Carbon-integrated vanadium oxide hydrate as a high-performance cathode material for zinc-ion batteries

Courtney-Elyce May Lewis

Bachelor of Science (Chemistry)

Submitted in fulfilment of the requirement for the degree of **Master of Philosophy**

Centre for Materials Science

School of Chemistry and Physics

Faculty of Science

Queensland University of Technology

2022

This page is intentionally left blank.

Keywords

Abstract

Zinc battery systems hold great importance in fulfilling the World's inherent need for clean energy storage, as a water and air stable system they pose as an ideal technology to be pursued in preparation for the oncoming spike in demand for clean, reliable energy. The problem, however, is that zinc isn't reliable. At its current stage in development zinc ion batteries are prone to significant capacity fade and premature cell failure. As such, it is the purpose of this Thesis to explore suitable materials and methods to rectify this and implement them into a new, high-performance cathode for use in a zinc ion full battery. The resulting was a layered vanadium oxide showcasing a stacked nanosheet morphology comprised of smaller nanoflakes. This was prepared through simple solvothermal synthesis and experienced the benefits of performance enhancing additives including an *in situ* carbon framework and interlayer water pillaring. A chemical formula of this material was verified through the use of XRD analysis cataloguing it to be $V_5O_{12} \cdot nH_2O$. The amount of water integrated into the material was altered in further experimentation yielding interesting results and the content per formula unit was determined by TG analysis allocating high and low water components of 2.7 and 0.4 respectively.

The designed material (CHVO) gave a high capacity of 396 mAh g^{-1} at 250 mA g^{-1} and completed over 100 cycles. Equally impressive was the cells' cycling life, completing over 3300 cycles at 4 A g^{-1}. The capacity was however impeded by the over-crowding of the intercalation tunnels due to the high presence of structural water within the material. As a result, the low water sample (CHVO-LW) was conceived. This opening of the intercalation pathways allowed for a phenomenal maximum capacity of 582 mAh g^{-1} at 200 mAh g^{-1} This success however was quite short lived as the lack of support from the structural pillaring allowed for the collapse of many of the tunnels, haltering the flow of ions to intercalation sites. An outcome which prompted a 64% drop in capacity before cell failure at a disappointing 80 cycles. From

this comparative analysis we can see that a balance must be maintained between the cells' capacity and cycling-life as an increase in one will sacrifice the other. This theory is well supported by the data obtained via EIS analysis with the CHVO material showing a notably higher initial impedance than the CHVO-LW alternative. These assumptions were further supported by additional electrochemical experimentation and analyses including GITT, as well as extensive characterisation of the materials' physiochemical properties and reaction chemistry throughout the galvanostatic charge/discharge process. Particularly notable was the conducting of *ex situ* XPS analysis through which we were able to investigate the internal redox reaction chemistry as a result of the galvanostatic cycling showing the presence of vanadium's various oxidation states at different stages throughout the charge/discharge process. Further study could however be conducted to improve the case of the capacity to cycling life relationship with the potential to optimise both variables. At a glance, this Thesis provides significant insight not only into a potential new cathode material for zinc battery systems, but also valuable information regarding the use and effect of structural water in layered material, a concept that is widely used across the electrochemical materials field.

Table of Contents

List of Figures and Tables

List of Abbreviations

ARB	Aqueous Rechargeable Battery
CE	Coulombic Efficiency
CHVO	Carbon integrated vanadium oxide
CHVO-LW	Carbon integrated vanadium oxide – low water
CNT	Carbon Nanotube
CV	Cyclic Voltammetry
EDX	Energy-dispersive X-ray spectroscopy
EIS	Electrochemical Impedance Spectroscopy
ESS	Energy Storage System
EV	Electric Vehicle
EHV	Electric Hybrid Vehicle
HER	Hydrogen Evolution Reaction
HVO	Hydrated Vanadium Oxide
GITT	Galvanostatic Intermittent Titration Technique
LIB	Lithium ion Battery
MOF	Metal Organic Framework
PBA	Prussian Blue Analogues
PVDF	Poly-Vinylidene Fluoride
XRD	X-ray Diffraction
SAED	selected Area (Electron) Diffraction
SEM	Scanning Electron Microscopy
SHE	Standard Hydrogen Electrode
SIB	Sodium Ion Battery
TGA	Thermogravimetric Analysis
TEM	Transmission Electron Microscopy
V-O	Vanadium Oxide
XPS	X-ray Photoelectron Spectroscopy
ZIB	Zinc ion Battery

Statement of Original Authorship

The following thesis contains only original works that have not been submitted for any award or to any other higher education institution, nor does it; to my knowledge, contain works written by an author other than myself unless referenced as such.

Signature: Courtney-Elyce Lewis

Date: 04/04/2022

QUT Verified Signature

Acknowledgements

I would like to give recognition to my principal supervisor and group leader Prof. Dmitri Golberg for his ongoing encouragement and wisdom throughout the course of my candidature, I have been extremely privileged to have him as a mentor and have gained a wealth of knowledge for his supervision. I would also like to acknowledge my associate supervisor Dr. Joseph Fernando who has provided me with consistent teaching and guidance in both my laboratory practices and research experience through which this project was able to be successful.

Next, I would like to thank Prof. Hongxia Wang for her support as well as the staff at the QUT Central Analytical Research Facilities (CARF) for their training and instruction of the many instruments that were used throughout the project. I would also like to acknowledge the QUT science and engineering faculty for providing the research scholarship to fund my studies.

Additionally, I would like to address my group members Dr. Konstantin Fareshteyn, Dr. Chao Zhang, Mr. Dumindu Thanaweera Achchige, and Mr. Joel Treifeldt for their encouragement and assistance throughout my studies. During my time here they have all become close and valued colleagues who I hope to work with again in the future. I would furthermore like to express my gratitude to all of my parents and my other family members along with my friends Ms. Alexandra Sykes, Ms. Kassandra Edie, and Ms. Kelly Bower, all of whom have provided me with so much support during the highs and lows of the past couple of years. With the care of all of these wonderful people I have been able to perform to the best of my ability and reach this great milestone in my life.

Chapter 1: Introduction
1.2. Background Information

Technology is in a trend of unforeseeable growth and with mass increases in the Worlds' population,[19] the demand for energy storage is at an all-time high[20] expecting to double by 2040.[21] But with the availability of fossil fuels at a historic low, only a few decades remain before they are no longer a viable energy source.[21] To prepare for the inevitable shift in resourcing, much of the world has turned their attention to new, eco-friendly energy storage systems (ESS)[20] to effectively implement renewables into the currently in-place systems.[22]

The most promising of the upcoming forms of renewable energy sources include solar, wind, hydropower and geothermal.[23] The underlying problem with the mass use of renewable energy however, is that the energy is not used immediately,[22] thus requiring a high energy density energy storage system (ESS) to store the energy until it is employed. With current technologies this may be achievable on a small, single home system, however to be implemented into a grid-scale project, further development and improvement into the capacity and safety of such storage systems is vital.[24, 25]

The use of enhanced ESSs will not only assist in the implementation of clean energy power grids, but also the expansion of 'green technologies' into the current market. A large amount of global pollution is due to the mass use of vehicles relying on fuels to power their combustion engines, rather than the recently introduced alternative of electric vehicles (EVs) and plug-in hybrid electric vehicles (PHEVs). To encourage the increased production of such technologies, a cheaper, safer, and more environmentally friendly ESS must be implemented into the vehicles than in current production vehicles.[26]

The current rechargeable ESS industry is undeniably saturated by lithium-ion batteries (LIBs). This technology has been the leading name since their commercialization and are commonly used in transportable devices such as mobile phones and laptops,[20] and in recent years have

even been implemented into EVs and PHEVs. The most significant drawback to the increased and prolonged use of LIBs is the ever decreasing availability of natural lithium sources which will not only increase the cost to produce such technologies, but also put other industries at risk such as glass and ceramics, which are the largest users of lithium in the world.[26]

Beyond this, the use of LIBs in large scale devices such as vehicles has raised many concerns about the safety of the cells due to the high toxicity of their components[27, 28] and a history of combustion under minor cell abuse.[20, 29-31] However, despite these risks, their overwhelming energy density and cycling life has seen them rise to the top of the ESS industry.

To overthrow the use of these LIB cells in years to come, many alternative ESS technologies are undergoing rapid development, yet none have reached commercial level at a notable scale. One such system is zinc ion batteries (ZIBs). ZIBs are a slightly more detailed approach to electrochemical battery technologies, due to the increased complexity of the ionic movement throughout the system and interactions between the positive and negative poles of the system, they require intricate design to operate at a level that is equivalent to LIBs.[28].

Despite this, they are quite ideal as an upcoming technology due to the abundance of zinc in the Earth's crust,[32] reducing production costs and increasing the longevity of the products viability[33-35]. Costs can be even further reduced by zincs high stability allowing for cell fabrication in air, rather than require an inert atmosphere environment.[36] Additionally, the cells themselves show lower redox potentials, higher theoretical capacities, and higher volumetric capacities, allowing for higher performance batteries.[32, 37] The concern over the safety of cell usage is negligible due to zinc's compatibility with water-based electrolytes, removing the most toxic and flammable component of the predeceasing LIBs.[23]

The use of water-based electrolytes is the defining feature of ZIBs, in addition to the drastic improvement of safety and eco-friendliness, it also has a greatly increased ionic conductivity providing a notable advantage in the electrochemical elements of the cells.[36, 38]

2

Despite the ideal nature of zinc ion batteries from a production standpoint, electrochemically they are not yet functional at the level of the commercial-grade battery cells they aim to dethrone. The three dominant sources of fault in these cells are:

- Lack of an appropriate wide-channelled, structurally sound, cathode material to allow for the efficient intercalation/ deintercalation of Zn^{2+} ions.

- Limited cycling-life due to passivation sites at the electrode interface caused by the occurrence of anodic dendrite evolution.

- Extensive leakage of liquid electrolytes causing an inability to properly facilitate the transport of Zn^{2+} between the positive and negative electrodes as well as throughout the structure of the cathode itself.

As a result of these drawbacks, ZIB are known to suffer from lack of sufficient energy density and power, as well as having limited cycling life being prone to cell failure especially so at lower current densities. As such, the technology is unable to be implemented into everyday devices nor able to be developed for grid-scale use. It is due to these issues that the research highlighted by this thesis document discusses the techniques in which high performance cathode materials can be developed for the implementation into ZIB systems to improve the viability of future commercial scale production.

Vanadium-containing materials have shown to be of high value to the industry and are the focus of many upcoming and high performance technologies including the aforementioned zinc ion systems.[39] This is likely due to the materials' unique multi-valent nature and highly tuneable structure. In addition, vanadium-containing materials are known for their low operating voltage and high theoretical capacity, making them an ideal cathode for transportable and renewable ESSs.[40]

When considering vanadium containing materials, they can be placed into a category of vanadium oxides, vanadates, oxygen-free vanadium compounds or vanadium phosphates.[41]

Whilst all are renowned for their electrochemical capabilities, only vanadium-oxides and vanadates are widely considered suitable for use in ZIB systems. This is due to the rigid structuring of oxygen-free vanadium compounds and vanadium phosphates, disallowing for the expansion of their intercalation pathways; a crucial factor when attempting to intercalate high energy ions such as Zn^{2+} as they are prone to electrostatic interaction with the cathode material.[42]

Vanadium oxides have a wide variety of morphologies allowing for enhanced surface interactions and shortened pathways to intercalation sites, furthermore they are also the foundation for many successful vanadate compounds.[23] Additionally, they display a large range of morphologies derived from very simple synthesis methods, the most common of which uses facile hydrothermal techniques. The vast variety of morphologies allows for the optimisation of intercalation pathway lengths and interactions between the electrode and electrolyte at the interface.[1]

They also show great surface tunability with enhanced pore size and increased surface area. Through this, vanadium oxides are highly capable of displaying pseudocapacitive characteristics.[43]

Pseudocapacitance is a highly sought after property in cathode development as the capacitive reaction at the surface balances the downfalls of the purely Faradic reactions typical of battery cells. Through this, not only is the cell able to store large amounts of charge, but also produce this energy with relative speed, as opposed to the slow kinetics of a traditional battery.[44, 45]

As well as being a porous material with a vast network of tunnels,[46] vanadium oxide (V-O) also often has a bi-layer structure. This layering easily allows for doping of the material with structural additives. The most common instance of this is the intercalation of water molecules. When forming strong bonds with the structure they provide a pillar-like effect between the bi-layers of the cathode due to their large atomic size[47] significantly increasing the structural

integrity and the size of the interlayer spacing.[48] The ratio of water to active material can greatly affect the resulting outcome as too little water is not structurally stable, whereas too much water can block possible intercalation pathways. Furthermore, doping with water molecules can also react with the vanadium compounds and form a hydroxyl layer on the walls of the cathode material, reducing the electrostatic interactions between it and the Zn^{2+} ions resulting in a lubricating effect,[28, 49] increasing the transport kinetics within the cathode and in turn improving the overall efficiency and reversibility of the battery cell.[49]

In addition to hydration, previous studies have shown that the integration of a carbon species into the cathode material can have multiple effects on the electrochemical performance of the battery cell.[50, 51] Firstly, the formation of a carbonaceous composite material can vastly improve the electrical conductivity of the electrode, pushing forward the redox reaction rate.[50] Furthermore, the carbon is highly porous and flexible, this allows it to have a cushioning effect on the base V-O structure during the intercalation/ deintercalation of Zn^{2+} ions.[52] Due to this, the mechanical strain experienced from the constant expanding and release of intercalation pathways is reduced, in turn increasing the overall cycling life of the cell by hindering the occurrence of electrode degradation.[7, 50, 52]

1.3. Thesis Objectives and Project overview

This thesis is a multi-focus process beginning with the collection and interpretation of available literature allowing for the formation of a tangible set of goals and objectives to be carried out throughout the completion of the work comprised of the following:

- Develop a clear understanding of the current limitations and ailments of zinc ion batteries as well as the effectiveness of the varying techniques designed to combat them.

- Using this knowledge to deduce the most effective cathode materials and relevant methods to introduce a promising new material in the ZIB research community.

- Devise a method to effectively synergise pre-established enhancement techniques applicable to vanadium oxide cathode materials

- Curate a detailed comprehension of the internal redox chemistry occurring within the $V_5O_{12} \cdot nH_2O$ cathode material throughout galvanostatic charge/discharge cycles and over the course of the cells cycling life.

- Use material characterisation techniques to highlight the physical drawbacks of $V_5O_{12} \cdot nH_2O$ and their effects on the electrochemical performance of the resulting cell.

Analyse the above data collections in the context of $V_5O_{12} \cdot nH_2O$ with both high and low structural water content, thus structuring a valid statement applicable to a variety of layered-hydrated cathode materials for use in ZIB technologies. Through fulfilling these aims, the project will have accomplished not only the study of a new high-performance ZIB cathode material, but also provide transferrable knowledge and techniques that will be usable for many materials and projects across the field of study.

1.1. Thesis summary

This Thesis document shall encompass the work I have completed throughout my Master of Philosophy candidature. The pre-established introductory chapter provides a fundamental understanding of the subject matter with a detailed background in relevant base theories, as well as detailing the significant gap in the current research providing requirements for the study area covered by this thesis project.

As implied in **Figure 1**, this shall be followed by a published review paper in place of a literature review chapter, allowing for a deeper understanding of the subject matter. This article provides an overarching evaluation of current technologies and materials involved in current zinc ion battery experimentation before entering a detailed analysis of vanadium-containing materials as one of the most promising contenders for ZIB cathode materials. Of the members of the vanadium family, the most prevalent are identified along with further enhancement techniques allowing for readers to identify the pros and cons of each and make the most informed decision when designing and synthesising experimental materials to overcome the current downfalls of the technology. This paper was created to function as a comprehensive tool allowing readers to not only examine past experimental data, but also to evaluate comparisons and analyses made throughout in order to develop relevant technologies with the highest possible capabilities. This information allowed for the designing of the resulting experimental research project. To undertake an experimental project of this fashion, a wide variety of techniques must be utilised to fully understand the scope of the material, as such, the methodology section gives insight into the practices used to provide the data required for the project.

This information allowed for the design and implementation of a hydrated, carbon incorporated, layered vanadium oxide cathode in a ZIB coin-cell system. Chapter three of this document is a collective overview of the various techniques and instruments used for data

collection throughout the duration of the thesis project. This section includes the relevant sample preparations required, as well as synthesis procedures used and battery cell fabrication details. In order to efficiently implement structural additives into the material, a simple solvothermal synthesis method was employed. Both physiochemical and electrochemical experimentations are covered in this chapter and give a clear insight into the skills that were developed and utilized throughout the candidature.

From here, the aforementioned techniques are applied in carrying out a complete physiochemical characterisation in order to accurately detail the structure, chemical composition, morphology, and architecture of the synthesised material. The purpose of a highly detailed characterisation of the nanomaterial is to completely determine its chemical formula and makeup, identify any impurities within the sample, and deduce its crystallinity and morphology as well as various physical properties. It is vital to analyse all these components of a sample to ensure it is the target material as well as being able to justify its electrochemical performance in ensuing battery cell testing. This is due to the extreme effect that structure and morphology have on its performance properties such as electrochemical capability, cycling stability and intercalation abilities, which are carefully documented in the fifth chapter of this document. The electrochemical testing of our material is conducted through a series of stringent experimentations targeting certain aspects of a batteries cell capabilities including capacity, capacity retention, cyclability, ability to perform at both low and high currents, and recoverability. Further data analysis techniques as highlighted in the following chapters will also afford us the insight into the reaction chemistry that occurs within the active material as a result of the cells' charge/discharge cycles.

The material of interest throughout the course of this Thesis is $V_5O_{12}\cdot nH_2O$, a cathodic active material not yet implemented into ZIB technologies, not only will the viability of this material be thoroughly examined using a variety of electrochemical and physiochemical techniques, a

secondary analysis will take place investigating the effects of different ratios of structural water within the bilayers of the material. Such information not only gives greater insight into the interactions between the intercalating zinc ions and the water molecules, but also allows for a greater understanding of the mechanics such additives introduce, a concept that is able to be applied across a great variety of layered materials.

Projects such as this are highly beneficial to the scientific community as they provide an in-depth look into the details of various vanadium-containing material compounds, explore the use of various material enhancements, as well as introducing a new material into the ZIB research field. Such points are further elaborated in the subsequent Discussion and Concluding Statements chapter of the document. This chapter examines the works accomplished throughout the candidature and highlights the dominant features in context of quality of the findings, and the overarching significance to the scientific community.
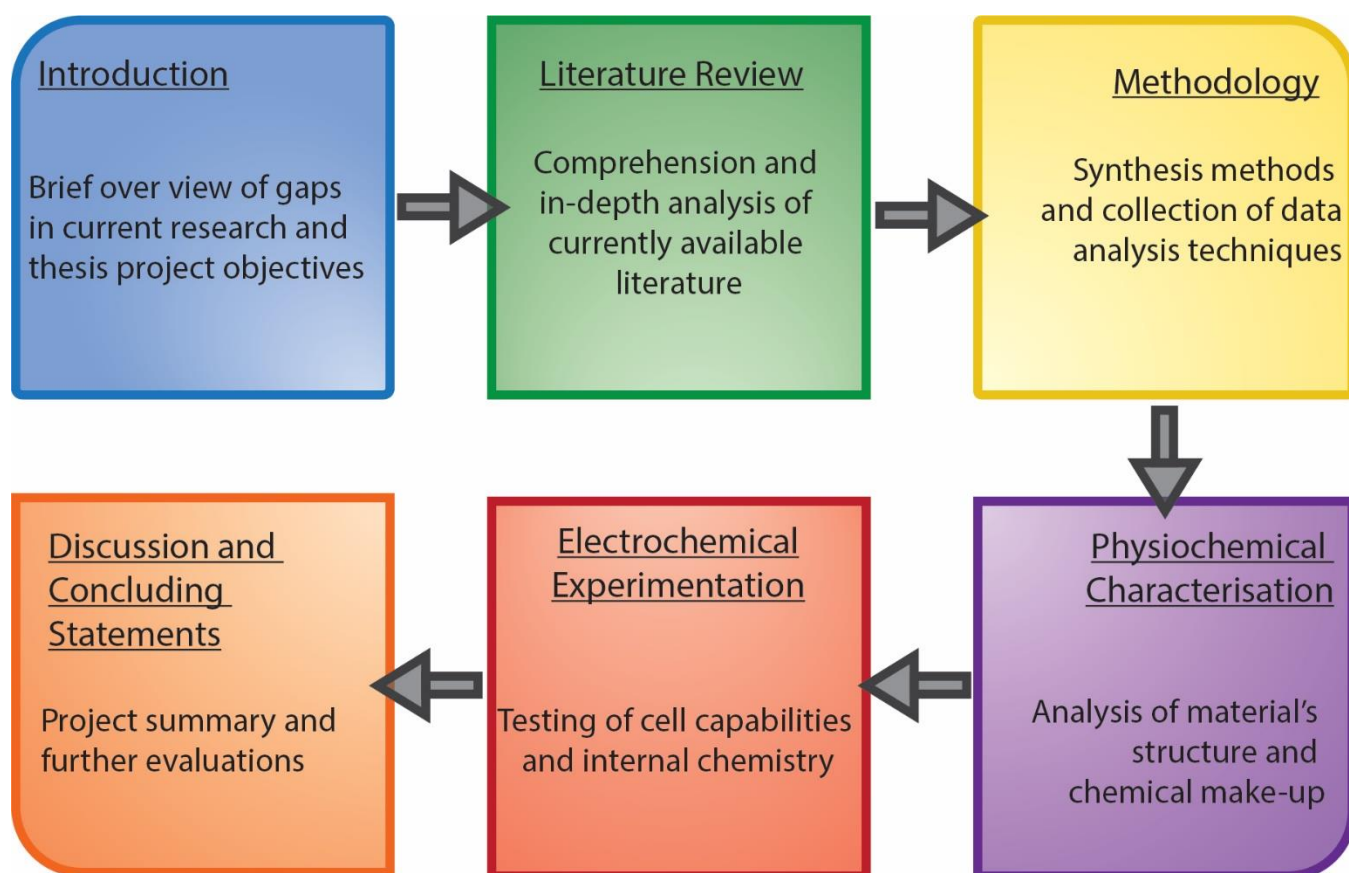
Figure 1: Flowchart diagram of Thesis documents chapters.

Statement of Contribution of Co-Authors for Published Paper

The authors listed below have certified that:

1. they meet the criteria for authorship and that they have participated in the conception, execution, or interpretation, of at least that part of the publication in their field of expertise;
2. they take public responsibility for their part of the publication, except for the responsible author who accepts overall responsibility for the publication;
3. there are no other authors of the publication according to these criteria;
4. potential conflicts of interest have been disclosed to (a) granting bodies, (b) the editor or publisher of journals or other publications, and (c) the head of the responsible academic unit, and
5. they agree to the use of the publication in the student's thesis and its publication on the QUT's ePrints site consistent with any limitations set by publisher requirements.

Please state the publication title and date of publication or status:

"Vanadium-Containing Layered Materials as High-Performance Cathodes for Aqueous Zinc-Ion Batteries" Published 14 July 2021.

Contributor	Statement of contribution*
Courtney-Elyce Lewis	Manuscript writing, Analysis of literature.
Courtney Lewis	
17/11/2021	
Dmitri V. Golberg	Supervision of project, reviewing of manuscript
Joseph F. S. Fernando	Aided manuscript writing and review.
Konstantin L Firestein	Reviewing of manuscript
Chao Zhang	Reviewing of manuscript
Dumindu P. Siriwardena	Reviewing of manuscript
Joel E. von Treifeldt	Reviewing of manuscript

Principal Supervisor Confirmation

I have sighted email or other correspondence from all Co-authors confirming their certifying authorship. (If the Co-authors are not able to sign the form please forward their email or other correspondence confirming the certifying authorship to the GRC).

Name: Dmitri Golberg   Signature: QUT Verified Signature   Date: 17/11/2021

Abstract

The World is currently in the midst of a climate crises and many across the globe are competing to find new technologies to create clean, and effective ways of harnessing renewable energy sources. However, this energy needs to be stored and the current systems simply would not last. Zinc-ion batteries with vanadium-containing cathodes are a recently arising technology providing a cheap, safe and eco-friendly alternative to the current systems. Vanadium is a material that has long been used for electrochemical systems due to its large range of stable oxidation states. Most common is the vanadium oxide (V_2O_5) renowned for its open layered framework and manipulatable structure. However, this is not the only vanadium-containing material that has been proposed for use in ZIBs. The vanadium family is comprised of four main sub-categories under which materials can be classified: vanadium oxides, vanadium phosphates, vanadates, and O_2-free vanadium compounds. This report delves into the specifics of each of these sub-families to further develop our understanding of their functionality by highlighting their structural and morphological characteristics, aptitude for modification, and the corresponding electrochemical properties. Through this investigation, the application of these materials in ZIB systems is highlighted and future development aims considered.

2.1. Introduction

The world is currently set to experience one of its most drastic energy crises with future forecasts expecting the demand for energy to double by 2040, and by 2050 reaching up to 1000 exajoules.[21] The largest contributors to this being population growth and major technological advancements.[19] With fossil fuel resources being expected to only last another few decades, and CO_2 emissions (currently 74%) pushing atmospheric levels to alarming heights (407.8 $\pm$ 0.1 ppm), much attention has been directed at employing global use of renewable and green

energies.[21] In preparation for such an event the world is seeing an extensive rise in demand for energy storage devices to contain this energy that is both non-toxic and eco-friendly.[20]

The fundamental problem with mass use of renewable energy (such as solar, wind, hydropower and geothermal) is that there is often a long period of time between when the energy is produced and when it is required for use. Storing energy for such a period of time requires high-functioning energy storage systems.[22] Conversely, for those that are connected to a grid source, the quality of the individual system will define the quality and stability of the overall power output. Integrating energy storage technologies into renewable energy systems will reduce this uncertainty in power output, thus steadying day-night fluctuations.[1, 25] And it is also a simple task to implement these technologies to grids that meet the requirements of EVs and HEVs.[25]

2.1.1 Current technology

As far as reusable energy storage systems are concerned, Lithium-ion batteries (LIBs) are one of the most successful advancements of our time and are highly sought after as a commercial battery.[20] However, LIBs are restricted in terms of large grid scale use due to drawbacks such as their increasing costs, safety hazards, and potential for environmental damage.[15, 53] One of their major downfalls is that there are very few viable electrolytes for use in LIBs and all of them are flammable organic electrolytes posing concerns in both their explosive tendencies and high toxicity.[15] Since the commercialization of LIBs, many reports on self-ignition and combustion of the cells have been made which have triggered extensive research into viable alternatives.[29]

Due to the skyrocketing interest in electric and hybrid vehicles, much research has gone into the sustainability of the lithium industry and what it would mean for the environment if LIBs were the vehicles' main source of energy. On average, EVs and HEVs use 4 kg and 1.4 kg of lithium *per* unit, respectively. If these mass requirements are to remain throughout the green vehicle boom, the demand for raw lithium metal will increase so significantly that even

'best-case' production yields will be vastly outweighed by the amount required. As it stands, the current lithium resources will not supply enough material to power the increasing number of battery powered vehicles let alone, as well as the demands of the glass and ceramics industry which is currently the highest consumer of lithium in the world.[26]

2.1.2 Aqueous rechargeable batteries (ARB)

Many research projects have focussed on the development of safe, cost effective and environmentally friendly ARBs, including those with monovalent alkali metals and multivalent metals, many of which are in significantly greater abundance than lithium.[54] Aqueous electrolytes demonstrate a significantly higher ionic conductivity[55] with an average improvement of two orders of magnitude depending on the specific solution.[36] However, the number of options is limited, as many transition metals have redox potentials too low for reversible reactions to occur without decomposing and producing hydrogen within the cell.[56] Monovalent systems often display similar de/intercalation mechanisms to LIBs and could serve as viable alternatives. Common examples of such technologies include aqueous sodium- and potassium-ion batteries. However, multivalent systems are more desirable given that their multiple redox states promise high specific capacity and energy density.

Theoretically, metals with multivalent ions are able to transfer more charges *per* ion that monovalent species, such as Li and Na,[57] and as such can display a much higher energy density, as well as a higher specific capacity.[56] Such materials include Mg, Zn, Ca and Al. Foreseeable complications with multivalent ions, however, stem from their large atomic size, which during de/intercalation has the potential to damage the host cathode material.[40, 58, 59] Thus, much like monovalent alternatives, they require very specific cathodes that contain large enough vacant sites and are stable enough to transfer and store the ions without collapsing the structure.[58] They are also assumed to diffuse slower due to the strong electrochemical interactions between them and the cathode material due to their increased energy densities.[40] However, this is not necessarily always the case. By borrowing theories from supercapacitor

studies, it is possible to achieve high charge-discharge rates using multivalent ion reactions. Research into this theory was conducted using zinc- and nickel-ion batteries with α-type manganese dioxide cathodes. The results showed a total energy density higher than lead-acid batteries, and almost equivalent to that of LIBs.[56, 60] Additionally, Mg^{2+} and Ca^{2+} ions in batteries often struggle to intercalate into the cathode material,[58, 61] as well as Al^{3+} ion batteries are suffering from intrinsically low energy densities.[62] Furthermore, all three types of batteries have limited electrolytes with which they are compatible, and many of those are viable often lead to the formation of passivation layers on the electrodes.[58] It is due to this and to its high kinetic overpotential to the hydrogen evolution reaction (HER)[63, 64] that Zn is a highly preferred candidate among multivalent anode materials.

2.1.3 Aqueous zinc ion batteries

Metallic zinc has historically been used in the energy storage industry since the first battery was invented in 1799.[54] Since then it has been a fundamental backbone in the development of new electrochemical storage technologies, growing to facilitate the first modern alkaline battery; the $Zn-MnO_2$ cell[4] invented in 1860.[46]

However, rechargeable aqueous ZIB require a more detailed design than that of LIBs due to the complex interactions between the cathode and the electrolyte/anode.[49] This also means that they suffer from a number of additional downfalls which in turn limit their commercialization viability. These issues include electrode decomposition, dendrite formation, over-abundance of electrostatic interactions, and the production of by-products within the system.[65] If these can be resolved, ZIBs would be the ideal battery, showing high potential, low production cost (approx. US$2 kg^{-1}),[66] and high abundance of primary materials[34, 35, 56] with zinc being 300 times more abundant in the Earth's crust than lithium.[67] For example, ZIBs with V_2O_5 cathodes cost approximately US$65 kW^{-1} h^{-1} including all raw materials for the electrodes and electrolyte, whereas the equivalent cost of LIBs with $LiCoO_2$ cathodes is on

average around US$300 *per* kW^{-1} h^{-1}.[65, 68] Additionally, ZIBs also exhibit a lower, more ideal redox potential (-0.763V *vs.* SHE) than that of competing technologies, as well as notably higher theoretical capacity of 820 mAh g^{-1},[67, 68] and volumetric capacity of 5585 mAh cm^{-3}.[67, 69] Production costs are also a notable benefit to the use of ZIB as they are compatible with air and therefore do not require specialized inert environments for fabrication.[36, 70] Furthermore, ZIBs with several alterations from the base form have been shown by prior research to have great promise for future grid application due to their reliability, safety and capacity, which are key goals in the search for storage of renewable energy sources.[34, 54, 57, 71]

ZIBs, despite being the most promising alternative to LIBs, also have a significant number of setbacks for which varying solutions are being developed. These drawbacks result in the battery cells displaying low specific capacities despite zinc having a high theoretical capacity of 820 mAh g^{-1}. However, this is not a detrimental factor to the development of ZIB technologies, as most of the issues, which stand at the heart of the capacity loss, and other issues, have been identified and are currently undergoing significant testing to eradicate these problems.[68] Despite the significant progress made towards the suppression of the aforementioned drawbacks, it is still prudent to investigate ZIBs in detail, ensuring that their amendments are better understood.

The first and most notable of issues that plague ZIBs is the growth of zinc dendrites on the anode surface during cycling, resulting in a significant drop in reversibility. When dendrites form, the amount of active material available for ion transfer is significantly reduced, resulting in a drop in the cells' Coulombic efficiency and thus its reversibility.[35] Significant and ongoing growth can also result in the eventual short circuiting of the battery cell.[72] In fact, there are a number of articles that specifically review the underlying issues and advancements of Zn anodes.[64]

The most basic and fundamental thing to note about designing a ZIB is that despite Zn^{2+} ions relatively small ionic radius (0.75 Å), zinc ions struggle with intercalation due to electrostatic interactions with the cathode host material caused by the ions of notably high charge energy.[23] When this phenomenon occurs during ion transfer through the cathode, it has the potential to affect the structural bending vibration of the host structure, as well as forcibly increasing the interlayer spacing putting immense strain on the structure and potentially leading to a breakdown in the cathode structure. The most promising method of reducing the effects of this resultant mechanical strain is to utilize a cathode material with a flexible and stable morphology, allowing it to stretch and undergo movement without putting the structure at risk.[54, 65]

2.2. ZIB cathode materials

The most significant issues surrounding electrochemical performance are associated with the cathode materials, many of which surround the struggle of ion intercalation, most prominently affecting the sustainability and high-rate performance.[37, 71] The specific cause of this occurrence is the potential for phase change, dissolution, and self-aggregation during the zinc ion intercalation process. There are often problems surrounding poor cyclability. These are often due to strong polarization of the zinc ions and can be improved upon or resolved through the implementation of cathode materials with stable crystal structures and significant flexibility, allowing dopped molecules to widen the ionic channels without jeopardising the materials overall integrity.[71] If a suitable cathode material can be developed, ZIBs will have taken a great leap past competing technologies in the race to be the best LIB alternative.[57] Most commonly nanostructured materials have been put to this use as they show shorter ion diffusion paths, better tolerance for physical strain and a larger interior surface area.[41]

Many materials have been developed over the past years, most of which are variations of three base compounds: manganese oxide, Prussian blue, and vanadium-based materials.[50]

Cathode materials including MnO_2 and Prussian Blue Analogues (PBAs) have been investigated and found to suffer from several detrimental faults. Despite the high specific capacity displayed by the cathodes, manganese oxides often display poor cycling at low currents,[4, 73] significant declines in the cells capacity throughout cycling,[37, 74] and discharged by-products limiting the Coulombic efficiency of the cell.[55, 75] Conversely, Prussian blue cathodes struggle with their low capacity that occurs as a result of defects in the lattice structure, which with continued intercalation of large ions such as zinc, has a tendency to collapse, destroying many of the intercalation sites.[23, 55]

There has also been a recent rise in interest surrounding the possibility of organic cathode materials such as quinone and polyaniline compounds for ZIB systems, however despite their high reversible capacity, they suffer from extremely limited lifespans owing to detrimentally low conductivity,[42] material decomposition and dissolutions during cycling.[76]

Comparatively, vanadium-based materials have an increased functionality potential than competitors. Although their operating voltage (0.75 V) is lower than that of Prussian blue (1.7 V) and manganese oxide (1.3 V), their higher capacity, as well as increased structural stability across a larger spectrum of valence states and frameworks, are still thought to be superior. **Figure 2a** illustrates output voltage and specific capacity values of several ZIB cathode materials where the high energy density of vanadium-containing materials is evident, albeit the low operating voltage. Moreover, they allow for more ideal morphologies encouraging increased ion intercalation and reversibility.[40] For instance, as illustrated in **Figure 2b,** vanadium-containing materials tend to from layered or tunnel like crystal structures that readily facilitate reversible Zn^{2+} (de)intercalation. With additional research and development, these materials could be the most viable option for ZIB commercialization as they are also non-toxic, simple to produce, and are of comparatively low cost.[39] Owing to this reason, the past 5 years have seen a rapid growth in the research area of vanadium-based cathode materials for

ZIB (**Figure 2c**). This review focuses mainly on ZIB cathodes from the vanadium family, covering the main groups of vanadium-oxides, vanadates, vanadium-phosphates, and oxygen-free vanadium compounds.

Reviews by Liu *et al*.[77] and Zhang *et al*.[78] give an extensive list of all common vanadium-containing compounds despite the presence of shared structural characteristics (such as crystal structure, morphology, and doping effects) as well as charge storage mechanisms between them. Conversely in this paper we offer a focused review of vanadium-containing materials in ZIBs, presenting a succinct yet meaningful analysis of the vanadium family, critically comparing and analysing the various material, giving readers the opportunity to extract the knowledge required to design the most ideal cathode for their desired outcome.

2.3. Vanadium-containing materials

Vanadium metal is naturally abundant in the Earth's crust as well as cheap to acquire (~US\$2.5 Lb^{-1}).[50] As such, vanadium-based materials have enticed much attention for battery cathode application, especially in LIB and SIB technologies[79] due to their large array of oxidation states (ranging from +2 to +5),[41] as well as their superior ability to host metallic ions attributed to their open structure, layered frameworks, and manipulatable interlayer spacing.[80] Furthermore, most vanadium structures can utilize metal ions to further stabilise the structure, namely alkali metals, as they form strong covalent bonds within the material.[20] Vanadium oxide cathode materials, despite their comparatively lower operating voltage, exhibit a high performance rate as well as a longer cycling life than many alternatives.[23, 81] This is likely assisted by their high theoretical capacity of $\leq$300 mAh g^{-1}.[81]
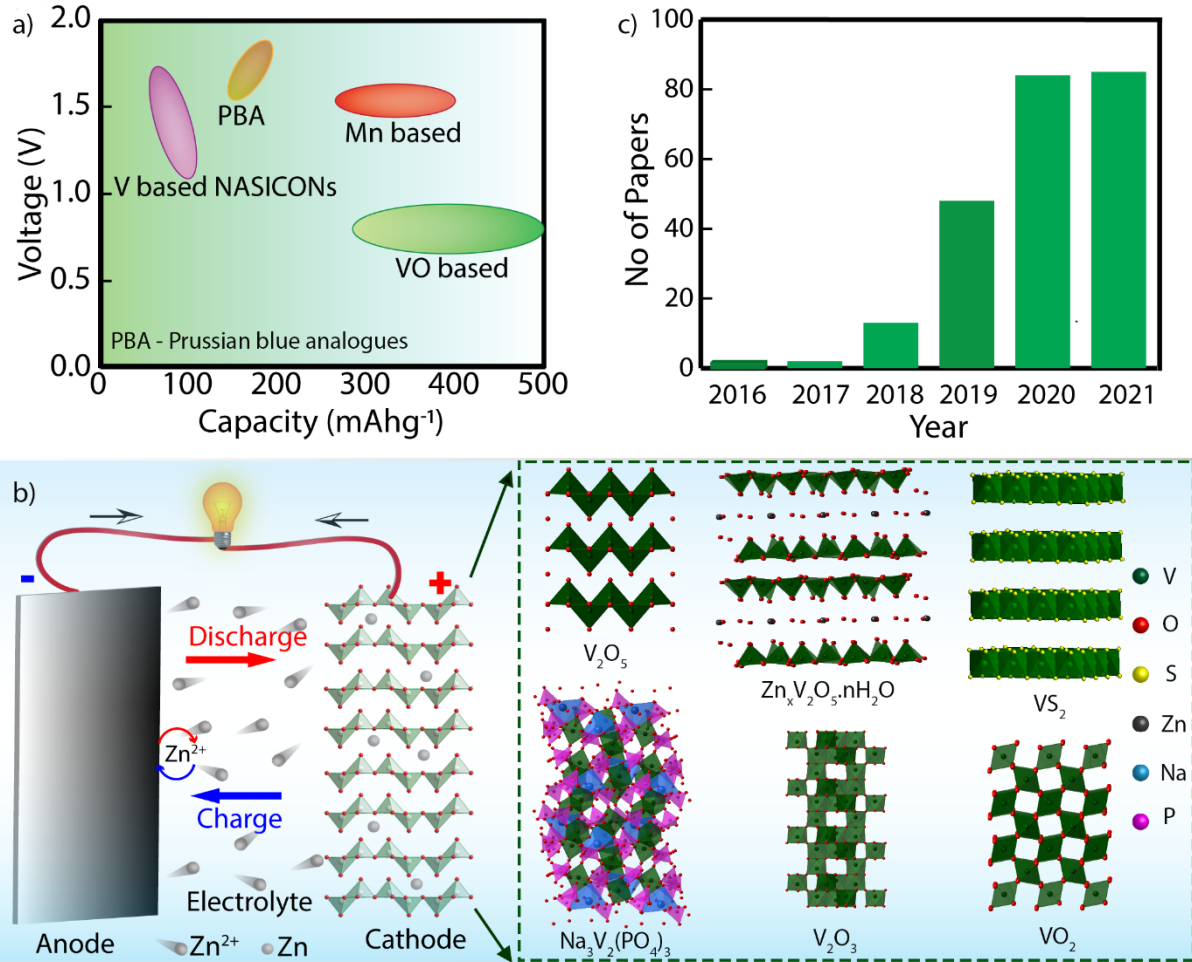
Figure 2. a) Comparison of output voltage and specific capacity values of a few ZIB cathode materials. b) Number of journal articles/*per* year reporting vanadium-containing cathode materials for ZIB in the past 6 years. Data extracted from Scopus on 2nd June 2021. c) Schematic illustration of aqueous ZIB and crystal structure of some common vanadium-containing cathode materials.

Due to the multiple valence states, the redox reaction that occurs within the vanadium cathode is a multi-electron redox reaction showing increased kinetics.[68, 73, 79] Vanadium's multi-valent nature also allows it to exist stably in many morphologies and frameworks, different combinations of which can have a significant effect on the intercalation capabilities

of the resulting material. This fact alone makes it one of the most promising ZIB cathode material options.[23]

One notable drawback of vanadium-based materials is that due to their loosely bound, layered crystal structures, it is likely that during ion exchange vanadium ions will be produced. If these new ions can dissolve in the electrolyte, the production will be encouraged and gradually decrease the amount of active material available at the cathode site resulting in significant capacity deterioration as the amount of zinc reaction sites becomes limited. Studies on the topic have shown that when operating at a faster charge-discharge rate, the dissolution of the cathode materials is significantly reduced. The opposite is also true that when slow charge-discharge is applied, the dissolution occurs much faster than it otherwise would. Beyond cycling speed, it is also recommended to use a cathode material with a highly stable crystal structure as it is less prone to lose ions or dissolve readily in solutions.[74] The cathode material is also less likely to dissolve in a 'salt in water' electrolyte, however, a high salt concentration inhibits ion flow through the electrolyte, and as such, this is not always the most recommended course of action.[46, 65]

A major advantage of vanadium-based cathodes, however, is that they are easily able to adopt pseudocapacitive characteristics. Pseudocapacitance occurs when fast and reversible Faradic reaction occurs near the surface of the electrode material. As such, it has an above average capacitance compared to standard battery cells and its power density mimics that of a supercapacitor.[44, 45] This is an ideal element within battery technology as it not only balances the need for fast energy transfer, but also the demand for storing larger amounts of energy, making such materials essential for new and more demanding technologies. The pseudocapacitance of a cathode can be encouraged within a material through the manipulation of crystal structure and morphology of its surface layer, as well as the electrolyte used within the cell.[82] Pseudocapacitance can also be greatly increased with the inner porosity of the

material creating a much larger active surface area. For example, research by Li *et al*. explored

porous V_2O_5 yolk-shell microspheres (**Figure 3a**) as a cathode in ZIB and found that surface

controlled capacitive processes account for a higher proportion of charge storage, which was

attributed to the microporous architecture.[1] The contribution of diffusion-controlled and

capacitive processes can be separated using a cyclic voltametric analysis, as depicted in **Figure**

3b-c. Another effective method of ensuring pseudocapacitance is to prepare amorphous-like

structures and implement oxygen defects into materials as in V_2O_5/Graphene heterostructures

synthesized by Wang *et al*.[2] (**Figure 3d**). The increased active sites enhance

electroconductibility and allow for faster rates of ionic transfer at the surface (**Figure 3e-f**).
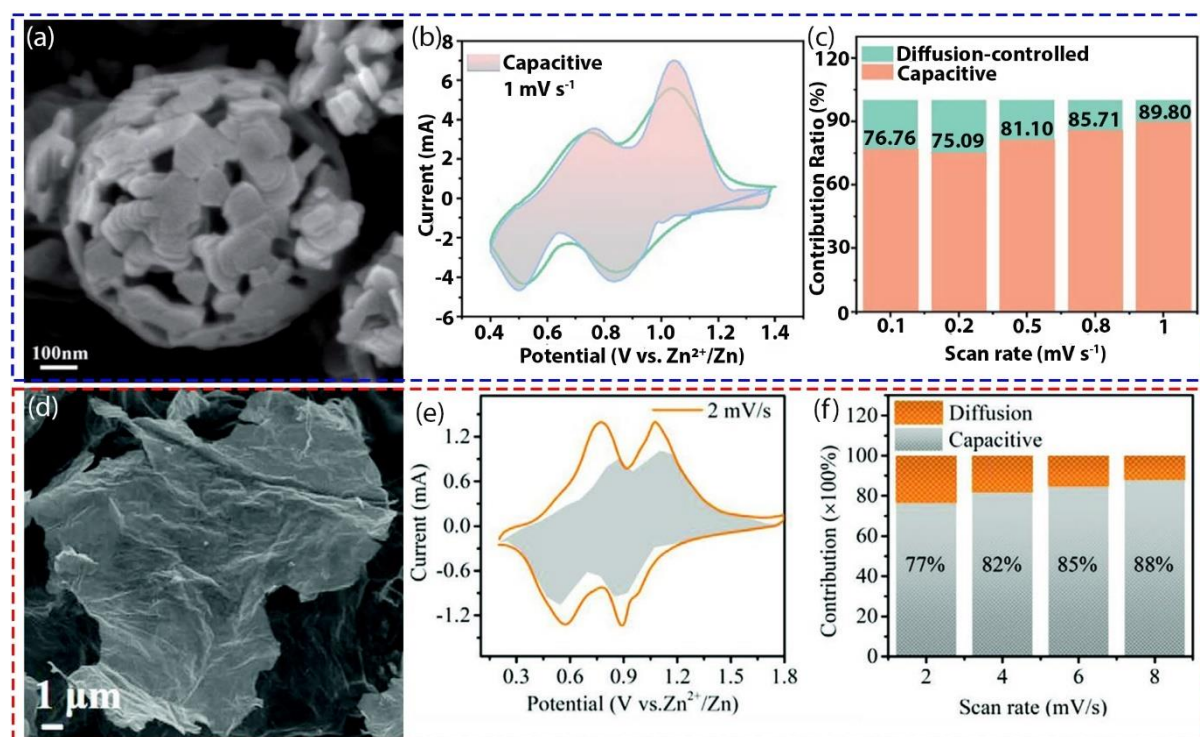
Figure 3. a) SEM image of V_2O_5 yolk-shell microspheres. b) CV curve showing capacitive

contribution (greyish area) at a scan rate of 1 mV s^{-1}. c) Percent capacitive and diffusion-

controlled capacities at different scan rates. d) SEM image of V_2O_5/graphene heterostructures.

e) CV curve showing capacitive contribution (greyish area) at a scan rate of 2 mV s^{-1}. Percent

capacitive and diffusion-controlled capacities at different scan rates. a-c) Reproduced with

The vanadium family can be broadly categorised into four groups: vanadium oxides, vanadates, vanadium phosphates and oxygen-free vanadium-based compounds.[41] While vanadium oxides and vanadates are the most commonly used of the vanadium family, recent research has delved further into oxygen free V-based composites such as vanadium transition metal dichalcogenides, as demonstrated by Zhu *et al.*[83] and Chen *et al.*[50] implementing VS_4 and VS_2, respectively, as well as Wang *et al.*[73] using VSe_2 as the base cathode material in ZIBs. The less common sub-category - vanadium phosphates, despite typically having a higher redox potential than its sister species, suffers from having notably low electrical conductivity which greatly decreases their practicality as a cathode material.[41]

2.3.1 Vanadium oxides

Vanadium-oxides exhibit diverse V-O coordination polyhedra,[32] such as tetrahedral, trigonal bipyramidal, square pyramidal, octahedral, and distorted octahedral, giving rise to alternate forms of vanadium oxides with electrochemical performance differing greatly between the materials and their structures.[32, 68] Furthermore, vanadium oxides are able to simultaneously exhibit both +4 and +5 valency states (and in some circumstances +3 as well) without altering the framework or limiting the stability of the material.[40, 81] As previously mentioned, vanadium oxides provide a wide variety of interchangeable frameworks, such as those of V_2O_5, allowing for particular manipulation of the material. Some structures, however, are more desirable than others. The case is the popular V_2O_5 compound which often exhibits a square pyramidal, double chain structure. Although in some cases, due to its sharing oxygen atoms between layers, it can also be considered as a distorted octahedron.[23] This material, due to its many viable configurations, is able to exist stably in varying frameworks.

Tetrahedron frameworks always contain V^{5+}. Any attempt to change the valency state will result in a transition to a new structure. Due to this, tetrahedral configurations have poor reversibility and are not ideal for battery use.[23] They do have a use however, as a precursor to form trigonal bipyramid and square pyramid structures consisting of both V^{4+} and V^{5+} ions. These materials are sometimes able to be further manipulated into distorted octahedral frameworks.[81]

Distorted octahedron frameworks also contain both V^{4+} and V^{5+} ions, unlike the pyramidal structure, however, they are also able to achieve V^{3+} ions with slight structural changes into regular octahedrons. This does not alter the materials morphology.[23, 84] Vanadium oxide materials with mixed oxidation states exhibit increased electrochemical activity, as the presence of +4 results in lower polarisation, thus resulting in faster ion diffusion and higher electrical conductivity than V_2O_5 (containing purely +5 valence ions). This makes it an ideal structure for electrochemical purposes. An example of this is shown in studies by Liu *et al.* presenting a multivalent structure of +4/+5 V_2O_5 hollow nanospheres constructed of layered nanoflakes. The material showed good rate capability and displayed high cycling rates up to 1000 cycles.[85]

Due to the recent interest in the development of vanadium-oxide based cathodes in ZIBs, there are now a large variety of structures and morphologies that are being investigated stemming from a large range of synthesis methods. These cathode materials and their resulting battery cells have had varying degrees of success.

2.3.1.1 V_2O_5

Vanadium (V) oxide (V_2O_5) materials that are typically applied as cathodes in ZIBs possess an orthorhombic phase (*Pmmn* – 59).[3] This material has a layered structure where each layer is composed of VO_5 pyramids **(Figure 4a)**.[86] The large interlayer spacing between (010) planes along *b*-axis (~ 4.7 Å) can facilitate Zn^{2+} (de)intercalation.[6]

Commercial V_2O_5 powders have displayed high capacity and remarkable cycling stability when incorporated as a cathode material in ZIB.[3, 86] For instance, Zhou *et al*. prepared a V_2O_5 cathode material by processing a commercial V_2O_5 powder.[86] This material displayed the best performance in a $ZnSO_4$ electrolyte (121 mAh g^{-1} at 1 A g^{-1} after 400 cycles) compared to when other electrolytes, such as $Zn(CH_3COO)_2$, $Zn(NO_3)_2$ and $ZnCl_2$ were used. Moreover, the energy density and stability of commercial V_2O_5 powders can be significantly improved by blending graphite using high energy ball-milling techniques.[3] V_2O_5-graphite mixture displayed superior rate capability (**Figure 4c**) and a high capacity of 372 mAh g^{-1} at a specific current of 5 A g^{-1} after 4000 cycles. Interestingly, the pristine solid morphology of V_2O_5 was gradually transformed to porous nanosheets during Zn^{2+} de(intercalation) (**Figure 4b**), where co-intercalation of H_2O was found to be advantageous to limit electrostatic reactions between Zn^{2+} ions and the host structure. **Figure 4a** displays a schematic illustration for co-intercalation of Zn^{2+} and H_2O between (010) planes of the V_2O_5 crystal structure.

Hydrothermal and solvothermal syntheses are frequently used to obtain V_2O_5 type materials with improved Zn^{2+} cycling performance.[1, 2, 4, 6, 85, 87] The different manipulations of these sol-gel techniques, as well as secondary modifications, allow to produce diverse morphological complexes with nano- and microscale structural features. In fact, by manipulating the reaction conditions, varying architectures can be formed such as that of Li *et al*.'s[1] yolk-shell structure comprised of porous spheres (**Figure 4d, e**). The yolk-shell morphology was expected to buffer volume expansions of the structure during Zn^{2+} de(intercalation). At a specific current of 5 A g^{-1} this material delivered a reversible capacity of 200 mAh g^{-1} after 1000 cycles. Although ~90% of the charge stored at a scan rate of 1 mV s^{-1} was calculated to be through a capacitive process, the rate capability of this material was not as good as the commercial V_2O_5-graphite discussed earlier (**Figure 4f**). Interestingly, akin to commercial V_2O_5-graphite, co-intercalation of H_2O and a reversible formation of nanosheet-

like structures on the surface of spheres were observed during the (dis)charge process. Integration of polymeric chains, such as polyaniline into the interlayers of V_2O_5 can also enhance the Zn^{2+} storage capability. Chen *et al*. used a hydrothermal technique for *in situ* intercalation of polyaniline within the crystal structure of V_2O_5 (PANI-V_2O_5).[4] They reported an increase in interlayer spacing from 0.44 nm to 1.42 nm (**Figure 4g**), however, it should be duly noted that integration of PANI completely alters the crystal structure of V_2O_5 (as evidenced by XRD). PANI-V_2O_5 displayed an appreciable rate capability (**Figure 4h**) and a reversible capacity of 360 mAh g^{-1} at 0.5 A g^{-1} and 208 mAh g^{-1} at 5 A g^{-1}, respectively. *In situ* XRD measurements have revealed that interlayer spacing can expand up to 1.62 nm upon insertion on Zn^{2+}, while PANI buffers any unfavourable expansion of the material. Narayanasamy *et al.* developed a hydrothermal route to prepare a layered V_2O_5/V_2C hybrid material through oxidation of V-MXenes.[57] The V_2C component effectively improved the charge transfer kinetics and the mechanical stability of the electrode material. V_2O_5/V_2C displayed a reversible capacity of ~300 mAh g^{-1} at 4 A g^{-1} after 2000 cycles.
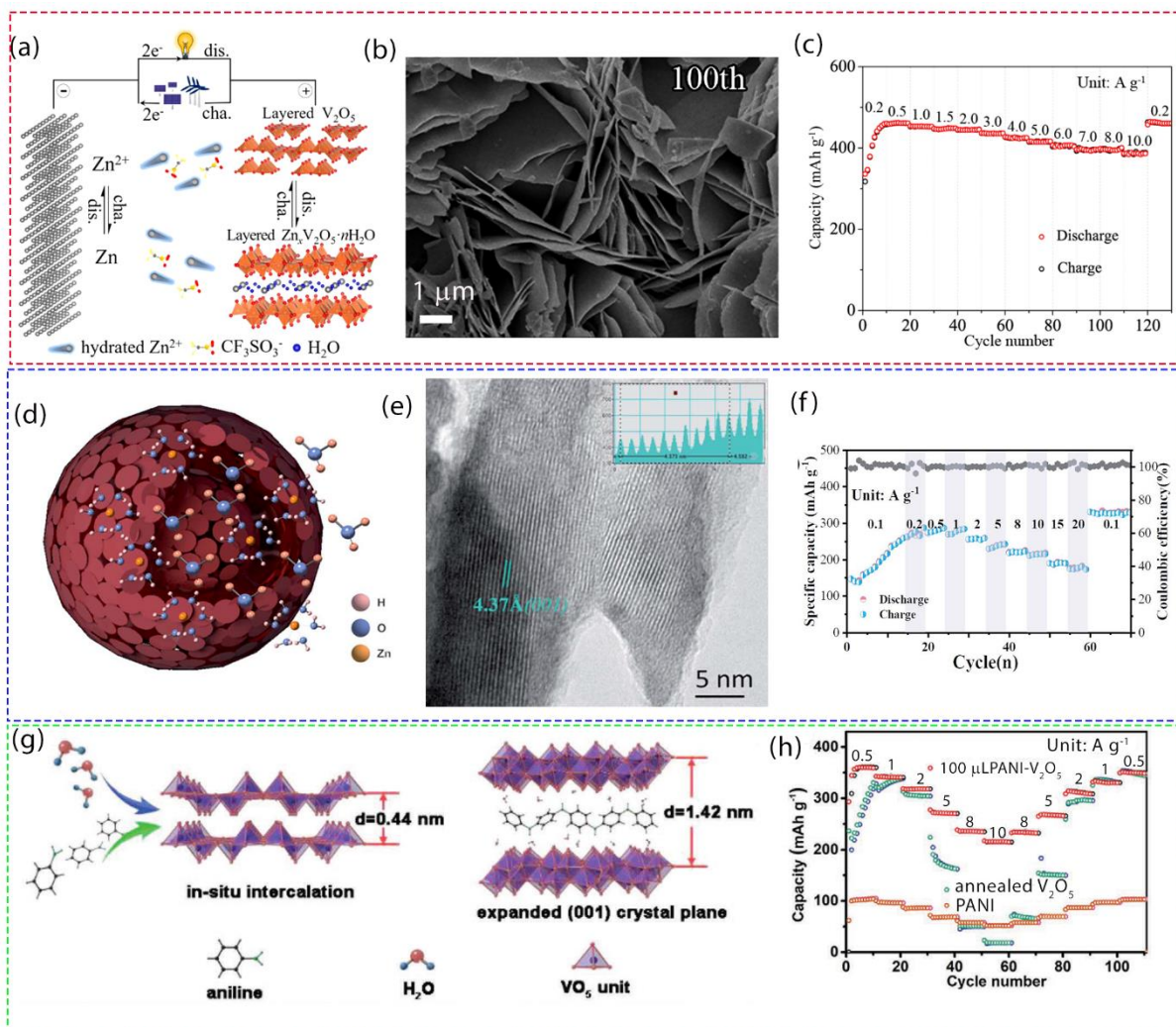
Figure 4. a) Schematic illustration of a Zn/V_2O_5 battery chemistry including crystal structures of layered V_2O_5 and $Zn_xV_2O_5.nH_2O$. b) SEM image of V_2O_5-graphite cathode after 100 cycles. c) Rate capability of V_2O_5-graphite cathode. d) Schematic of V_2O_5 yolk-shell microspheres. e) high resolution TEM image of V_2O_5 yolk-shell microsphere showing an interlayer spacing of 4.37 Å. f) Rate capability of V_2O_5 yolk-shell microspheres. g) Schematic illustration of Zn^{2+} (de)intercalation in PANI-V_2O_5 cathode material. h) Rate capability of PANI-V_2O_5 cathode. a-c) Reproduced with permission.[3] Copyright 2018, American Chemical Society. d-f) Reproduced with permission.[1] Copyright 2020, Royal Society of Chemistry. g-h) Reproduced with permission.[4] Copyright 2020, Wiley.

In addition to hydro/solvothermal approaches, electrospinning techniques have been used to prepare porous V_2O_5 nanofibers (**Figure 5a**).[5] However, the reversible capacity of the material was only 166 mAh g^{-1} at a C-rate of 2 C (1 C = 294 mA g^{-1}), which is comparatively low compared to V_2O_5 materials synthesized *via* hydrothermal techniques (**Figure 5b**). Interestingly, authors observed the transformation of V_2O_5 to zinc pyrovanadate (ZVO) during the first discharge. ZVO has a layered structure comprising of ZnO_6 octahedral layers, and functions as the reversible active material in subsequent cycles (**Figure 5c**).

The materials that were further enhanced beyond their initial product saw significant impacts on their electrochemical performance, especially those that were developed without the use of binder materials during the cathode assembly process. This can be seen in the data collected by Javed *et al.*[6] who showed that their V_2O_5 nanosheet material grown directly onto the Ti foil substrate (**Figure 5d**) can deliver a reversible capacity of 340 mAh g^{-1} after 700 cycles at a specific current 500 mA g^{-1}. This binder-free approach demonstrated significantly better long-term cycling and rate capability (**Figure 5e**) than their counterparts such as the cathode material proposed by Zhou *et al.*[86] which, despite having the same chemical makeup (V_2O_5) and similar morphologies (nanosheets), performed significantly worse than the binder-free equivalent. Whilst comparing against Javed's own binder included tests, the increased porosity *via* calcination seems to have improved the performance of Zhou's material, but it is still not enough to overcome the impediment of containing binder materials. The idea behind binder-free cathodes is to remove the binding agent in the slurry as it makes up a large amount of 'dead-weight' that contributes greatly to the mass loading, but not to the electrochemical performance, causing the specific capacity of the material to suffer greatly. This approach to cathode material synthesis can not only increase the flexibility of the electrode but also to some extent address the issue of vanadium compounds' sluggish intercalation kinetics which has plagued the material.
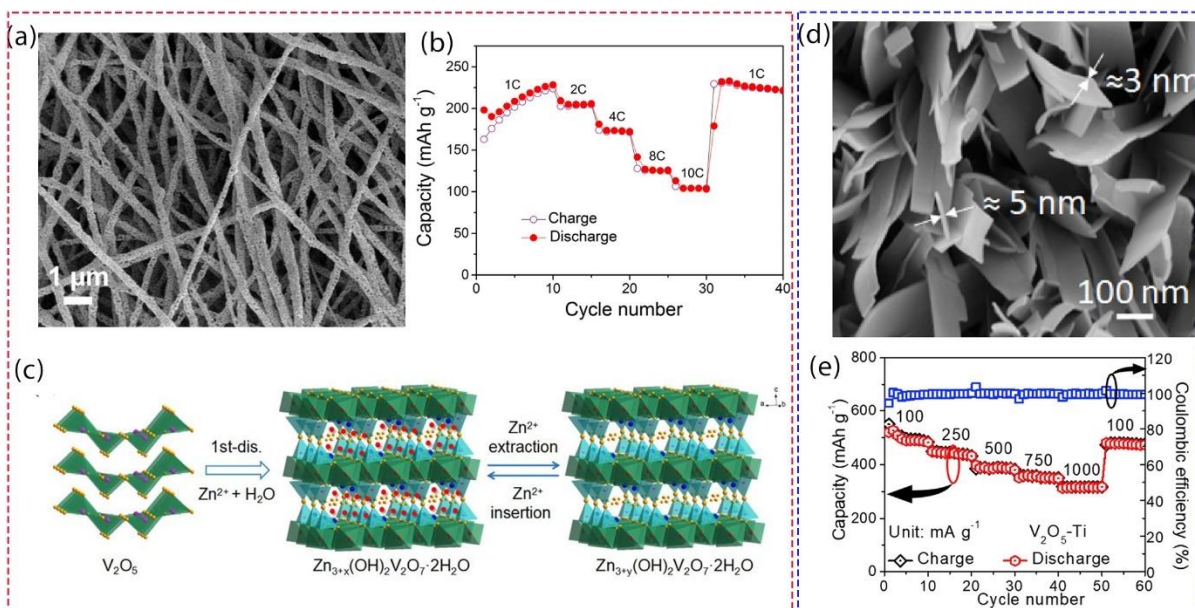
Figure 5. a) SEM image of V_2O_5 nanofibers. b) Rate capability of V_2O_5 nanofibers. c) Schematic illustration of Zn^{2+} ions storage mechanism in V_2O_5 nanofibers. d) SEM image of V_2O_5-Ti nanosheets. e) Rate capability of V_2O_5-Ti nanosheets. a-c) Reproduced with permission.[5] Copyright 2019, Elsevier. d-e) Reproduced with permission.[6] Copyright 2020, Elsevier.

2.3.1.2 V_2O_3

V_2O_3 type materials with both cubic and hexagonal crystal structures have been reported as cathodes for ZIBs.[7, 8] As noted in our previous works, cubic phase V_2O_3 is air/moisture sensitive and undergoes a slow oxidation to a hydrated vanadium oxide form.[43] A similar transformation was observed by Luo *et al.* when V_2O_3 microcubes (**Figure 6a**) were applied as a cathode material in aqueous ZIBs. V_2O_3 material was obtained by calcination of a hydrothermally synthesised vanadium-MOF.[7] Notably, non-layered cubic phase V_2O_3 oxidized to a layered hydrated vanadium oxide ($V_2O_{5-x} \cdot nH_2O$) during the first charging of the battery (**Figure 6c**). The newly formed layered structure functions as the active material in subsequent cycles. The electrochemically transformed V_2O_3 material displayed excellent rate capability (**Figure 6b**) and a high capacity of 547 mAh g^{-1} at 5 A g^{-1} after 1000 cycles. The superior rate

capability was attributed to the high proportion of surface controlled capacitive charge storage in the material (~ 91% at a scan rate of 1.5 mV s^{-1}).

Intriguingly, V_2O_3 materials with rhombohedral crystal structure are stable in aqueous electrolytes and do not undergo structural alterations. Rhombohedral V_2O_3 has a tunnel-like structure composed of VO_6 octahedrons, where these tunnels offer a room for Zn^{2+} (de)intercalation (**Figure 6d**). V_2O_3 type cathode material prepared by Ding *et al.* is a key example for this observation.[8] Although obtained *via* the pyrolysis of a vanadium-MOF akin to the work of Luo *et al.*, the use of a different V-precursor for the preparation of V-MOF led to a rhombohedral structured V_2O_3. This material displayed a porous spherical morphology, which was deemed favourable for (de)insertion of Zn^{2+} ions. It should be noted here (as later discussed) that pyrolysis of V-MOFs promotes the *in situ* formation of carbon frameworks over the V_2O_3 particles which can greatly enhance the conductivity. This material displayed a capacity of ~180 mAh g^{-1} at 5 A g^{-1} after 4000 cycles, and the rate capability was satisfactory (**Figure 6e**), however not as impressive as for the cubic V_2O_3 materials discussed before. The likely reason could be the structural rigidity of rhombohedral V_2O_3 resisting the transformation to a large spaced layered structure during Zn^{2+} (de)intercalation, as opposed to cubic-V_2O_3 particles.
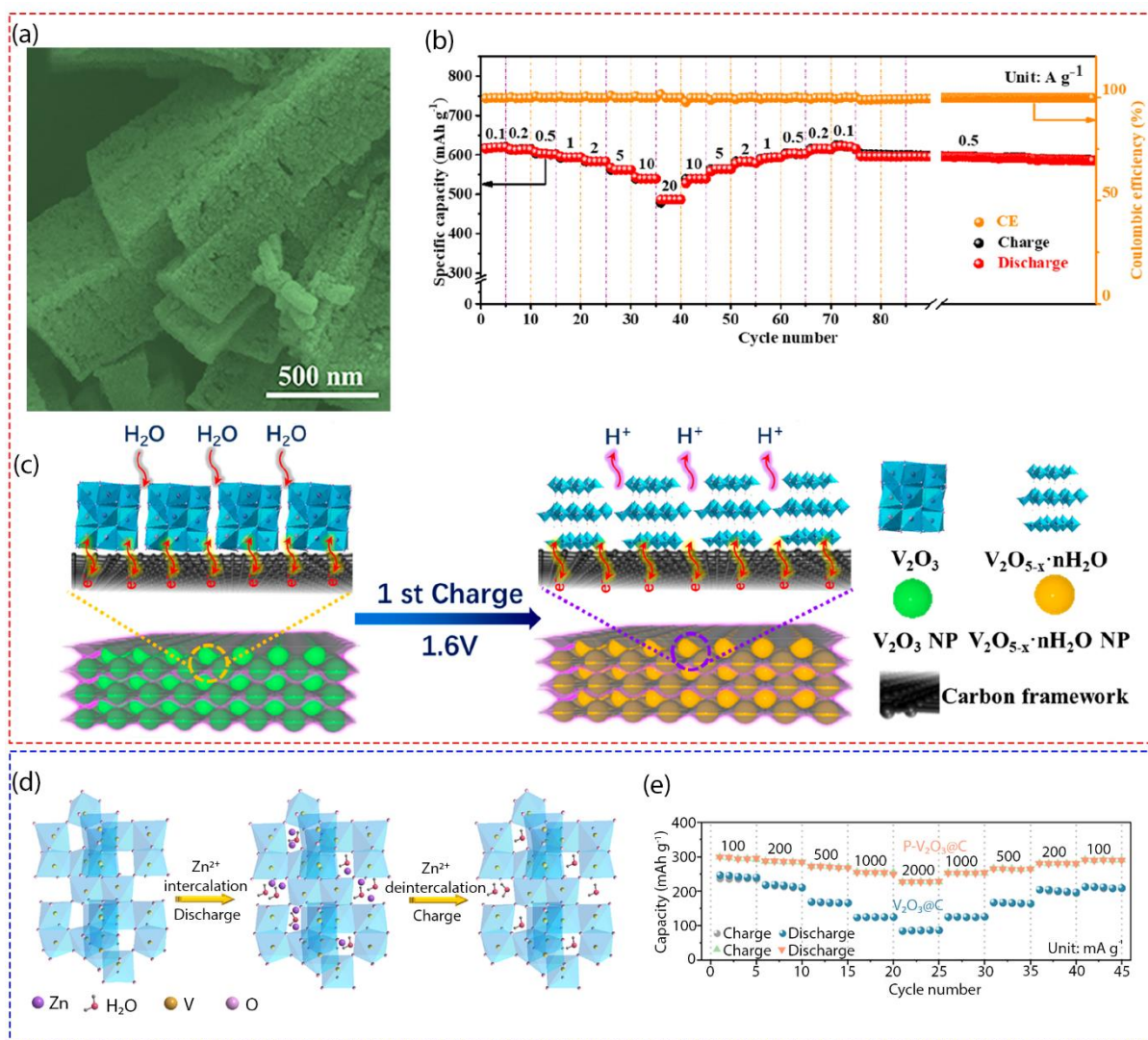
Figure 6. a) SEM image of carbon-coated V_2O_3 microcubes. b) Rate capability of C-V_2O_3 microcubes. c) Schematic illustration of oxidation of V_2O_3 to a layered hydrated vanadium oxide during the first charging. d) Schematic illustration of crystal structure and Zn^{2+} (de)intercalation mechanism in rhombohedral V_2O_3 material. e) Rate capability of carbon coated porous V_2O_3 particles (P-V_2O_3@C). a-c) Reproduced with permission.[7] Copyright 2020, American Chemical Society. d-e) Reproduced with permission.[8] Copyright 2019, American Chemical Society.

2.3.1.3 VO₂

Vanadium (IV) oxide (VO_2) has been frequently applied as a cathode material in ZIBs.[9, 11, 12, 48, 79, 88] Most of the materials were synthesized through either hydrothermal or

solvothermal techniques. VO_2 materials reported for ZIBs are most commonly in the monoclinic crystal structure,[9, 48, 79, 88], however, rutile and tetragonal structures are also characteristic of VO_2,[89] and on rare cases nsutite-type hexagonal phase is also reported.[12] VO_2 has a tunnel-like structure composed of VO_6 octahedra analogous to the rhombohedral-V_2O_3 discussed previously. Zinc storage in VO_2 is enabled by these tunnels, where fast reversible (de)intercalation of Zn^{2+} ions takes place (**Figure 7a**).[9] As discussed below, there is a disagreement in literature whether the crystal structure parameters (such as distance between *(001)* planes) increase or decrease upon insertion of Zn^{2+} ions into the monoclinic VO_2 materials. Chen *et al.* reported a hydrothermally synthesized nanorod-type VO_2 material (**Figure 7b**) with moderate electrochemical performance in $ZnSO_4$ electrolyte (~100 mAh g^{-1} at 3.0 A g^{-1} after 5000 cycles).[10] By means of *in situ* XRD measurements they observed an increase in the distance between *(002)* planes upon Zn^{2+} insertion, and an increase in all three lattice parameters resulting a unit cell volume expansion of 6.69 % (**Figure 7c**). *In situ* XRD also confirmed that Zn^{2+} (de)insertion process is completely reversible, however, there was no mention of the deposition of zinc sulfate hydroxides on the cathode surface. In a separate study, Li *et al.* critically analysed the Zn^{2+} storage mechanism of VO_2 nanorods in $ZnSO_4$ electrolyte.[11] The rate capability (**Figure 7d**) and overall electrochemical performance of these nanorods were marginally better compared to the latter. Based on *in situ* XRD analysis, Zn^{2+} ions were stored *via* reversible deposition of $Zn_4(OH)_6SO_4 \cdot 5H_2O$ on the cathode surface, and simultaneous (de)insertion of protons (H$^+$) into the VO_2 structure (**Figure 7e**). Such a mechanism is not expected for electrolytes such as $Zn(CF_3SO_3)_2$, owing to the ability of $[CF_3SO_3]^-$ anions to form a large solvation shell around Zn^{2+}, which can block the access for H_2O molecules. However, when conductive PEDOT-doped VO_2 nanobelts (VO_2-PEDOT) were applied as a cathode in ZIBs there was a clear evidence for the reversible formation/decomposition of $[CF_3SO_3]^-$-based layered double hydroxide ($Zn_m(OTf)_n(OH)_{2m-}$

$_n$.xH$_2$O),[79] indicating the (de)insertion of both Zn^{2+} and protons. It was noted that without the assistance of a conductive substrate, the cathode suffered greatly and thus was incorporated with 20% carbon nanotubes. Moreover, as opposed to observations by Chen *et al*. VO$_2$-PEDOT showed a decrease in *(001)* interplanar distance (or a diminish in *c*-value) upon Zn^{2+} insertion, which was attributed to the electrostatic attraction between layers induced by Zn^{2+} ions. Such divergences in observations for the VO$_2$ materials (with identical crystal structure) highlight the significant effects of synthetic methods, dopants, and the nature of electrolyte pose on the charge storage mechanism. In another notable work, Li *et al.* developed a modified solvothermal method (repeated phase transition approach) to prepare oxygen vacancy rich VO$_2$ materials (V$_O^{..}$-VO$_2$).[48] It was deemed that that V$_O^{..}$ can produce large tunnel cavities along *b-axis* enabling efficient Zn^{2+} (de)intercalation. V$_O^{..}$-VO$_2$ displayed a specific capacity of 175 mAh g^{-1} at 5 A g^{-1} after 2000 cycles.

Discussed VO$_2$ materials (nanobelts, nanofibers and nanorods) possessed a monoclinic crystal structure. In contrast, hydrothermally prepared coin-like VO$_2$ nanoplates had a nsutite-type hexagonal crystal structure (**Figure 7f**).[12] In Zn(CF$_3$SO$_3$)$_2$ electrolyte this material displayed reasonably good rate capability (**Figure 7g**) and a specific capacity of ~ 150 mAh g^{-1} at 3 A g^{-1} after 1200 cycles. **Figure 7h** displays a schematic image of Zn^{2+} ions insertion into the tunnel structure of coin-like VO$_2$ nanoplates. Interestingly, *ex situ* XRD measurements confirmed the reversible formation and decomposition of Zn$_x$(OTf)$_y$(OH)$_{2x-y}$.nH$_2$O similar to the observations in Liu *et al.*'s study.[79]
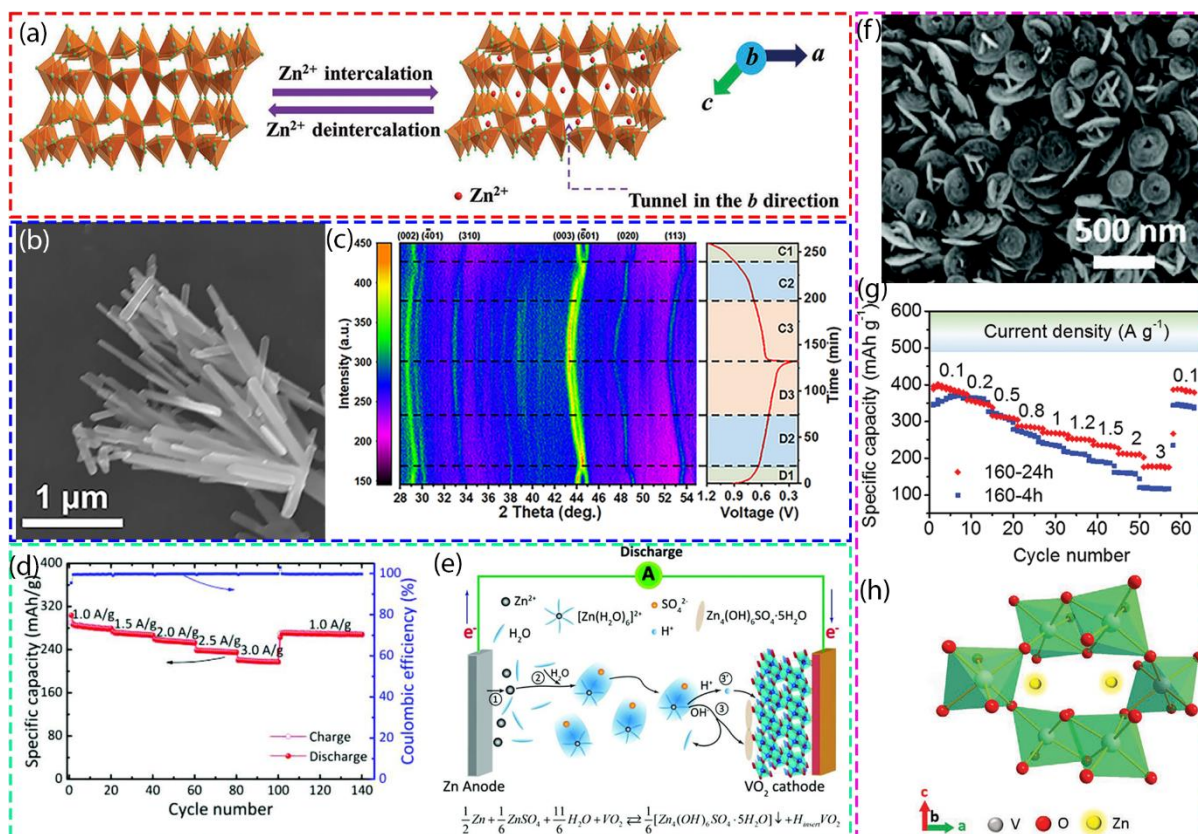
Figure 7. a) Schematic illustration showing Zn^{2+} (de)intercalation in tunnel-like framework of VO_2 crystal structure. b) SEM image of VO_2 nanorods. c) 2D *in situ* XRD pattern collected during the first cycle at 0.1 A g^{-1} for VO_2 nanorods-based cathode. d) Rate capability of VO_2. e) Schematic representation of the working principal of Zn/VO_2 battery, highlighting $Zn_4(OH)_6SO_4 \cdot 5H_2O$ deposition and H^+ insertion. f) SEM image of coin-shaped VO_2 nanoplates. g) Rate capability of coin-shaped VO_2. h) Schematic image of Zn^{2+} ions insertion into the tunnel structure of coin-like VO_2 nanoplates. a) Reproduced with permission.[9] Copyright 2019, Wiley. b-c) Reproduced with permission.[10] Copyright 2019, American Chemical Society. d-e) Reproduced with permission.[11] Copyright 2019, Wiley. f-h) Reproduced with permission.[12] Copyright 2020, Wiley.

V_6O_{13} is another oxide of vanadium that has displayed promising electrochemical performance as a cathode material in ZIBs.[13, 14, 90-93] V_6O_{13} is a mixed valence state oxide of

V^{4+} and V^{5+} which typically crystalizes in the monoclinic crystal system. It has a tunnel-like structure, however unlike other vanadium oxides, V_6O_{13} is composed of alternating single and double VO_6 octahedral layers joined by edge sharing O atoms as depicted in **Figure 8a**. There are four cavities per unit cell that can facilitate reversible Zn^{2+} (de)insertion. Tamilselvan *et al.* report on V_6O_{13} nanobelts directly grown on carbon cloth substrates, which were directly applied in ZIBs without the addition of any binders.[90] This binder free cathode showed satisfactory rate capability and delivered a reversible capacity of 268 mAh g^{-1} at 4.5 A g^{-1} after 50 cycles. As in the case of VO_2-based materials, integrating O vacancies into the V_6O_{13} could improve the charge transfer kinetics, reversibility and the Zn^{2+} storage capability.[13, 14] For instance, carbon integrated nanoscroll-like O-deficient V_6O_{13} ($V_6O_{13-\delta}$@C or DVOC) material (**Figure 8b**) prepared by Lin *et al*. displayed an impressive capacity of ~ 300 mAh g^{-1} at 10 A g^{-1} after 2000 cycles.[13] Moreover, $V_6O_{13-\delta}$@C clearly out-performed well-crystallized V_6O_{13} (RF) as depicted in **Figure 8c**. In a similar work, Liao *et al*. evaluated the Zn^{2+} storage mechanism in O-deficient textile-like V_6O_{13} material.[14] It was found that O-deficient V_6O_{13} can provide extra entry points for Zn^{2+} ions along the *c*-axis, compared to only *a* and *b* -axes routes in pristine V_6O_{13} materials as schematically depicted in **Figure 8d-e**. The superior rate capability of O-deficient V_6O_{13} over pristine V_6O_{13} is evident in **Figure 8f**. Hence, O-vacancies can improve the overall electrochemical performance of V_6O_{13}-based materials. Lin *et al*. proposed that incorporation of small molecules such as CO_2 could improve the electrochemical performance of V_6O_{13} materials.[91] Based on theoretical simulations and experimental work they found that CO_2 molecules can lower the energy barrier for Zn^{2+} diffusion across channels within the V_6O_{13} structure, enabling faster kinetics and high capacity. Integration of metal ions (e.g., Mn), and carbon and nitrogen-containing scaffolds are other methods that have been used to enhance the electrochemical performance of V_6O_{13}-based ZIB cathodes.[92, 93]
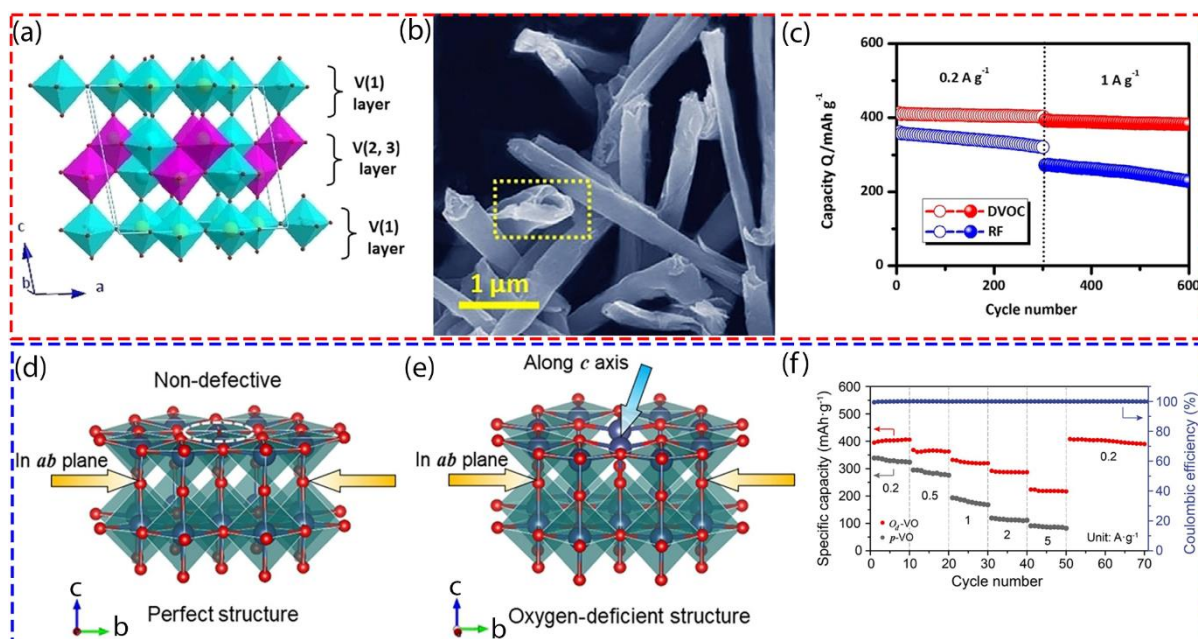
Figure 8. a) Schematic view of a tunnel-like V_6O_{13} crystal structure. b) SEM image of O-deficient nano scroll-like V_6O_{13} material ($V_6O_{13-\delta}$@C or DVOC). c) Comparison of ZIB performance of DVOC and well crystallized V_6O_{13} (RF). d-e) Schematic illustrations showing Zn^{2+} ions access points in well crystalized and oxygen-deficient V_6O_{13} crystal structures. f) Comparison of rate capability of O-deficient V_6O_{13} and pristine V_6O_{13}. a-c) Reproduced with permission.[13] Copyright 2020, Wiley. d-f) Reproduced with permission.[14] Copyright 2019, Wiley.

As discussed in section 3.1, vanadium oxide materials are capable of having many interesting and intricate morphologies. However, these do not always result in the best functionality as a battery cathode. In fact, many of the noted materials with unusual designs did not perform any better than the battery cells containing cathodes of commercial V_2O_5-based materials.[3]

2.3.2 Vanadium oxide hydrates and metal ion integrated vanadates

Most vanadium-containing cathodes do not solely consist of vanadium oxides as they have been specifically modified to combat the bottlenecks that the original material is likely to encounter. There are several methods of improving the effectiveness of the material, mostly

involving the introduction of new species into the structure. And as such, it has almost become common practice to integrate performance enhancing molecules into the complex.[23] With the occasionally outlier, almost all vanadate materials have been prepared *via* a hydrothermal method. Not only is this highly cost effective, but its facile nature allows for easy integration of additional components.

It can be noted that unlike the prior vanadium oxide sub-categories, the variation in morphologies exhibited by vanadates is extremely limited and is almost entirely comprised of nanorods, fibres, belts and other common, similarly shaped structures. One of the most notable morphologies is that prepared by Li *et al*.[68] who manipulated simple nanoribbons into an urchin-like micro-morphology. A sound hypothesis for the lack of deviation from this traditional long and thin morphology is that due to the added complexity of the material (due to the intercalated molecules) it may simply not be possible to force the compound into different shapes. This is due to the rigidity and strength of bonds within the structure. It could also be assumed that the common morphology is due to a lack of post-production treatment such as calcination, heat treatment and freeze-drying, at risk of removing or in any way interfering with the intercalated species.

2.3.2.1. Hydration

A major variable that determines the materials' intercalation capabilities is the interlayer spacing within the structure. This spacing can be increased through the integration of structural molecules between the bi-layers that will not react with the host structure.[47] The most common molecule used for this purpose is water. This doping not only changes the interlayer spacing but also the interlayer force and the material's structural strength,[15, 49] causing vast improvements to properties such as cycle life and reversibility. Cathode materials are also able to use structural water molecules to create a barrier of hydroxyl and/or water molecules over the host material surface,[68] reducing the electrostatic interactions between zinc ions and the cathode material.[15] This in turn increases the ion movement and intercalation speed,

enhancing many aspects of the battery's electrochemical performance including specific capacity, energy density and power density.[49] It also serves to reduce the activation energy of interactions at the cathode-electrolyte interface, allowing for smoother introduction of ions into the cathode from the electrolyte.[68]

A few different forms of hydrated vanadium oxides (HVOs) or gels are reported in literature as cathodes for ZIBs, most commonly $V_2O_5.nH_2O$, $V_5O_{12}.nH_2O$ and $V_{10}O_{24}.nH_2O$-based materials.[15, 32, 49, 77] The number of water molecules *per* formula unit of HVO can be tuned *via* controlled heating of the materials. It should be recalled here that even pristine vanadium oxides (*i.e.*, V_2O_5, V_2O_3) discussed in section 3.1 could transform to hydrated layered structures during the operation of ZIB in aqueous electrolytes. This process is often termed as an *in situ* electrochemical activation and manifested as a capacity increase in GCD profiles (**Figure 5b**). All HVO materials tend to show a low angle peak (~6 °2θ) in XRD patterns, denoting a large interlayer spacing between *(001)* or *(002)* planes. The interlayer spacing range from 11 – 14 Å and depends on the number of water molecules *per* formula unit of HVO. Typically, HVO compounds are in monoclinic crystal system and each layer is composed of edge-sharing VO_5 pyramids and VO_6 octahedra as depicted in **Figure 9a**. Moreover, HVOs are mixed valence compounds of V^{4+} and V^{5+} although often written as $V_2O_5.nH_2O$.[15, 32, 53] It is quite common to combine HVOs with carbon frameworks like graphene and/or carbon nanotubes to enhance the conductivity of materials.[49, 53, 77] Zhang *et al.* synthesised free-standing $V_5O_{12}\cdot 6H_2O$ materials utilizing a simple electrodeposition technique (**Figure 9b**).[15] This material displayed excellent rate capability and a stable reversible capacity of ~ 300 mAh g^{-1} at 2 A g^{-1} after 1000 cycles (**Figure 9c**). Due to the structural enhancement of the material *via* hydration, the intercalated ions can enter and exit the material without damaging the integrity of the cathode. This allows for long-term stability and cycle-life in addition to the increase of reversibility from the water molecules' lubricating effect. This is

clearly demonstrated in the $V_2O_5 \cdot nH_2O$/graphene (VOG) composite cathode materials prepared by Yan *et al.* The compound without hydrations (VOG-350 – note: compound without hydrations was obtained by annealing the sample at 350 °C) promptly fails under the strain of higher current rates reaching only 78 mAh g^{-1} after 50 cycles at 6 A g^{-1}. Conversely, VOG (hydrated form) has the effect of the H_2O pillaring to maintain its structural stability and delivered ~200 mAh g^{-1} after 900 cycles at 6 A g^{-1}.[49]
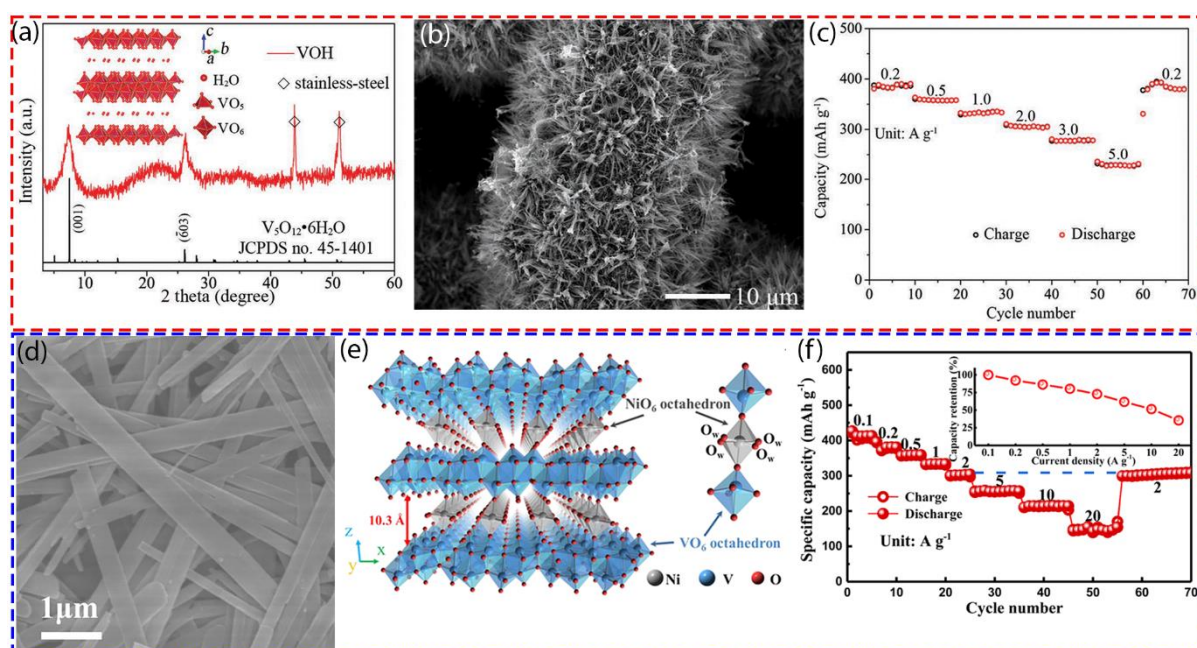
Figure 9. a) XRD pattern and crystal structure of $V_5O_{12} \cdot 6H_2O$ material. b) SEM image of freestanding $V_5O_{12} \cdot 6H_2O$ material. c) Rate capability of $V_5O_{12} \cdot 6H_2O$ cathode. d) SEM image of $Ni_{0.25}V_2O_5 \cdot 0.88H_2O$ (NiVO) nanobelts. e) Schematic illustration showing crystal structure of NiVO material. f) Rate capability of NiVO cathode. a-c) Reproduced with permission.[15] Copyright 2019, Wiley. d-f) Reproduced with permission.[16] Copyright 2020, American Chemical Society.

2.3.2.2. Metal cations

Integration of metal cations is another widely applied approach to enhance the electrochemical cycling performance of vanadium oxide-based cathode materials. Metal ions not only work as pillars to stabilize the layered structure but also act as dopants to improve the

ion diffusion kinetics.[19] Despite there being many possible structural cations available,[41] the integration of cations with larger radii is more commonly undergone to further increase the interlayer spacing[94]. It is considered that transition metal ions for structural additives are superior to the alternatives such as alkali/ alkali-earth metals, and non-metals, as they can exhibit catalytic effect on the redox reaction rather than being a purely physical assistance.[32, 95]

In most cases metal ions are integrated into HVOs, to synergistically combine with useful structural features of inter-layer H_2O molecules.[96-98] Characteristically, these vanadates have a layered structure where V-O layers are bridged by metal cations within the inter layer spacing. However though, atomic structures of metal vanadates are more complex compared to pristine vanadium oxides and HVOs. Metal vanadates are formed in various crystal systems (such as triclinic, orthorhombic, monoclinic etc.) depending on the kind of metal ion used and the synthetic approach.[19, 80, 96-99] As seen in Table 1, many metal vanadates have been tested as cathode materials in ZIBs to date. Despite slight variations in the atomic structure the operation and charge storage mechanisms of most vanadate-based cathodes appear to be related. Hence, a selected set of model compounds were taken as examples for the discussions below.

Kundu *et al.* proposed Zn^{2+} ions and H_2O integrated vanadium oxide ($Zn_{0.25}V_2O_5 \cdot nH_2O$) nanobelts as a high performance cathode material for ZIB.[96] This compound formed in the triclinic crystal system where double-sheet V_2O_5 layers were composed of VO_6, VO_5 and VO_4 polyhedra. V_2O_5 double sheets were bridged together by ZnO_6 octahedral pillars. Insertion of H_2O molecules from the electrolyte can further expand the inter-layer spacing (12.9 Å) making room for additional Zn^{2+} storage. This material displayed exceptional rate capability and a reversible capacity of 208 mAh g^{-1} at 2.4 A g^{-1} after 1000 cycles. *In situ* XRD measurements found that interlayer distance between *(00l)* planes contracts upon Zn^{2+} ions insertion, which was attributed to shielding of electrostatic repulsion by Zn^{2+} ions and the ejection of H_2O

molecules. This process was found to be reversible, hence Zn^{2+} ions and H_2O molecules play a key role by providing structural stability and flexibility. In a related study, Feng *et al.* reported 'structure-evolving' $Ni_{0.25}V_2O_5 \cdot 0.88H_2O$ (NiVO) nanobelts (**Figure 9d**) as high-performance cathode materials for ZIBs in $Zn(CF_3SO_3)_2$ electrolyte.[16] NiVO material was formed in monoclinic crystal system where edge-sharing bilayer VO_6 octahedrons were joined by NiO_6 octahedrons as depicted in **Figure 9e.** Each NiO_6 octahedron was also bound to four structural water units. This material displayed excellent rate capability (**Figure 9f**) and an impressive long term cycling capability (226 mAh g^{-1} at 10 A g^{-1} after 10000 cycles). *In situ* XRD measurements saw the contraction of *(00l)* interlayer spacing upon Zn^{2+} insertion, akin to $Zn_{0.25}V_2O_5 \cdot nH_2O$ materials discussed before. NiVO transformed through a reversible monoclinic phase during (de)intercalation of Zn^{2+} and water molecules. Additionally, they observed the deposition of $Zn_x(OTf)_y(OH)_{2x-y} \cdot nH_2O$ on the electrode surface, as has been observed in other ZIB systems utilizing the $Zn(CF_3SO_3)_2$ aqueous electrolyte. At high rates, NiVO nanobelts transformed to hierarchal sheet like structures with more active sites and short diffusion paths further improving the cycling stability.

Another notable work is that by Liu *et al*.,[99] where CuV_2O_6 was reported as a high performance cathode material for ZIB. CuV_2O_6 had triclinic crystalline structure where edge sharing VO_6 octahedral layers were separated/connected by CuO_6 octahedrons. This material when coupled to graphene oxide, displayed very good rate performance and a reversible capacity of close to 300 mAh g^{-1} at 5 A g^{-1} after 3000 cycles. Interestingly, *ex situ* XRD and XPS measurements showed that Zn storage in CuV_2O_6 material is based on a displacement reaction between zinc and copper, involving reversible reduction/oxidation of $Cu^{2+}(aq)/Cu(s)$ during Zn^{2+} (de)insertion process. Since, Cu^{2+} ions are replaced by Zn^{2+} the structural integrity of cathode material was maintained. Moreover, the presence of Cu metal within the system can significantly enhance the host material electrical conductivity and subsequent redox reactions.

Researches by Liu *et al*. and Li *et al*. enlighten the importance of choosing the correct metal ions for incorporation in HVOs.[98, 100] It can be seen from the results obtained by Li *et al*. that despite the smaller inter layer spacing, the superior ion diffusion properties of $Ni_{0.25}V_2O_5 \cdot nH_2O$ encourage deeper intercalation of the Zn^{2+} ions and thus noticeably enhance the cathodes' capacity with $Ni_{0.25}V_2O_5 \cdot nH_2O$ achieving 218 mAh g^{-1} after 1200 cycles at 5 A g^{-1} compared to $Co_{0.25}V_2O_5 \cdot nH_2O$ displaying only 144.4 mAh g^{-1} after 500 cycles at 5 A g^{-1}. An additional comparison between Cu^{2+} and Mg^{2+} (intercalated vanadium oxides) by Liu *et al*. allows an insight into the beneficial effects of transition metal ions over alkaline-earth metal ion dopants.[100] Cu^{2+} integrated HVO yielded nearly 10 % more capacity compared to the Mg^{2+} doped equivalent at a current of 0.5 A g^{-1} which was attributed to the catalytic redox properties of Cu^{2+} ions.

2.3.2.3. Non-metal cations

As well as metal ion integration, non-metal cations, such as NH_4^+, have gained much traction in recent studies due to their large ionic radius being more practical to expand the inter layer spacing of vanadium oxides.[32, 95, 101] Moreover, NH_4^+ can form hydrogen bonds between VO layers to improve the structural stability, effectively acting as "pillars" within the framework. In a notable work, Zhao *et al*. explored $(NH_4)_{0.58}V_2O_5 \cdot 0.98H_2O$ nanobelts as a cathode material in ZIBs.[95] This material had a monoclinic crystal structure, where the framework was constructed by edge and corner sharing VO_6 octahedral units. NH_4^+ ions were incorporated along the *c-axis* of the crystal structure (like the structural framework of $Ni_{0.25}V_2O_5 \cdot 0.88H_2O$) resulting an interplanar distance of 10.9 Å. This material delivered a reversible capacity of 137 mAh g^{-1} at 2000 mA g^{-1} after 400 cycles. *In operando* synchrotron measurements revealed that hydrated $[Zn(H_2O)_6]^{2+}$ is intercalated at the high potential region (1.4 – 0.85 V), followed by Zn^{2+} ions at the low potential region (0.85 – 0.4 V) leading to reversible solid solution reactions and two-phase transitions of the cathode material during

(dis)charge of the battery. Although non-metal components are lighter in weight, metal ion/HVO compounds tend to outperform non-metal ion/HVO compounds in terms of both energy density and rate capability, possibly owing to the added benefit of faster ionic conductivity.

2.3.3 Vanadium phosphates

Due to the strong inductive effect of $(PO_4)^-$ anion, vanadium phosphates often have a greater output voltage than other vanadium-based materials.[102] Alongside the PO_4 tetrahedral units, vanadium phosphates are composed of strongly bound VO_6 octahedral units. The combination of both frameworks results in a structurally durable, open framework compound that performs better than other materials under the mechanical strain of Zn^{2+} ion (de)intercalation. However, vanadium phosphates have low conductivity since VO_6 octahedral units are kept apart by $(PO_4)^-$ anions.[41] Hence, it is quite routine to incorporate carbon additives into vanadium phosphate-based cathode materials to enhance conductivity.[17, 18]

Li *et al.* employed a NASICON-structured $Na_3V_2(PO_4)_3$ (NVP) to host Na^+ ions, as the atomic radius of Na^+ exceeds that of Zn^{2+}, creating wider pathways. This in turn greatly improved the materials ability to transfer and host intercalating Zn^{2+} ions. The material was then wrapped in graphene-like nanosheets to amend the cathodes low electroconductivity.[17] NVP had a rhombohedral crystal structure composed of PO_4 tetrahedral and VO_6 octahedral units. The ideal structure for Zn^{2+} (de) intercalation is obtained by the extraction of 2 Na^+ ions from the parent material (this can be achieved by initial charging of the material to upper cut-off potential). The desodiated $NaV_2(PO_4)_3$ has a large open framework to accommodate reversible Zn^{2+} (de)intercalation (**Figure 10a**). However, this material was able to deliver only 72 mAh g^{-1} at 50 mAh g^{-1} after 100 cycles *i.e.*, poor electrochemical performance as opposed to vanadium oxides and vanadates. Vanadium fluoro phosphates, due to their inherently durable structure, are expected to show excellent cycling life and stability, notably the $Na_3V_2(PO_4)_2O_{1.6}F_{1.4}$ (NVPOF) material (**Figure 10b**) reported by Ni *et al*. could be

mentioned.[18] This material had a tetragonal crystal structure, composed of VO_5F octahedral and PO_4 tetrahedral units (**Figure 10c**). As in the case of NVP it is necessary to activate the material by extraction of 2 Na^+ ions by an initial charging to upper cut-off voltage. NVPOF delivered a reversible capacity of 139 mAh g^{-1} at 500 mA g^{-1} after 2000 cycles in a water-in-bi-salts electrolyte system (25 m $ZnCl_2$ + 5 m NH_4Cl) (**Figure 10d**). Thus, electrochemical performance of vanadium phosphates is vastly surpassed by cathodes of vanadium-oxide and vanadate materials. This is likely because of the difficulty to stretch the structures' intercalation channels to a width at which the transfer kinetics is not affected by Zn^{2+} ions (of extremely high charge energy) and thus the resulting electrostatic interactions. Hence, the materials are often utilized in Na-ion battery systems where the intercalating ions, despite having a slightly larger radius, have significantly lower charge energies and are able to move through the space provided by the structural Na^+ cations without difficulty.[41]
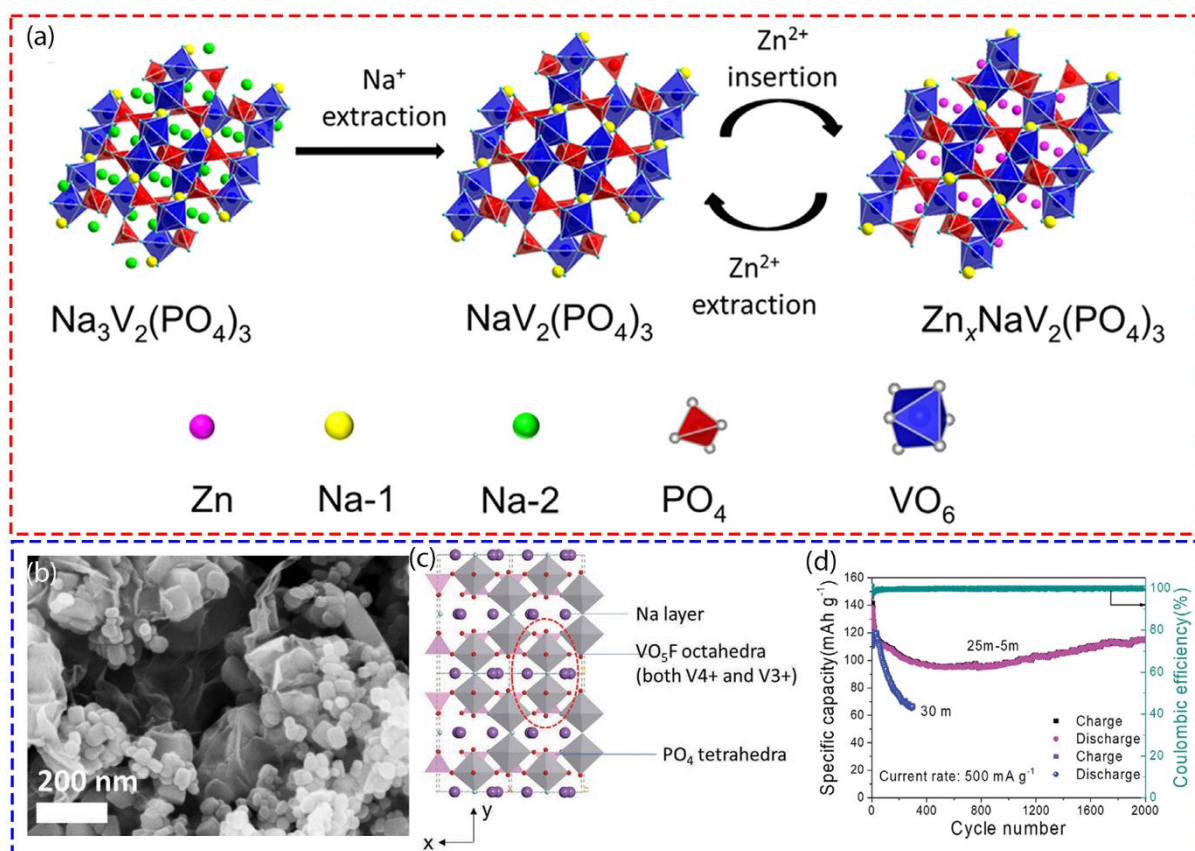
Figure 10. a) Schematic representation showing Na^+ extraction from $Na_3V_2(PO_4)_3$ crystal structure on 1st charge and subsequent Zn^{2+} (de)insertion during cycling. b) SEM image of $Na_3V_2(PO_4)_2O_{1.6}F_{1.4}$ (NVPOF) material. c) Schematic view displaying the crystal structure of NVPOF. d) Long-term cycling performance of NVPOF cathode in 25 m $ZnCl_2$ + 5 m NH_4Cl (water-in-bi-salts) electrolyte. a) Reproduced with permission.[17] Copyright 2016, Elsevier. b-d) Reproduced with permission.[18] Copyright 2020, Wiley.

It is also noted that due to the rigid structure of the base material, most vanadium phosphate compounds have been shown to display a nanoparticle architecture rather than the simple yet effective nanostructures of other vanadium-based cathodes, such as nanorods and nanosheets. By having limited morphological features, vanadium phosphates are unable to optimise the architecture for short ion diffusion paths and high electrode-electrolyte interface area. Between this and the limited intercalation pathway radius, the material at its current stage of development is incapable of reaching high capacities even at lower current rates.

2.3.4 Oxygen-free Vanadium-based Compounds

While vanadium oxides and vanadates are the most commonly used of the vanadium family, recent research has delved further into oxygen free V-based composites, primarily vanadium-based dichalcogenides, such as VS_4, VS_2, V_3S_4 and VSe_2 as the cathode material in ZIBs.[73, 83, 103, 104]

Owing to the layered structure of vanadium disulfide (VS_2) reminiscent of graphite,[71] He *et al*. prepared and applied VS_2 nanosheets as a cathode material in ZIB.[103] Layered VS_2 typically forms in the trigonal crystal system where V atoms in each layer are covalently bonded to 6 sulfur atoms. These layers are held together *via* weak van der Waals forces giving the compound an open structure. The notable distance between each interlayer (5.76 Å) can allow for large intercalation pathways leading to effective ion diffusion. VS_2 nanosheets delivered reasonably good rate performance and a reversible capacity of 110.9 mAh g^{-1} at 0.5

A g^{-1} after 200 cycles. *Ex situ* XRD measurements indicated reversible (de)intercalation of Zn^{2+}, which involved expansion (during intercalation) and contraction (during deintercalation) of the VS$_2$ crystal structure. In a subsequent study, Chen *et al*. managed to improve the Zn^{2+} cycling performance of VS$_2$ nanosheets by combining with reduced graphene oxide (rGO).[50] This material had a considerably large interlayer spacing (9.7 Å) and delivered a reversible capacity of ~168 mAh g^{-1}. The enhanced performance was attributed to the excellent electrical conductivity and the cushioning effect (or limited volume expansions) induced by the rGO component. Vanadium diselenide (VSe$_2$) also has a similar structural framework to VS$_2$. Layered VSe$_2$ material prepared by Wang *et al*. had a large interlayer spacing of 6.1 Å. Electrochemical performance of VSe$_2$ materials is quite comparable to that of VS$_2$, where a reversible capacity of 109 mAh g^{-1} was obtained at 2 A g^{-1} after 800 cycles.

Vanadium tetrasulfide (VS$_4$) in another compound that was applied as a cathode material in ZIBs. Like VS$_2$, VS$_4$ also has a layered structure held together by week van der Waals forces. The interlayer spacing is quite large (~ 5.83 Å) and each layer is composed of V atoms surrounded by four sulfur dimers (S$_2$)$^{2-}$. The charge storage mechanism and the electrochemical performance of VS$_4$ was akin to that of VS$_2$, where a reversible capacity of 110 mAh g^{-1} was achieved after 500 cycles at 2.5 A g^{-1}.[83] In another notable work, Liu *et al*. applied V$_3$S$_4$ nanoparticles anchored on a modified carbon substrate as a cathode material in ZIBs.[104] Again the electrochemical performance was quite comparable to VS$_2$ (102 mAh g^{-1} at 5 A g^{-1} after 1000 cycles).

Almost all oxygen-free compounds face significant complications or are unable to be produced *via* facile methods; and as of yet the area of structural cation/ H$_2$O doping has not yet been explored. However, that is not to say it will not be a viable option in the future for implementation into ZIB cells, as the research of oxygen free-vanadium compounds as a whole is still in the very early stages of development. Despite this, it cannot be neglected to note that

the oxygen-free vanadium-based cathode materials currently implemented into ZIB systems show only a slightly higher average capacity than vanadium phosphates, without the added advantage of long cycling life. It must be seriously considered whether it is of value to continue down this direction of investigation, or seek more viable materials in other, more successful areas.

2.3.5 Carbon Additives

Alternatively, or additionally, in order to increase the materials performance *via* cationic doping, it is also possible to create a composite of a carbonaceous material within the cathode that can have significant improvements on the functionality of the electrode. Such materials include graphene/oxide, carbon nanotubes, carbon fibres, activated carbon and so on.[50, 51] The most basic function of implementing a carbonaceous material to the cathode is the increase the overall electrical conductivity of the component. However, a carbon matrix within the material can also increase the electrochemical performance as it decreases the mechanical strain caused by expansion during ion transfer, as well as decreases aggregation during ion deintercalation.[7, 50, 52] Throughout cycling, the constant intercalation and deintercalation of ions into and out of the cathode material can cause permanent expansion damage to the structure due to the mechanical strain put on the framework. This often results in blocked ion transfer paths, reducing the materials reversibility and cycling stability. The inclusion of a carbon matrix throughout the material has a cushioning effect reducing the strain of constant volumetric expansion as well as increasing the overall strength and integrity of the material framework.[52]

Most of the materials described in sections 3.1 to 3.4 were in fact composed of a carbonaceous component. Beyond the internal doping of carbon throughout the material, increases to conductivity and structural stability have also been demonstrated with coating the base cathode material with a nitrogen-doped carbon[105] or graphene oxide layer, as the later showing up to 30% increase of the cells specific capacity. This occurs as the cathode surface

becomes protected against by-product passivation layers which halter the interfacial mechanisms of the cathode, thus limiting the effectivity of the cell. An example was given by Liu *et al*.[99] The addition of the graphene oxide not only increases the conductivity, but also the overall capacity of the cathode material. Alternatively, carbon content can be implemented into the material as part of the original structure through annealing vanadium MOFs, for example, $V_2O_3@C$, a vanadium (III) compound with carbon integration for increased porosity of tunnel structures and overall electrode conductivity.[8] A MOF-derived synthesis technique proposed by Deng *et al*. has shown to yield a high capacity V_2O_5 cathode showing up to 620 mAh g^{-1} at a current of 0.3 mA g^{-1}, however despite the high performance of the material, the procedure is costly and more complex than traditional methods limiting its viability for later commercial use.[106]

A structurally ideal ZIB cathode was developed by Wan *et al*. incorporating several of the aforementioned techniques into the formation of a freestanding, CNT-incorporated, $KV_3O_8 \cdot 0.75H_2O$ cathode. This cell displayed an extremely long cycling life of 10,000 cycles and a high capacity of 397 mAh g^{-1} at 0.1 A g^{-1}.[21] Whilst this technology is not able to be implemented into the flexible and wearable devices market, it ticks both major boxes of stationary energy storage systems being safety and cost.[66]

The vast number of vanadium-containing cathode compounds has given rise to a family that can produce materials ranging from dismal to superb electrochemical performance depending on the individual makeup, many of these materials are highlighted and compared in **Table 1** below.

Table 1: Physical and Electrochemical Comparisons of V-containing Cathodes in Zinc Ion Batteries.

Material	Morphology	Enhancements	Maximum capacity	Maximum No. of Cycles	Cite
V_2O_5	nanosheets	synthesis straight onto Ti	503.1 mAh g^{-1} (@0.1A g^{-1})	700 (@0.5Ag^{-1})	[6]
V_2O_5	nanosheets	calcined	128 mAh g^{-1} (@0.5A g^{-1})	400 (@2A g^{-1})	[86]
V_2O_5	hybrid structures	+ oxidation of MXenes	397 mAh g^{-1} (@0.5A g^{-1})	2000 (@4A g^{-1})	[57]
V_2O_3	nanocubes	calcination	625 mAh g^{-1} (@0.1A g^{-1})	10000 (@10A g^{-1})	[7]
VO_2	nanobelts	free-standing/ added CNTs	540 mAh g^{-1} (@0.05A g^{-1})	1000 (@5A g^{-1})	[79]
V_2O_5	nanosheets	Polyaniline intercalated	372 mAh g^{-1} (@0.5A g^{-1})	2000 (@5A g^{-1})	[4]
V_3O_7/V_2O_5	nanorods	Composite material	218.4 mAh g^{-1} (@1A g^{-1})	1100 (@2A g^{-1}) and 7000 (@5A g^{-1})	[107]
VO_2	nanoplates	Ostwald ripening	394 mAh g^{-1} (@0.1A g^{-1})	1200 (@3A g^{-1})	[12]
V_2O_5	heterostructures	Grown onto graphene	489 mAh g^{-1} (@0.1A g^{-1})	3000 (@30A g^{-1})	[68]
VO_2	nanobelts	N/A	375 mAh g^{-1} (@0.1A g^{-1})	2000 (@5A g^{-1})	[48]
V_2O_5	yolk–shell microspheres	N/A	410 mAh g^{-1} (@0.1A g^{-1})	1000 (@5A g^{-1})	[1]
V_2O_5	nanospheres	N/A	262.1 mAh g^{-1} (@1A g^{-1})	1000 (@10A g^{-1})	[85]
V_2O_5	microplates	N/A	258 mAh g^{-1} (@0.05A g^{-1})	2000 (@2A g^{-1})	[87]
V_2O_3	spherical	Carbon framework	319 mAh g^{-1} (@0.02A g^{-1})	4000 (@5A g^{-1})	[8]
V_2O_5	nanofibers	Calcination	275 mAh g^{-1} (@0.65 C)	500 (@2C)	[5]
V_2O_5	nanoparticles (to sheets w/ cycling)	Carbon additives	225 mAh g^{-1} (@0.05A g^{-1})	4000 (@5A g^{-1})	[3]
V_2O_5	prismatic	MOF derived, carbon additives	620.2 mAh g^{-1} (@0.3A g^{-1})	20,000 (@40A g^{-1})	[106]
$(NH_4)_2V_6O_{16}\cdot1.5H_2O$	nanowires	N/A	385 mAh g^{-1} (@0.1A g^{-1})	500 (@2A g^{-1}) and 10,000 (@8A g^{-1})	[101]
$Mn_{0.15}V_2O_5\cdot nH_2O$	nanoflower (of sheets)	N/A	367 mAh g^{-1} (@0.1A g^{-1})	8000 (@10A g^{-1})	[97]
$Zn_3V_2O_7(OH)_2\cdot2H_2O$	nanowires	N/A	213 mAh g^{-1} (@0.05A g^{-1})	300 (@ 0.2A g^{-1})	[66]
$Zn_{0.25}V_2O_5\cdot nH_2O$	thin nanobelts	Carbon additives	300 mAh g^{-1} (@0.05A g^{-1})	1000 (@8C)	[96]
K+ intercalated V_2O_5	nanorods	N/A	439 mAh g^{-1} (@0.05A g^{-1})	1500 (@8A g^{-1})	[19]
$Mg_{0.19}V_2O_5\cdot0.99H_2O$	nanobelts	N/A	352 mAh g^{-1} (@0.1A g^{-1})	5000 (@5A g^{-1})	[59]
$Mg_{0.23}V_2O_5\cdot1.0H_2O$	nanospheres	N/A	393 mAh g^{-1} (@0.2A g^{-1})	20,000 (@20A g^{-1})	[80]
$Na_xV_2O_5\cdot nH_2O$	nanobelts	CNTs/ free-standing	459.1 mAh g^{-1} (@0.5A g^{-1})	1800 (@10A g^{-1})	[47]
$(NH_4)_{0.5}V_2O_5$	nanoflakes	N/A	418.4 mAh g^{-1} (@0.2A g^{-1})	2000 cycles (@5A g^{-1})	[108]
$KV_3O_8\cdot0.75H_2O$	nanobelts	CNTs/ free-standing	379 mAh g^{-1} (@0.1A g^{-1})	10,000 (@5A g^{-1})	[109]
$(NH_4)_xV_2O_5\cdot nH_2O$	nanobelts	N/A	391 mAh g^{-1} (@0.5A g^{-1})	400 (@2A g^{-1})	[95]
$NaV_8O_{20}\cdot nH_2O$	nanobelts	Hierarchically porous structure	417.5 mAh g^{-1} (@0.2A g^{-1})	6000 (@10A g^{-1})	[37]
$Zn_3(OH)_2V_2O_7\cdot2H_2O$	nanosheets	Stitched with CNTs	114 mAh g^{-1} (@0.1A g^{-1})	2000 (@1A g^{-1})	[51]

$Co_{0.247}V_2O_5 \cdot 0.944H_2O$	nanobelts	N/A	432 mAh g^{-1} (@0.1A g^{-1})	7500 (@4A g^{-1})	[110]
CuV_2O_6	nanobelts	graphene oxide wrapped	427 mAh g^{-1} (@0.1A g^{-1})	3000 (@5A g^{-1})	[99]
CaV_3O_7	nanobelts	Binder-free/ O$_2$ defects	471.04 mAh g^{-1} (@0.83A g^{-1})	400 (@3.7A g^{-1})	[111]
$Ni_{0.25}V_2O_5 \cdot nH_2O$	nanoribbons	N/A	402 mAh g^{-1} (@0.2A g^{-1})	1200 (@5A g^{-1})	[98]
$NH_4V_4O_{10} \cdot nH_2O$	urchin-like nanoribbons	Oxygen defects	435 mAh g^{-1} (@0.2A g^{-1})	1500 (@10A g^{-1})	[68]
NaV_3O_8	nanoparticles	N/A	353 mAh g^{-1} (@0.07A g^{-1})	500 (@1.75A g^{-1})	[112]
$NH_4V_3O_8 \cdot 0.5H_2O$	nanobelts	N/A	423 mAh g^{-1} (@0.1A g^{-1})	1000 (@1A g^{-1})	[32]
$(NH_4)_2V_{10}O_{25} \cdot 8H_2O$	nanobelts	N/A	417 mAh g^{-1} (@0.1A g^{-1})	500 (@0.5A g^{-1})	[67]
$(NH_4)_2V_{10}O_{25} \cdot 8H_2O$	nanosheets	Free-standing	523 mAh g^{-1} (@0.1A g^{-1})	1000 (@1A g^{-1})	[32]
$(NH_4)_xV_2O_5 \cdot nH2O$	nanoribbons	N/A	372 mAh g^{-1} (@0.1A g^{-1})	2000 (@5A g^{-1})	[113]
$Mg_{0.1}V_2O_5 \cdot H_2O$	nanobelts	N/A	470 mAh g^{-1} (@0.1A g^{-1})	3000 (@5A g^{-1})	[114]
$Cu_3V_2O_7(OH)_2 \cdot 2H_2O$	nanoribbons	N/A	216 mAh g^{-1} (@0.1A g^{-1})	500 (@0.5A g^{-1})	[84]
$MgV_2O_6 \cdot 1.7H_2O$	nanobelts	N/A	425.7 mAh g^{-1} (@0.2A g^{-1})	1500 (@4A g^{-1})	[115]
$Al_{0.24}V_2O_5 \cdot 0.78H_2O$	nanobelts	Tailored carbon substrate	534 mAh g^{-1} (@1A g^{-1})	1000 (@10A g^{-1})	[116]
NaV_6O_{15}	nanorods	N/A	427 mAh g^{-1} (@0.05A g^{-1})	300 (@1A g^{-1})	[20]
Al-Doped $V_{10}O_{24} \cdot 12H_2O$	nanosheets	N/A	415 mAh g^{-1} (@0.2A g^{-1})	3000 (@5A g^{-1})	[117]
$NaV_3O_8 \cdot 1.5H_2O$	nanobelts	Dual carriers	380 mAh g^{-1} (@0.05A g^{-1})	1000 (@4A g^{-1})	[118]
ZnV_2O_4	nanoparticles	Electroactivation	312 mAh g^{-1} (@10C)	1000 (@10C)	[80]
$V_{10}O_{24} \cdot 12H_2O$	nanotubes	Freeze drying/ CNTs/ freestanding	191 mAh g^{-1} (@0.5A g^{-1})	1000 (@10A g^{-1})	[77]
$V_2O_5 \cdot nH_2O$	nanoplates	N/A	372 mAh g^{-1} (@0.3A g^{-1})	950 (@6A g^{-1})	[49]
$V_5O_{12} \cdot 6H_2O$	nanobelts	Binder-free	354.8 mAh g^{-1} (@0.5A g^{-1})	1000 (@2A g^{-1})	[15]
$V_2O_5 \cdot nH_2O$	nanosheets	Polyaniline intercalated	346 mAh g^{-1} (@0.3A g^{-1})	800 (@1A g^{-1})	[119]
$V_2O_5 \cdot nH_2O$	microsphere of nanosheets	Cu or Mg catalysis	VOH: 337, +Cu:379, +Mg: 349 (all 0.5A g^{-1})	all 1000 (@4A g^{-1})	[100]
VPO_4F	nanoparticles	N/A	150 mAh g^{-1} (0.02C)	N/A	[120]
$Na_3V_2(PO_4)_2O_{1.6}F_{1.4}$	nanocubes	Water in bi-salt electrolyte	155 mAh g^{-1} (@0.05A g^{-1})	7000 (@2A g^{-1})	[18]
$Na_3V_2(PO_4)_3$	nanoparticles	Wrapped in carbon sheets	97 mAh g^{-1} (0.5C)	100 (@0.05A g^{-1})	[17]
V_3S_4	Spherical nanoparticles	Novel carbon substrate	148 mAh g^{-1} (@0.10A g^{-1})	1000 (@5A g^{-1})	[104]
VSe_2	Micro-hexagonal plates	N/A	250.6 mAh g^{-1} (@0.2A g^{-1})	800 (@2A g^{-1})	[73]
VS_2	nanosheets	Grown onto graphene sheets	238 mAh g^{-1} (@0.1A g^{-1})	1000 (@5A g^{-1})	[50]
VS_4	nanoparticles	N/A	310 mAh g^{-1} (@0.1A g^{-1})	500 (@2.5A g^{-1})	[83]
VS_2	nanosheets	N/A	190.3 mAh g^{-1} (@0.05A g^{-1})	200 (@0.5A g^{-1})	[103]

2.4.0 Alternative Research of ZIBs

2.4.1 Current Collectors

The main requirements for an ideal current collector are high conductivity, low mass, and low cost. It should also be easily machinable. Materials, such as thin stainless-steel mesh or foil, are often used as they are also solderable, allowing for simple implementation into technologies. Conversely, materials such as carbon cloth are ideal due to their superior electrical conductivity and minimal mass, however, cloths are unable to be soldered, limiting their viability in the manufacturing processes of some technologies.[40] Despite their superior electrochemical properties, carbon substrates are often hydrophobic, causing issues surrounding the ability for the electrolyte to enter the electrode and ultimately hindering the efficient diffusion of intercalating ions. This can be resolved through extra procedures, such as acid treatment, plasma cleaning and ionising radiation.[77] Wu *et al.* found that through micro/nanostructure fabrication, a hydrophilic carbon cloth support allowed for the anisotropic growth of the active cathode material. This technique resulted in a high performing cell showing 534 mAh g^{-1} at 1 A g^{-1}.[116] However, the requirement for extra processing before use makes them less desirable in an industrial environment due to cost and time considerations. It is likely due to such issues, as well as previously mentioned manufacturing drawbacks, that materials, such as stainless steel meshes, are more commonly implemented into ZIBs than carbon cloth despite their slightly poorer performance as a current collector. However, that is not to say this will not change in the future, with new developments of carbon-based current collectors such as that designed by Liu *et al.* in which a highly conductive, flexible and hydrophilic carbon substrate was successfully implemented into ZIBs as the current collector for a vanadium sulfide (V_3S_4) cathode material.[104]

2.4.2 Electrolytes

The choice of electrolyte that is used within a battery cell can have a great impact on the cells electrochemical performance as it is closely related to the reaction in which the active

ions are removed from and returned to the cathode.[121] It has been duly noted that one of the major advantages of ZIBs is their compatibility with a large variety of electrolytes (both aqueous and organic) due to their wide pH window (pH: 3.6-6.0) allowing for a larger range of compatible solutions and thus can be chosen depending on the desires of the developer[40, 51]. ZIBs often utilize electrolytes with neutral or mild acidic pH values as alkaline environments encouraging dendrite formation and highly acidic electrolytes are prone to H_2 evolution.[81] Often KOH electrolytes were used in zinc primary batteries, however, due to their tendency to allow anodic dendrite production in secondary batteries, many have seen them exchanged for non-alkaline alternatives.[23]

2.4.2.1 Organic Electrolytes

Due to overwhelming safety and environmental factors, it is ideal to prioritise aqueous electrolytes when considering the development of ZIBs, but even more so because many aqueous electrolytes have improved ionic conductivity over their organic counterparts showing 0.1-6 S cm^{-1} and ~10^{-3}-10^{-2} S cm^{-1} respectively,[66, 68, 96] as well as a much larger electrochemical window (~ 2.5 V).[18] This is demonstrated by Zhang *et al.* in a comparison of aqueous $Zn(CF_3SO_3)_2$ against organic ($Zn(CF_3SO_3)_2$) (in acetonitrile) in conjunction with a V_2O_5 cathode, showing the former to provide a much high cycling capacity and more stable CE.[3]

2.4.2.3 ZnSO$_4$

Many of the electrolyte compounds utilized in Zinc-ion battery systems suffer from slow transfer kinetics, this is due to unstable compounds such as CH_3COOH^-, NO_3^- , and Cl^-. However $ZnSO_4$ does not suffer this and as such is known for stability and readily allows the transfer of Zn^{2+} ions.[86] In combination with its extreme cost efficiency (US$7-20 kg^{-1}), this has seen $ZnSO_4$ become one of the most common electrolyte solutions used in conjunction with zinc anodes and vanadium containing cathodes. However, due to the low mass of the molecules, much of the electrolytic solvation sphere is taken up by water which is prone to deprotonation and in turn OH^- and H^+ ions are often present.[46] This leads to interactions with soluble

vanadium ions causing the gradual dissolution of the cathode material as well as the build-up of inactive passivation materials such as Zn hydroxides and zincates.[65]

2.4.2.2 Zn(CF₃SO₃)₂

Conversely to $ZnSO_4$, the equally common electrolyte $Zn(CF_3SO_3)_2$ is a larger salt that does not suffer such effects. This is due to the bulky anions encompassing dominating the solvation sphere of transferring ions, drastically reducing the reactivity at the electrolyte-electrode interface[55] This is demonstrated in a comparison of $(Zn(CF_3SO_3)_2)$ and $ZnSO_4$ electrolytes by Zhang *et al.* who show the bulkier salt to have a smaller potential between the Zn^{2+} platting and stripping of the zinc anode (-0.14 and 0.05 V) as well the CE climbing to 100% where it remained stable. The $ZnSO_4$ however had a larger potential difference (-0.17 and 0.055 V) and a constantly decreasing CE until the eventual failure of the cell.[38] Furthermore, much like $ZnSO_4$, $Zn(CF_3SO_3)_2$ is highly compatible with zinc electrodes showing enhanced stripping and plating during the galvanostatic cycling process.[40] However, the considerable price jump between the two has seen $Zn(CF_3SO_3)_2$ take the back-seat when exploring industrial ZIB technologies.

2.4.2.4 Zn(TFSI)₂

Due to its limited compatibility with the zinc electrode, $Zn(TFSI)_2$ is more often used as an enhancing agent in ZIB electrolytes, much like $Zn(CF_3SO_3)_2$, the salts' bulky anions alter the solvation sphere of the transferring ions, drastically changes the reactivity as the zinc has a higher tendency to form Zn-TFSI rather than $(Zn-(H_2O)_6)^{2+}$.[65] The addition of $Zn(TFSI)_2$ into an electrolyte is also a highly efficient preventative against the growth of dendrites on the surface of the electrode, as it allows for selective reductive decomposition of the TFSI⁻ ions resulting in uniform Zn^{2+} deposition. $Zn(TFSI)_2$ is not widely used however due to its being extremely costly (even more so than $Zn(CF_3SO_3)_2$) thus reducing its viability for commercial scale use.[81]

It is also possible to combine the effects of different solutions by using a bi-salt electrolyte such as that developed by Ni *et al.*, showing a solution of 25 M $ZnCl_2$ and 5 M NH_4Cl.[18] Another example of this is a dual electrolyte solution that results in a Zn/V_2O_5 hybrid-ion battery containing both Zn and Li ion transfer, this is done through the implementation of a $Zn(CF_3SO_3)_2$ – LiTFSI electrolyte, allowing the zinc anode to release Zn^{2+} ions, which in turn allows the Li^+ ions to be intercalated into the cathode material. This approach, whilst creating an interesting mechanism, is not ideal as the capacity reached ($\leq$200 mAh g^{-1} at 200 mA^{-1}) is easily achievable through traditional ZIB methods[87] as well as the fact that the use of LiTFSI takes away the safety aspect of having a salt in water electrolyte.

Concentration of the electrolyte also plays a significant role in the cell's performance as low concentration electrolytes can allow increased water activity and water-induced side reactions.[35] Therefore, higher concentrations reduce dissolution of active cathode materials in aqueous solution. An investigation by Zhou *et al.* compared the effects of electrolyte concentration on the electrochemical performance of V_2O_5 cathode in a ZIB system. The cells with varying concentrations of $ZnSO_4$ between 0.5 M and 3 M underwent galvanostatic cycling. From the resulting data, it was concluded that the higher concentrations yielded not only higher capacities, but also higher levels of capacity retention.[86]

2.5. Summary

ZIB systems are one of the most promising focuses in the face of the oncoming energy crisis. With high potential, almost incomparable safety components, and significantly lower production costs than the alternatives, if they are able to be optimized to rival the performance of the current LIB systems, it could be turning point in the way we look at commercial batteries and their environmental effects. This progression towards eco-friendly storage systems is being more aggressively proposed in recent years due to the dramatic effects of climate change and

the immediate need for safe and suitable storage systems to house the output of green energy-production technologies.

Due to their structural advantages and high theoretical capacity, vanadium containing materials have seen a dramatic rise in popularity in recent years. Through this, many types, compounds, and morphological variations have been investigated for use in ZIB systems.

To rectify this complication, new and improved cathode nanomaterials are being proposed from many different base materials and production methods. Thus far the most common materials are manganese oxides, vanadium oxides, and Prussian blue analogues.

Both vanadium-phosphates and vanadium-free compounds, whilst being highy regarded in the energy storage industry for a while, have little viable application in zinc battery systems due to their low capacity for Zn^{2+} transport and their limited aptitude structural manipulation. However, both vanadium-oxides and their related vanadates show significant promise. Vanadium oxides allow for a wide variety of morphologies and interlayer spacings due to the simplicity of the base structure. These can have significant impacts on the capacity and intercalation abilities of the cathode. Conversely, vanadates due to their more complex atomic structures often do not show a large range of morphologies. They do however have differing electrochemical results based on the cations and molecules which they have been altered with. Water molecules allow for ease of ion transport and increase the cycling life of the cathode by reducing mechanical strain during the de/intercalation process. Various cations can not only act as secondary support alongside the hydration of the material but can also have catalytic effects increasing the reaction kinetics during the redox and ion intercalation.

2.5.1 Future Developments
From the current state of the energy storage industry, it is clear that changes must be made. The development of ZIBs utilizing vanadium oxide cathodes is progressing smoothly and has made great advancements towards becoming a commercially viable option for grid

scale use to assist the World's transition to renewable energy sources as well as varying other areas of interest in which both ZIB system and cathode development would greatly advance technological development as summarised in **Figure 11**.

Uses for such technologies, while often focussed on the storage of renewable energies, is not limited to it. With the World's population becoming more reliant on transportable and wearable devices, creating flexible ZIBs for implementation into such technologies would greatly assist their integration into the industry.[40] It is theorized that the future of such technologies is for the devices to be more conforming with, and possibly integrable into human skin. To accomplish such a feat, current storage devices must be further developed to form flexible apparatus that are able to replicate properties of skin such as modulus and strain.[122] One of the methods of achieving this under current development, is to incorporate this feature into the current technology of ZIBs is through a design of solid state batteries with a gel electrolytes based on salt-in-water solutions.[18] These not only increase the stretchability of the cell but also prevent leaking that often occurs from flexible batteries with standard electrolyte.[80, 122] These leakages can cause significant decreases in the cycle life of the cell due to the limited transportability of ions. Furthermore, liquid electrolytes are often displaced as a result of strain upon the cell, misalignment within a battery can have great effects on the electrochemical performance as a result of the interfacial interactions of the components.[59] Research is however required in this area as the current solid-state batteries suffer from significantly lower capacity due to the low ionic conductivity of the gel electrolytes. It also is prone to allowing dendrite formation on the surface of the zinc anodes further reducing the efficiency of the cell over its limited cycling life.[80]

Additionally, several alterations can be made to current cathode materials in order to facilitate the mechanical requirements of flexible technologies. The most prominent of which includes the development of binder-free cathodes, as non-active additives (such as PVDF)

reduce the energy density of the cell as the extra material significantly increases the electrode's weight with no electrochemical benefit.[32, 77] The use of PVDF can also limit the interior porosity of the structure and increase the rigidity of the cathode material causing mechanical strain under the application of tensile stress, a characteristic that is not ideal for use in flexible technologies. Potential alternatives include the use of elastic substrates rather than the rigid polymeric binding seen by PVDF.[47, 122] Many such cathodes are already in development and are expected to make a significant breakthrough in the coming years. If the solid-state technology can be improved, in conjunction with the development of superior cathode materials, zinc-ion batteries could become the forefront of wearable technologies in years to come.[122]

It should also be noted that battery cells are often prone to failure in some regions of the world due to drastically low temperatures causing changes to the viscosity and phase of the electrolyte. For example, in some areas of northern China, which can reach as low as -30°C, this is a considerable problem and a major focus of electrolyte development. Several possible solutions undergoing investigation include the use of hydrogels, extremely high concentration aqueous electrolytes, and those with anti-freeze[110] agents such as ethylene glycol incorporated into the solution.[121] Many such electrolytes are gel solutions implemented as part of a quasi-solid-state battery.[18, 59] This is due to the ease with which the gel electrolyte can be adapted to suit different environments. One such case is the $Zn(CF_3SO_3)_2$ electrolyte mixed with PVA and glycerol developed by Zhou *et al.*[59] This creates a cost effective, anti-freeze gel electrolyte that is able to be easily adjusted for production on an industrial scale.[59]. Another example is that of Ma *et al.* which showed little drop in cell performance after recovery from 30 days of freeze drying under vacuum as well as cycling in temperatures as low as -25°C showing only a small drop to its capacity.[110] The major drawback of these cells, however, is that gel electrolytes often experience lesser electrical conductivity than had a liquid electrolyte been implemented into

the system.[111] If this technology can be improved, it could result in the widespread use of reliable, rechargeable energy storage systems in areas of the world that currently suffer without.

In addition to the application to the technologies, there are also future perspectives surrounding the way we fabricate the materials. Recent research has been conducted surrounding the use of additive manufacturing to produce gel electrolytes as well as nanostructured cathode materials in a more efficient and cost-effective manner. Currently, 3D-printed materials include mostly metal and their oxides/sulphides/etc. as well as carbon-based structures.[123, 124] However, it is not unlikely that in the future vanadium oxides and other like materials will be able to be produced through this method ensuring the most ideal structure, porosity and physical characteristics, increasing both the power and energy densities of the resulting cells. The technology is yet to be perfected and many of the desired materials require additives in order to be printed as desired, however, it is a worthy endeavour, and should it be perfected in the future, will prove to be invaluable to the battery making industry.
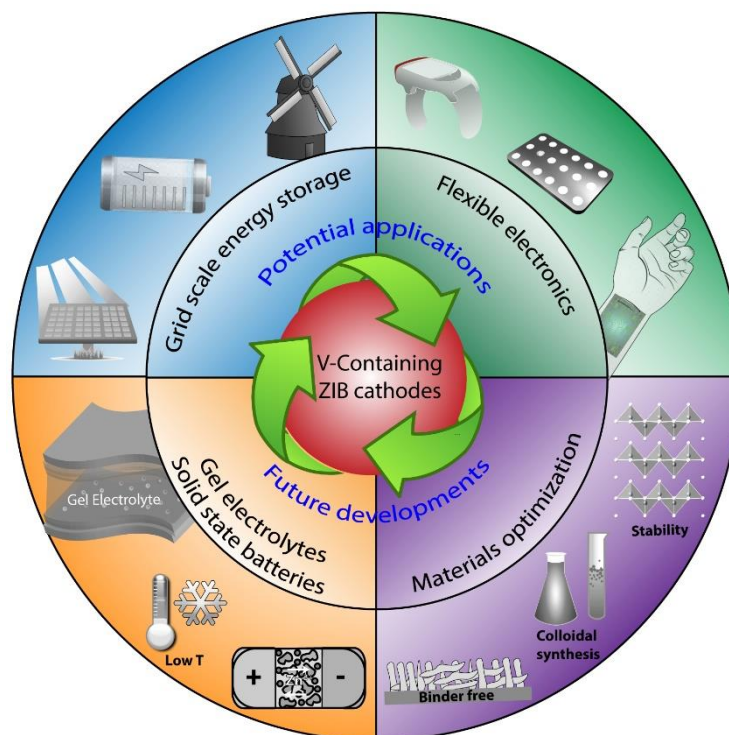
Figure 11. Schematic illustration of potential applications and proposed future developments of vanadium-containing ZIB cathodes.

2.5.2 Ongoing Research

In order to achieve the aforementioned future developments, much work must first go towards improving the cathodes and the overall electrochemical performance of the current technologies. Vanadium-containing cathode materials are an ideal foundation from which to build-up and develop ZIBs. Currently, many experimental cathodes excel in certain variables of performance while failing in others, for example those with large interlayer spacing and structural integrity due to intercalating ions often suffer from slow kinetics and limited intercalation capacity due to the blocking of the ion transport pathways. One of the most immediate and informative goals for the coming years is to focus the techniques currently available and develop ways to integrate them into the cathode materials allowing for equally high performance in capacity, reaction kinetics, cycling life, conductivity, structural integrity, and other variables. If this balance can be achieved, Vanadium-containing cathodes could push ZIBs to overtake the current interim, and lead the movement into safer, and more eco-friendly energy storage systems usage worldwide.

Acknowledgements

Chapter 3: Methodology

The information gleaned from the previous chapters allows us to narrow down the selection of viable cathode materials and also gives great insight into the effectiveness of the varying enhancements techniques available to each material, it is from this that we have chosen to synthesise and experiment on a carbon integrated, hydrated, layered vanadium oxide (CHVO) material. The CHVO material ($V_5O_{12}\cdot nH_2O$) is being tested for the first time in a ZIB system and as such, the following will provide great insight into its viability as a cathode material as well as giving insight into the mechanisms occurring in both this and other relevant materials. All of the following methodologies, results and analysis are contributions to an experimental paper that has been submitted for publication and is presently under peer review.

3.1. $V_5O_{12}\cdot nH_2O$ Material Synthesis

The CHVO powder was prepared through a solvothermal synthesis of 2.08 g vanadyl acetylacetonate and ethylene glycol (44 mL). The mixture was stirred at 80 °C in a round bottom flask until the vanadyl acetylacetonate was completely dissolved. Once complete, oleylamine (6 mL) was added and the heat increased to 160 °C for four hours under reflux. Upon cooling to room temperature, the precipitate was separated from the oil layer and transferred to a falcon tube to be centrifuged (9000 rpm for 3 min). The material was then washed with absolute ethanol until the precipitate showed a purple colour (vanadyl glycolate) with no green contaminants. The powder was dried under vacuum at 60 °C for 12 hours. Prior experimentation by Fernando *et al.* has demonstrated that metal glycolates can be used as a precursor for the synthesis of carbon-doped, functional metal oxides.[43] As such, the vanadyl glycolate powder was annealed at 400 °C in a three-zone tube furnace, for 30 min under argon environment. This yielded a black powder of carbon-doped V_2O_3.

Water was then introduced into the layered structure via the addition of deionized water (5 mL) to the material, allowing to stir for ~48 h under standard laboratory conditions. This mixture was then centrifuged (9000 rpm for 3 min) and the water decanted, before drying under vacuum at 60 °C for ~24 h, resulting in a green-tinged, black powder ($V_5O_{12} \cdot nH_2O$). This addition allowed for the production of a material of relatively high-water content. Subsequently, a lower water content compound was yielded by allowing the carbon-doped V_2O_3 to oxidize in standard lab conditions for 20 days, during which atmospheric water incorporated itself into the material, forming a notably green powder ($V_5O_{12} \cdot nH_2O$). Once complete, both materials were stored in an inert atmosphere (argon) glove box until ready for use.

3.2. Characterisation

Several forms of data collection will be used in order to completely and accurately characterize the synthesised nanomaterial.

3.2.1. Transmission Electron Microscopy (TEM)

TEM is a common characterisation technique that is used to identify the basic structure of a material be is amorphous or crystalline, as well as providing insight into morphological details such as layering and porosity. A common use for TEM imaging is to measure the interlayer spacing of relevant materials and as a precursor for SAED and EDX analysis. This technique requires a colloidal sample to be prepared by adding a small amount of material to ethanol and effectively dispersing the compound throughout the liquid by sonicating the mixture. This solution is then added as several drops to a 300 mesh Cu grid coated with a lacey formvar layer, allowing the ethanol to evaporate between each drop. The TEM instrument was conducted with an acceleration voltage of 200 kV and imaged using a Gatan OneView camera.

Instrument used: JEOL-ARM200F NEOARM atomic resolution analytical S/TEM equipped with a cold field emission gun (Cold FEG)

3.2.2. Selected Area Electron diffraction (SAED)

TEM be used for the acquisition of selected area electron diffraction (SAED) patterns of the material. This can be used to confirm the amorphous structure of a material, or to create a distinct diffraction pattern of a crystalline material that can be indexed to a database to obtain the exact structure in question. As a sub-technique of TEM, the sample preparation is identical to the aforementioned.

Instrument used: JEOL JEM-2100 microscope.

3.2.3. Scanning Electron Microscopy (SEM)

Creates a scanning image highlighting the surface makeup and characteristics (topography). This assists in the determination of the material's morphology. The surface morphology is particularly important as it is the materials' primary site of reaction, as such this data allows further insight of the redox chemistry within the battery cell. To prepare this sample a small amount of material is put onto carbon tape which is then attached to an SEM stub. The analysis was conducted at a 5 kV operating voltage using Secondary Electrons (SE) imaging mode.

Instrument used: JEOL JSM-7001F microscope equipped with a field emission gun.

3.2.4. Energy-dispersive X-ray spectroscopy (EDX)

EDX provides information about the elemental composition of the material within a selected region. This allows us to identify the makeup of our material, ensuring the target material has been achieved and with negligible/no impurities, ensuring a high purity level. This spectroscopy technique is utilised within the SEM and TEM and as such, the sample preparation is as noted above. The operating voltage was increased to 15 kV to undertake EDX analysis and utilised a Oxford X-Max, 50mm Silicon Drift Detector (SDD) EDX detector.

Instrument used: JEOL JSM-7001F microscope equipped with a field emission gun.

3.2.5. X-ray Diffraction (XRD)

Reveals crystallographic details of a material which can be matched against standardized data to assist in identifying the samples' crystal structure. For this analysis, the sample is prepared

using a Rigaku standard sample holder. The data obtained a Bragg Brentano Geometry utilizing Cu Kα radiation (λ = 1.54059 nm) with a 2 theta range of 2-80 degrees and a scan speed of 1.3 degrees per minute.

Instrument used: Rigaku SmartLab diffractometer.

3.2.6. X-ray Photoelectron Spectroscopy (XPS)

This characterisation technique allows for the clarification of the oxidation states of various components of the compound. The oxidation state of the transition metal within the compound is important, as it delegates the material's ability to undergo efficient and extensive redox reactions without a high risk of irreversibility. To prepare this material for analysis, press the sample onto an indium foil substrate, then place onto carbon tape, which is adhered to the sample holder. Data collection was undertaken using Monochromated Al K-alpha source (1486.7 eV) radiation with an emission current of 15 mA. The data was then analysed using CasaXPS software with calibrations to C 1s (284.8 eV) peak.

Instrument used: Kratos AXIS Supra Spectrometer.

3.2.7. Thermogravimetric Analysis (TGA)

Measures a material's thermostability as well as its volatile composition (structural water content) and the amount of carbon within the sample. The ratio of materials to crystal water and carbon framework can determine the entire molecular stability of the material as well as improving/limiting its ion intercalation abilities. The material was pre-heated to 140 °C under Ar environment before heating in air from 25 °C to 800 °C at 5 °C min^{-1}.

Instrument used: NETZSCH STA 449.

3.2.8. Raman Spectroscopy

Raman spectroscopy identifies the bond stretching of relevant target compounds to identify the presence of difficult to detect compounds such as graphite amongst an amorphous material.

The instrument does not require detailed sample preparation and the powder material is able to be deposited directly onto the stage.

Instrument used: Renishaw inVia Raman microscopea

3.3. Electrochemical Testing

The electrochemical characterisation of the battery cell allows us to determine whether our material is an effective cathode material and if so, to what extent.

3.3.1. Cell Fabrication

The working electrodes were prepared by mixing a slurry of active material, carbon Super P TIMCAL and PVDF (6% concentration in NMP) with a ratio of 7 : 2 : 1 parts respectively. This was then painted onto current collector sheets of carbon cloth and dried under vacuum at 60 °C for 12 h. The coated sheets were cut to disks of 15 mm. The surface of the zinc counter electrodes was sanded to remove the oxidized surface layer and cut into 15 mm disks. The CR2032 coin cell batteries were fabricated in ambient air, employing the prepared working and counter electrodes, glass fibre separators, and 3M $Zn(CF_3SO_3)_2$ electrolyte.

3.3.2. Galvanostatic Charge/Discharge Testing

This test measures the change in voltage and capacity over repeating charge/discharge cycles at a constant current. The data retrieved from this test is able to determine not only capacity, but also the cell's stability and cyclability. Cycling experiments were conducted using a voltage range from 0.2 to 1.6 V. To ensure complete charging of the cell, a constant voltage of 1.6 V was applied to the cell for five minutes or until the current reached 0.01 mA at the end of each galvanostatic charge. Testing was conducted at varying rates between 200 mA g^{-1} and 5000 mA g^{-1}.

Instrument used: LANHE CT2001A electrochemical station.

3.3.3. Cyclic Voltammetry

Cyclic Voltammetry (CV) testing measures the current across a sweeping voltage at a selected scan rate, and by doing so is able to determine the redox processes as well as the charge storage mechanism, whether charge is stored via diffusion-controlled charge storage processes or surface-controlled capacitive processes. This was completed at the potential window 0.2-1.6 using scan rates of 0.1 - 1.0 mV s^{-1}.

Instrument used: Keithley 2450 EC sourcemeter and Gamry 1010E potentiostat.

3.3.4. Galvanostatic Intermittent Titration Technique (GITT)

The cells were charged and discharged at a low current whilst alternating between 'on' and 'rest', showing the charge/discharge and voltage change during rest for each 'step'. The 'steps' were then further analysed to obtain information on the active materials kinetic characteristics. Using the formula $D_S = \frac{4}{\tau\,\pi} \times (\frac{n_m V_m}{S})^2 \times (\frac{dE_S}{dE_t})^2$ in which dEs and dEt are obtained from the raw graphical data, GITT analysis is used to calculate the diffusion coefficient over varying potentials. GITT cycles were conducted at a specific current of 50 mA g^{-1} (on time: 10 min, rest time 30 min, upper voltage: 1.6 V and lower voltage: 0.2 V).

Instrument used: Keithley 2450 EC sourcemeter and Gamry 1010E potentiostat.

3.3.5. Electrochemical Impedance Spectroscopy (EIS)

EIS allows for the formulation of a comparative analysis between materials showing their impedance with reference to the intercalation of zinc ions through the use of the Nyquist Plot method. Tests were conducted between 0.1 MHz and 10 mHz with a sinusoidal amplitude of 5 mV.

Instrument used: Keithley 2450 EC sourcemeter and Gamry 1010E potentiostat.

Chapter 4: Characterisation and Physiochemical Experimentation

The material was produced via a simple solvothermal synthesis followed by annealing, ageing, and water mixing as depicted in **Figure 12a**. Through this CHVO was fabricated with a stacked sheet-like morphology as depicted by the SEM imaging in **Figure 12b-d**. The particles vary greatly in size, ranging from ~8-50 µm as noted by comparisons of **Figure 12b and c** respectively. Closer inspection of **Figure 12d** via the inset image shows that the sheets are in fact made up of closely compacted flakes creating a porous architecture. The specifics of the materials characteristics will be uncovered through the use of various techniques including TEM, XPS, XRD and Raman spectroscopy.
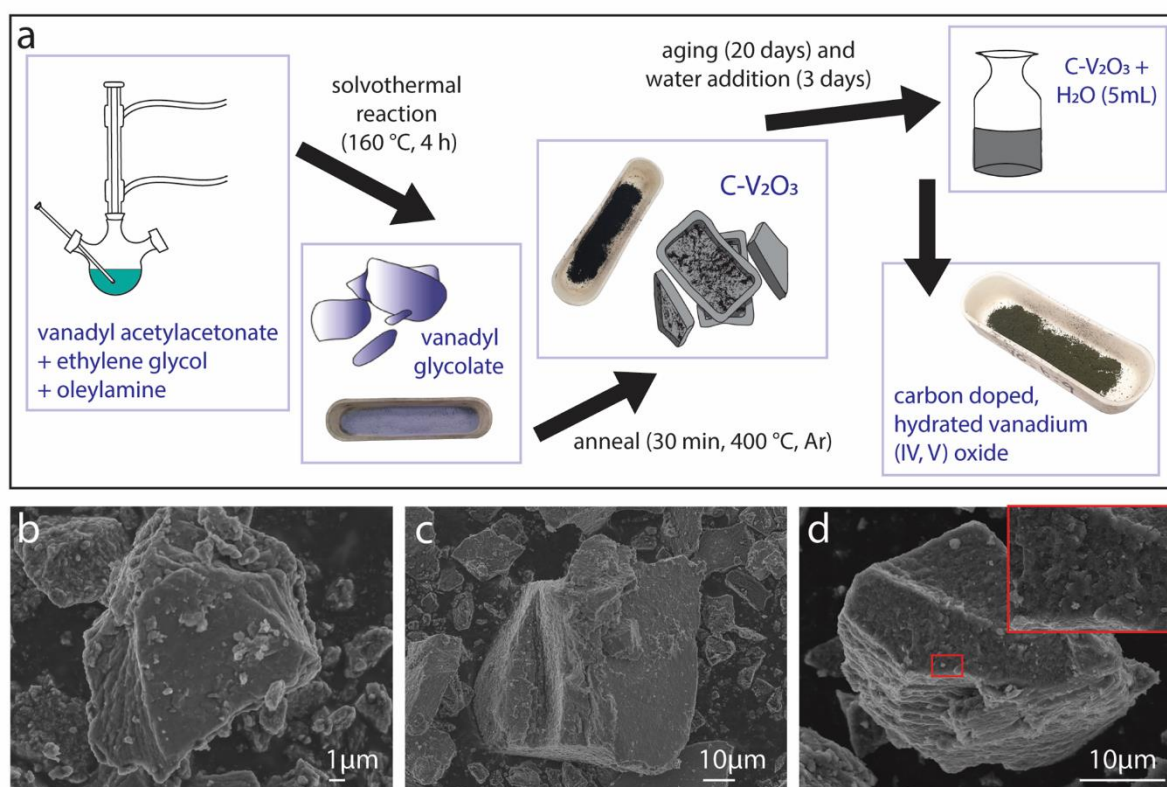
Figure 12: a) Schematic of CHVO synthesis procedure, b-d) SEM imaging of CHVO morphology (d-inset provides high magnification image showing flake-like composition of stacked sheets).

The TEM image in **Figure 13a** highlights the presence of large pores and tunnels at the surface of the material, allowing for better and more efficient ion transport throughout the cathode. During the aging process, the precursor material oxidises and forms an amorphous product.

This is clearly identifiable in **Figure 13b** showing overlapping layers of amorphous material. This is further emphasised using the FFT pattern in the figures' inset, showing a uniform, non-crystalline pattern. However, upon further analysis, small regions of crystalline impurities were noted as seen in **Figure 13c**. The d-spacing values of 0.27 and 0.24 nm are attributed to (222) and (400) planes of cubic V_2O_3, respectively. This indicates some trace starting material and it is assumed that the presence of this crystalline impurity maintains some of the materials' natural diffusion-controlled mechanisms during cell cycling. **Figure 13d** demonstrates the use of EDX mapping, graphically highlighting the approximate ratios of vanadium, carbon, and oxygen within the material as well as confirming the uniformity of each element throughout.
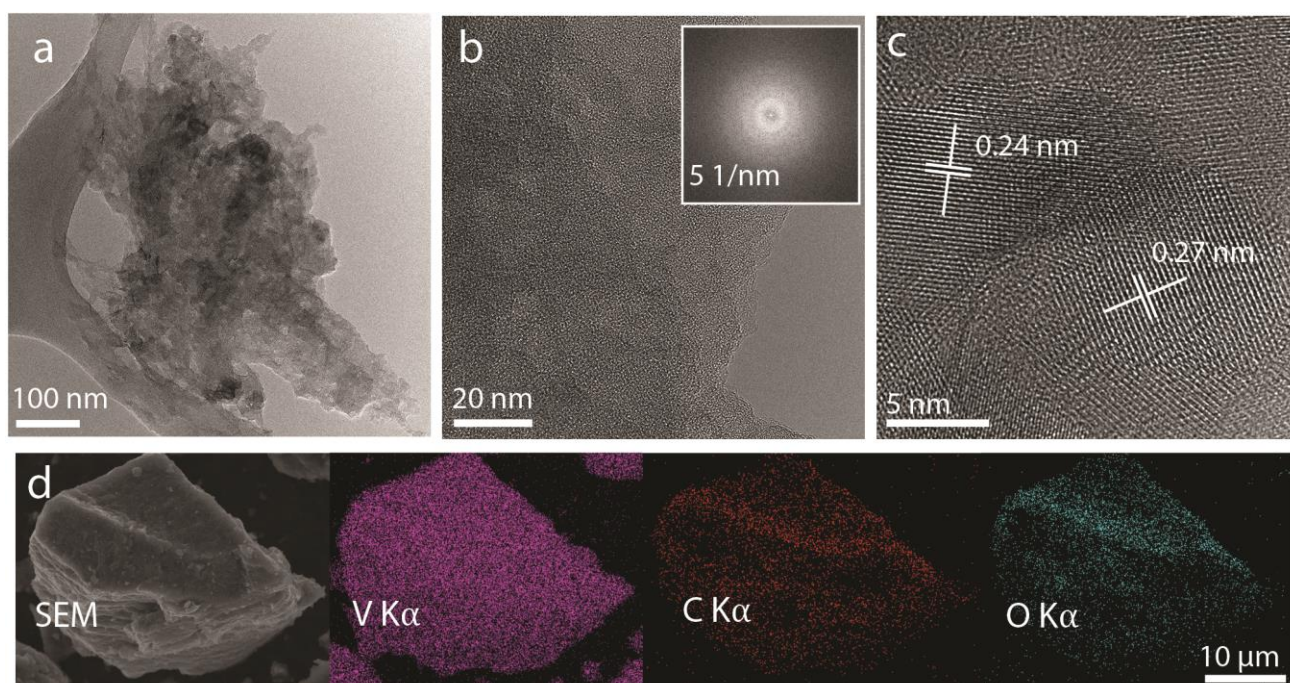
Figure 13: a) TEM image of CHVO product b) HRTEM image of amorphous region (inset shows the corresponding FFT pattern). c) HRTEM image of crystalline region. d) SEM-EDX mapping of CHVO material highlighting vanadium, carbon and oxygen.

To further elucidate the chemical character of the vanadium within the material structure, the powder sample underwent XPS analysis. **Figure 14a** shows the high-resolution spectra of V 2p, highlighting two sets of major and minor peaks. The major peaks are attributed to the 5+

oxidation state vanadium at values of 517.2 (V 2p $^3/_2$) and 524.8 (V 2p $^1/_2$), with the remaining

minor peaks representing vanadium with a 4+ valency at 516.3 (V 2p $^3/_2$) and 523.3 (V 2p $^1/_2$).

The ratio between V^{4+} and V^{5+} is 1:2.06, giving an approximate average oxidation state of +4.7

(close to oxidation state of vanadium in V_5O_{12} form). The crystal structure of the material was

endorsed by the data obtained from XRD characterisation (Figure 3b). The spectra saw notable

peaks occurring at 7.49, 26.11, and 50.7 °2θ corresponding to the 001, 603, and 020 planes

respectively. These peaks are matched to PDF# 00 045 1401 confirming the material

composition as $V_5O_{12} \cdot nH_2O$. The (001) planes have a spacing of ~13 Å, held at an expanded

distance due to the pillaring effect of structural water molecules. However, the XRD peaks are

broad and exhibits low intensity demonstrating the poor crystallinity (and amorphous

character) of the sample as evidenced by TEM data.

The carbon framework is a key constituent of the cathode material as it increases the electrodes

overall electrical conductivity as well as providing structural support. Due to the flexibility of

carbon, it can also have a cushioning effect to reduce the mechanical strain during ion

intercalation. As the integrated carbon is also an amorphous structure, it is unable to be

identified separately from the amorphous-like vanadium oxide material during TEM imaging.

Thus, it must undergo further analysis to identify and characterise the carbon components. A

Raman spectrum was taken of the material (**Figure 14c**) and showed a large peak at ~1590 cm^{-1}

alongside a slightly smaller peak at ~1360 cm^{-1} which were indexed to the amorphous

carbons' G and D bands respectively, confirming the presence of the carbon framework in the

active material.[125]

As previously stated, the amount of water that has been incorporated into the cathode can play

a pivotal role in the effect that the water has on the materials intercalation abilities. To quantify

the amount of structurally bound water within the material, TG analysis was undertaken. The

results of this technique are displayed in **Figure 14d**, showing a 10.5% water loss at

temperatures up to ~150°C, this mass is attributed to the loosely bound surface water. A further 4.8% was lost between temperatures 150-200°C, this loss is the desired structural water molecules strongly bound within the framework of the cathode material (accounting for 2.7 structural water per formula unit of V_5O_{12}). Therefore, it can be stated that the materials' chemical formula is $V_5O_{12} \cdot 2.7H_2O$.
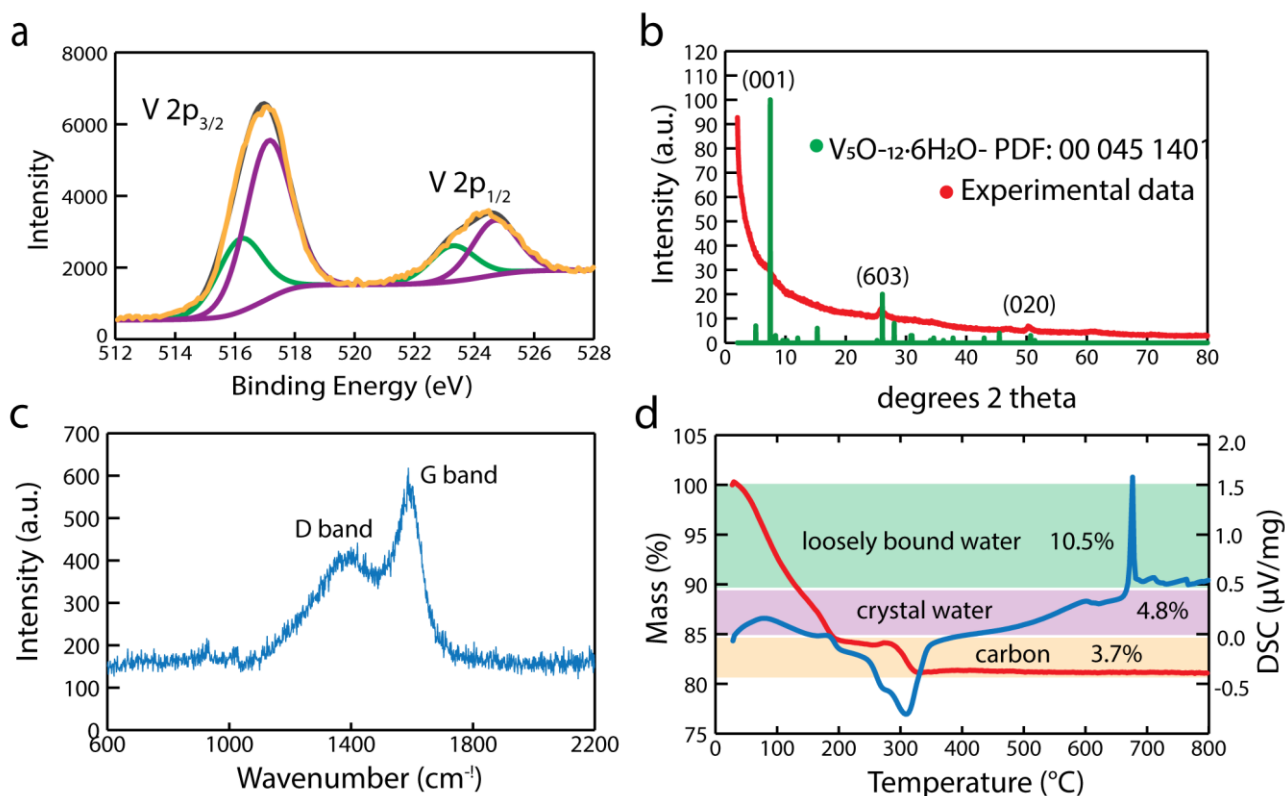
Figure 14: a) XPS spectrum of CHVO powder V 2p region, b) XRD spectrum showing CHVO powder indexed to PDF – 00 045 1401, c) Raman spectroscopy of carbon region of CHVO, and d) TGA-DSC curve for CHVO product.

However, the ratio of water implanted into the material can also improve or impede the electrochemical performance. As such, a low water ratio alternative of the proposed material was also prepared in order to identify the superior water mass to best benefit the materials' structural chemistry. This material was prepared as described in our previous work.[43] This low water content material displayed a molar ratio of $V_5O_{12} \cdot 0.4H_2O$ (CHVO-LW) and a simple

morphology of nano-particles (as seen in **Figure 15**), the implications of these discrepancies will be further evaluated and discussed in later analyses.

Figure 15. SEM images for CHVO-LW sample
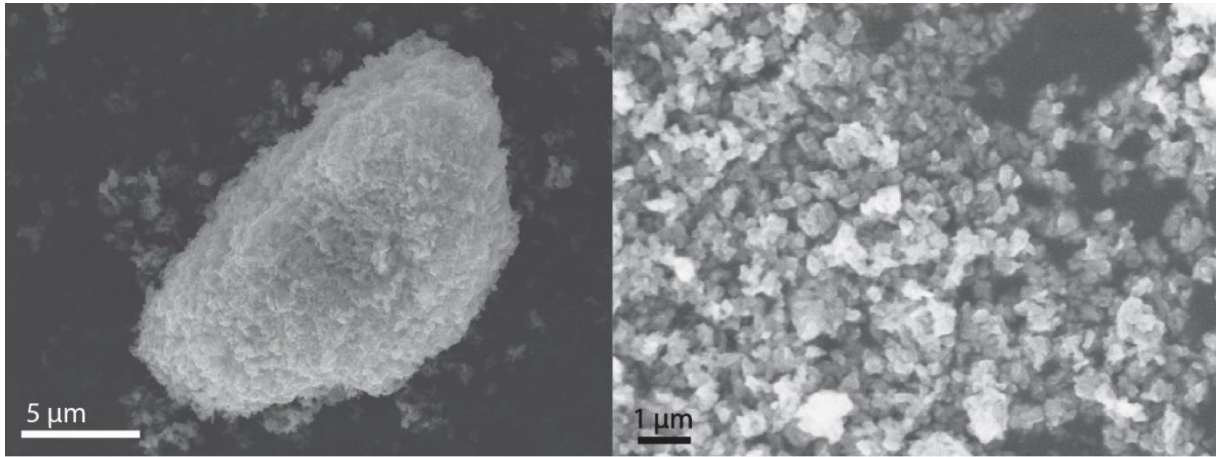
Chapter 5: Electrochemical Experimentation

The electrochemical data for this material was collected through the testing of the CHVO cathode against a Zn/Zn^{2+} anode in a coin cell with 3 M $Zn(CF_3SO_3)_2$ as the aqueous electrolyte. These cells were cycled between potential values of 0.2 V and 1.6 V at varying current densities as well as undergoing cyclic voltammetry and *ex situ* XPS analysis. The battery cell cycled at 250 mA g^{-1} showed an impressive capacity of 396 mAh g^{-1}. This value dropped to 278 mAh g^{-1} after 100 cycles giving a capacity retention of 70% (**Figure 16a**). The cell takes approximately 18 cycles to stabilize with initial cycles showing low capacity and low coulombic efficiency which gradually increases to reach the cells true starting capacity. This phenomenon is known as the gradual activation process and is typical of AZIBs containing cathodes of high internal surface area due to the slow diffusion kinetics typically exhibited by Zn^{2+} ions[19]. After this period however, the cell showed a high coulombic efficiency ~100 % displaying high reversibility of Zn^{2+} ions into the material. This is due to the stable, wide tunnel morphology of the host material, facilitated by the carbon framework and water pillaring as well as the decreased electrostatic interactions provided by the integrated water species. **Figure 16b** allows us to note that the cells' charge/discharge profile displays two slightly plateauing regions at approximately 0.4-0.6 and 0.9-1.1 V. This is attributed to the redox processes in CHVO material due to the insertion of Zn^{2+} ions.[28]. Additionally, the close overlapping of the voltage profiles implies the enhanced stability of the cathode material. A cycling test at 200 mA g^{-1} was conducted for the aforementioned CHVO-LW sample, this data is displayed by the blue datapoints in **Figure 16a** and shows an interesting trend as the material performs significantly better than the CHVO at low current densities in the initial cycles exhibiting a capacity of 582 mA g^{-1}, but only for a limited number of cycles before the cells' capacity drops dramatically (64% over 80 cycles) leading to inevitable early cell failure. This is likely due to the gradual collapse of the tunnel structure as a result of lacking structural support from the

lack of H_2O pillaring. Throughout cycling this will limit the size and availability of the interlayer tunnels in the morphology, disallowing ease of access for the intercalating Zn^{2+} into the material. The CHVO material suffers from a limitation to the maximum capacity (~396 mAh g^{-1}) due to the filling of internal tunnel structure by water molecules resulting in many of the intercalation pathways being blocked as well as limiting available active sites for Zn^{2+}ions. This does however provide excellent structural stability attributing to the cells notable cycling life, a feature that is significantly lacking in the CHVO-LW compound. This is specifically noted by the comparative cycling tests in which the CHVO-LW's open tunnels allow a higher initial capacity that subsequently plummets, driving the cell into failure as the tunnels begin to collapse under the strain of repetitive intercalation cycles.

This high specific capacity remains even when the cycling current is increased, this can be seen in **Figure 16c** where at a current of 1000 mA g^{-1}, the cell shows an initial capacity of 198 mAh g^{-1}. Due to the gradual activation process, this then increased to 333 mAh g^{-1} by cycle 10. The cyclability of the material can be noted by the capacity retention of 168 mAh g^{-1} after 150 cycles. It can also be noted that the CE value obtained after the gradual activation (~100 %) did not drop largely over the batteries cycle-life, showing 99.55% even after 150 cycles. An identical cycling test was conducted for cells using the CHVO-LW material. Not only did the capacities during galvanostatic cycling show much lower values, but the capacity retention was also much poorer than its high-water content counterpart. As seen in **Figure 16c**, at 1000 mA g^{-1} the low water cells showed initial capacities of only 171 mAh g^{-1} with an inconsistent capacity trend showing the cell struggling to reach 150 cycles and a capacity retention of 58.7%. This observation reiterates the poor structural stability of CHVO-LW as compared to CHVO, particularly at high specific currents.

The CHVO cell also underwent rate capability tests (**Figure 16d**), cycling at 250, 625, 1250, 2500, 3750 and 5000 mA g^{-1} for 10 cycles at each current density resulting in remarkable

capacities of 346, 319, 274, 246, 224 and 207 mAh g^{-1}, respectively. This exhibits the immense stability of the materials architecture throughout the intercalation/deintercalation process, a feature that is greatly assisted by the carbon framework limiting the effects of mechanical strain caused by the guest ions, as well as the reduced electrostatic interactions due to the structural water molecules' lubricant-like effect.

The material is further regarded as a viable cathode material due to the outstanding results obtained during the cyclability test as shown in **Figure 16e**. To reduce the interference of dendrites to the cyclability data, this test was conducted at 4000 mA g^{-1} as dendrites are greatly inhibited by cycling at higher current densities. These results were highly impressive, showing a long cycle life of over 3300 cycles whilst maintaining a CE value of ~99.9% and an average capacity of 188 mAh g^{-1}. The data showed an initial capacity drop from 340 to 250 mAh g^{-1} over the course of 300 cycles, from thereon out the capacity stabilized and dropped only very gradually for the remaining 3000 cycles. By discounting this preliminary stabilizing period, the capacity retention can be stated to be ~65 %. Comparatively to previously published data on carbon assisted, hydrated vanadium oxides, this material shows improvement in capacity retention comparing with data from Yan *et al.* reporting a V$_2$O$_5$·nH$_2$O/ graphene cell with 71% capacity retention at 6 A g^{-1}, over the course of 900 cycles.[49] At this number of cycles our material presented a capacity retention value of 77.4%.
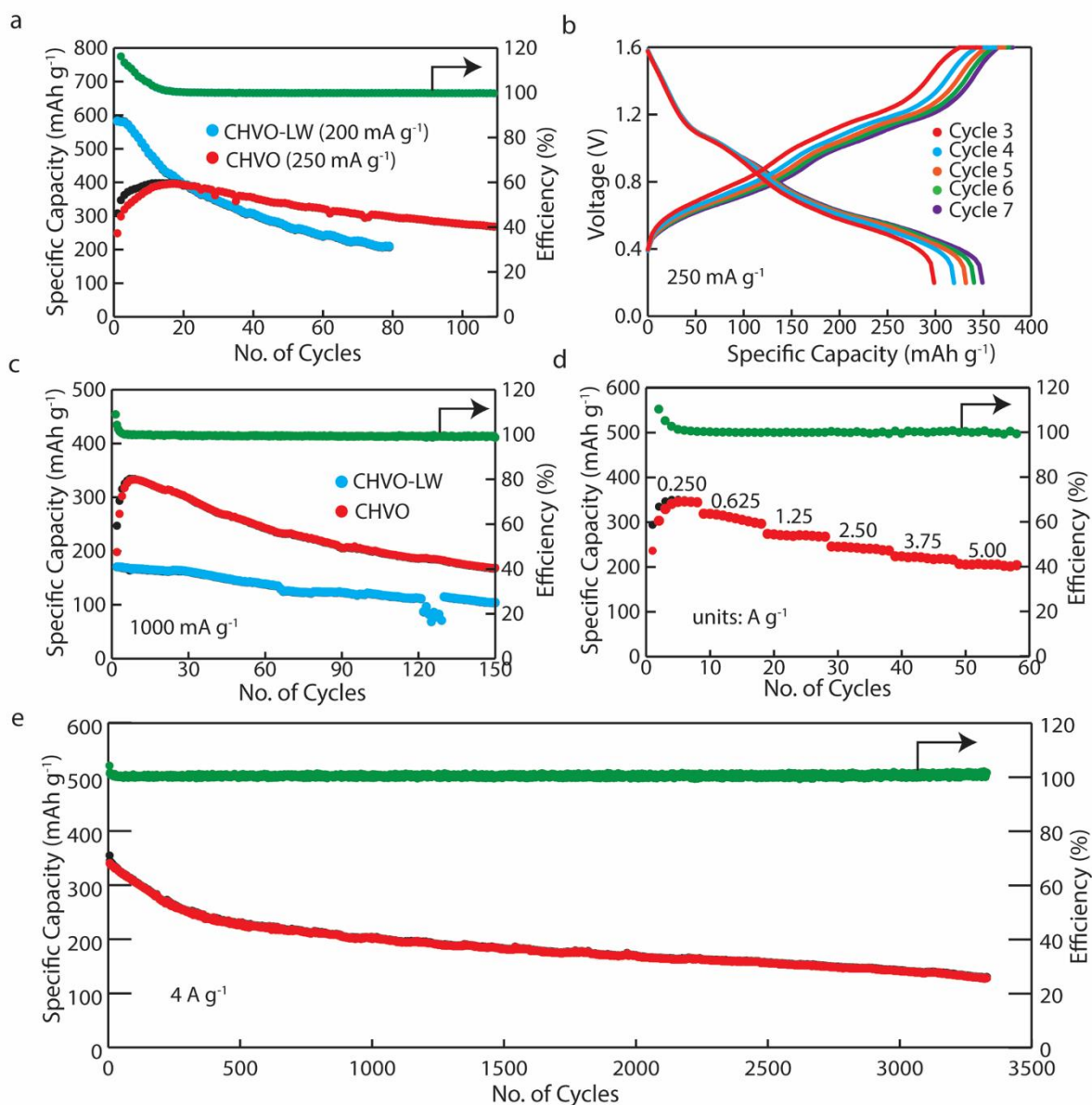
Figure 16: a) Galvanostatic cycling of CHVO (250 mA g^{-1}) and CHVO-LW (200 mA g^{-1}) samples, b) charge/discharge profiles of CHVO for five consecutive cycles at 250 mA g^{-1}, c) galvanostatic cycling at 1000 mA g^{-1}, d) CHVO rate test, and e) long-term cyclability test of CHVO at 4 A g^{-1}.

The aforementioned were repeated utilizing a cathode with a stainless-steel current collector to highlight the effect that varying the electrodes substrate can have on the electrochemical performance of the cell. It is demonstrated in **Figure 17** through the comparison of cyclability test results (4 A g^{-1}) that the cycling life of the stainless-steel mesh batteries is significantly less than its carbon cloth counterpart with a 92.5% reduction in charge/discharge cycles before cell failure. Additionally, the stainless-steel cells display a lacking tendency for capacity retention, this is noted during cycles at 200 mA g^{-1} in which the cells displayed a retention of only 80% over 50 cycles. It can also be noted that during the conducting of rate tests, cells with stainless steel substrates displayed larger drops in capacity between cycles at varying current densities. From this comparison we can duly assume that despite being compatible with the system, stainless steel is not an appropriate current collector substrate to accompany CHVO in creating a high performance cathode.
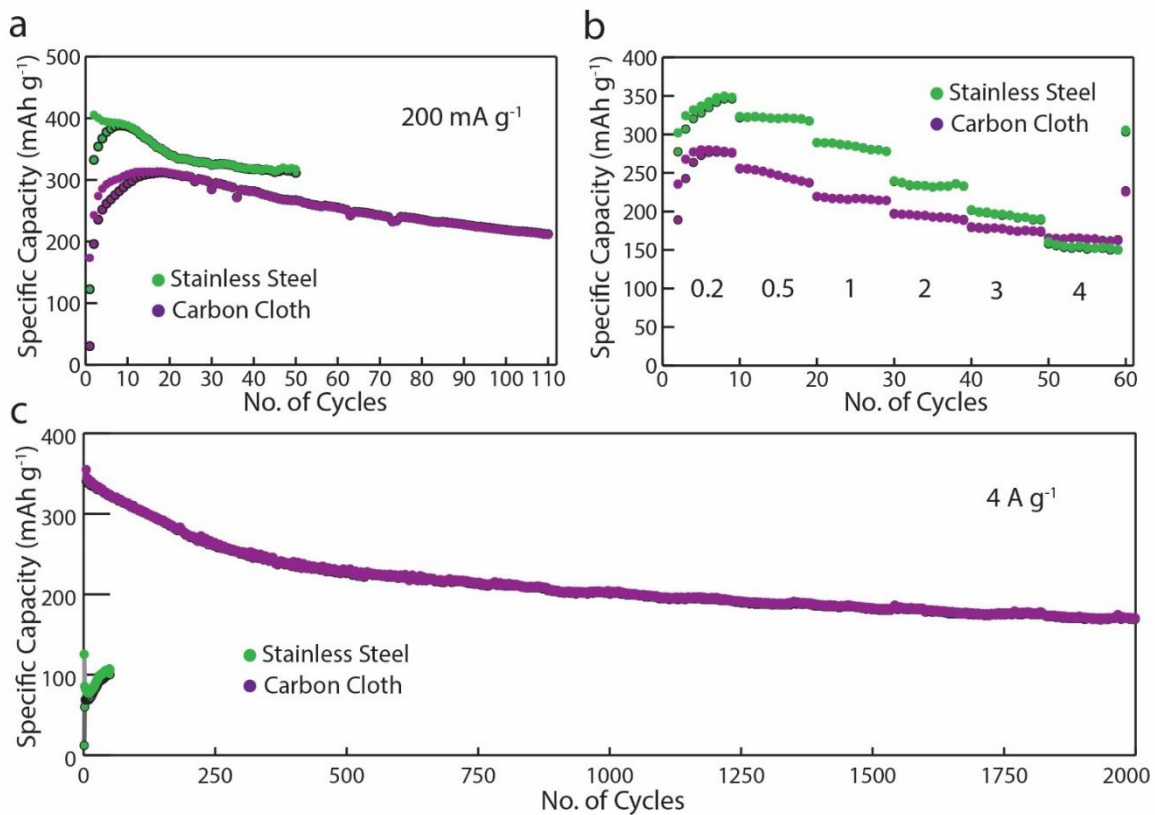
Figure 17: high water stainless steel electrochemical results comparison

Cyclic voltammetry testing was also conducted to highlight the reaction kinetics that occurs within the cathode during the cycling processes. The CV profiles were obtained between 0.2-1.6 V potential range at different scan rates (0.1, 0.2, 0.4, and 1.0 mV s^{-1}). **Figure 5a** shows the CV profile obtained at a scan rate of 0.4 mV s^{-1}. The curve showed two clear redox peaks at 0.53 and 1.04 V during reduction, and 0.73 and 1.2 V during oxidation. The values of these peak locations are identical to the aforementioned plateau-like regions of the charge/discharge profiles, demonstrating both consistency and accuracy across the data. These peaks represent the multi-step reaction mechanism that occurs as a result of the vanadium structure containing multiple valence states, allowing for the reversible redox reactions of +5/+4, +4/+3 and +3/+2 oxidation states. As depicted in **Figure 5b,** all sweep rates returned consistent characteristics further demonstrating the material's strong structural stability during de/intercalation.

The charge storage mechanism of the CHVO cathode can be diffusion-controlled, capacitive-controlled, or a combination of both processes. This can be further investigated through the typical power law relationship $i = av^b$ in which 'a' is a constant and 'b' is the power-law exponent.[54, 55] This equation can be rearranged to $\log(i) = b \times \log(v) + \log(a)$. Thereby, we can plot $\log(i)$ against $\log(v)$, to determine the distinct 'b' value as the gradient. This allows us to predict the level of diffusion-controlled charge storage ($b = 0.5$) compared to surface controlled one ($b = 1$).[10] This is demonstrated in **Figure 5c** by which the cathodic (0.53 V) and the anodic (0.73 V) values are determined to be 0.71 and 0.77, respectively. These voltage values are based on the peak position of the 0.4 mV s^{-1} scan rate, with the assumption that the process was subjected to only negligible amounts of polarisation. Hence, the charge storage mechanism in CHVO material is both diffusion-controlled and capacitive, rendering a high capacity and rate capability.

The CV data were further analysed to calculate the percentage contributions of the two charge storage mechanisms. The $i(V) = k_1 v + k_2 v^{1/2}$ formula can be used for this purpose, where k_2

$v^{1/2}$ and $k_1 v$ denote current response from diffusion-controlled and capacitive processes, respectively.[56] The plotting of $i(V)/v^{1/2}$ against $v^{1/2}$ gives the gradient value of k_1 which can be used to calculate the current response from capacitive processes. **Figure 5d** shows this analysis for scan rate of 0.4 mV s^{-1}, in which the capacitive input was represented as a portion of the complete CV curve. The CHVO electrode displayed 79 % of its charge storage to be capacitive, which is higher than the capacitive contribution of $V_5O_{12}·6H_2O$ nanobelts (50.5 % at 0.4 mV s^{-1}),[10] ball-milled V_2O_5 (56.2 % at 0.4 mV s^{-1}),[56] and $Li_3V_2(PO_4)_3$ (56.5% at 0.6 mV s^{-1})[55] reported in recent studies. The capacitive contribution of CHVO is comparable to that of $Ca_{0.25}V_2O_5·xH_2O$ (76 % at 0.3 mV s^{-1})[57] reported in the previous work. The higher capacitive contribution is attributed to the specific nanoporous architecture of the CHVO material. This indicates the potential of CHVO material to provide both fast and long-term charging capability, something that is essential in today's fast paced society. This analysis was also undertaken for the remaining scan rates of 0.1, 0.2, and 1.0 mV s^{-1} (**Figure 5e**) exhibiting 66%, 72%, and 95% capacitive contribution. Note: In **Figure 5d** shaded area overflows the original CV curve, this is likely due to the polarization of experimental CV curves, as seen in **Figure 5b**, because the use of $i(V) = k_1 v + k_2 v^{1/2}$ formula involves combined analysis of CV curves at different scan rates. For instance, anodic peak at ~0.73 V shifts to ~0.80 V when changing the scan rate from 0.4 mV s^{-1} to 1.0 mV s^{-1}, hence we can expect minor overflows in calculated CV curves.

EIS measurements were conducted to further clarify the observed difference in electrochemical performance of CHVO and CHVO-LW cathode materials. **Figure 5f** shows the EIS curves for CHVO and CHVO-LW electrodes (OCV of CHVO cell was 1.25 V, while the OCV of CHVO-LW cell was 1.30 V during measurement). Gamry Echem Analyst software was used to generate a fitting equivalent circuit, as shown in the inset of **Figure 5f.** R_e denotes the internal resistance of the cell; R_{ct} and W represent a charge transfer resistance and Warburg impedance,

respectively.[58, 59] R_f stands for the $Zn_x(CF_3SO_3)_y(OH)_{2x-y} \cdot nH_2O$- based surface film that can form on the electrode as has been observed in other ZIB systems utilizing the $Zn(CF_3SO_3)_2$ aqueous electrolyte.[60] R_b is added to represent the porosity of the carbon cloth current collector (Note: Bisquert element (R_b) is available in Gamry Echem analyst to represent porous elements). The simulation results are displayed in **Table S1**. As expected, R_e is comparable for both electrodes. However, R_f and R_{ct} of CHVO (25.9 and 60.9 Ohm) are notably higher compared to those of CHVO-LW (13.0 and 36.5 Ohm). This is attributed to the opened layered structure of the CHVO-LW material, encouraging the movement of ions through the material during the first cycles of galvanostatic cycling, thus yielding a high initial capacity as seen in **Figure 4a**. However, the subsequent capacity drop is likely a result of the breakdown of the tunnel structure during cycling owing to insufficient H_2O pillaring within the CHVO-LW material.
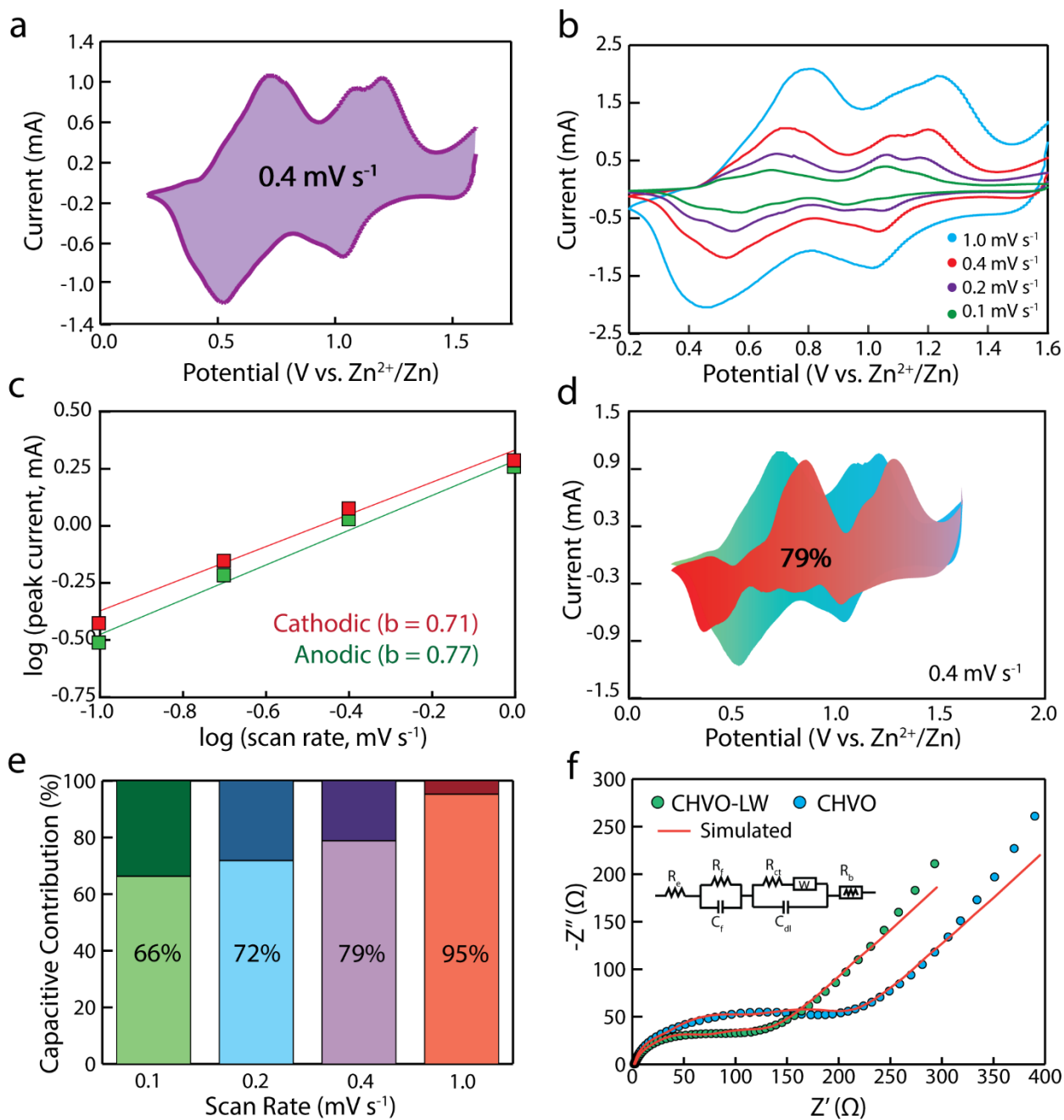
Figure 18: a) CV curve at 0.4 mV s⁻¹; b) CV curves at varying scan rates (0.1-1.0 mV s⁻¹); c) comparative cathode and anode log(peak current) *vs.* log(scan rate) relationship graph; d) Capacitive output percentage at 0.4 mV s⁻¹ scan rate; e) Capacitive output of all other scan rates; f) Comparative EIS analysis of CHVO and CHVO-LW samples.

GITT analysis is utilised to identify the chemical diffusion coefficient (D_s), this was conducted in the potential range 0.2 and 1.6 V depicting a full (dis)charge cycle and was conducted at 50

mA g^{-1}. The resulting curve as shown in **Figure 19a** gives an identical pattern to that of the charge-discharge profiles in **Figure 16b**. Due to the linear behaviour of the cell's potential during constant current input with $\tau^{1/2}$, a simplified version of Fick's Second Law was able to be implemented for the consecutive analysis:

$$D_s = \frac{4}{\tau\,\pi} \times \left(\frac{n_m V_m}{S}\right)^2 \times \left(\frac{dE_s}{dE_t}\right)^2$$

The duration of the 'on time' for each step (in seconds) is depicted by τ, followed by n_m, V_m, and S representing the number of moles, molar volume, and electrode interface area respectively. The molar volume was obtained from the PDF4 database after comparing the sample's XRD data to available compounds. The change in steady state voltage (dE_s) and change in overall cell voltage (dE_t) excluding the IR drop were obtained from the GITT analysis software provided by the Gamry interface 1010E instrument. A concentrated depiction of two steps from the charge cycle are highlighted in **Figure 19b** allowing for a better understanding of the equations' variables. **Figure 19c** demonstrated the change in D_s at different potentials taking the log of the diffusion coefficient (to increase the clarity of changes in the data). In both the charge and discharge cycles two weak minimum regions shown as drops in the y-axis, these are present at the same voltage potentials as the peaks previously noted in the CV analyses. These minima depict the $V^{3+/4+}$ and $V^{4+/5+}$ shifts that occur during cycling highlighting the reduction and oxidation mechanics of the cell. When considering **Figure 19d** in which CHVO is compared to the CHVO-LW, it can be seen that the latter has a higher diffusion coefficient at the second minima position. As the GITT analysis was conducted in the initial stages of the cells' cycling life, the data obtained agrees with the capacity trends displayed in **Figure 16a**.
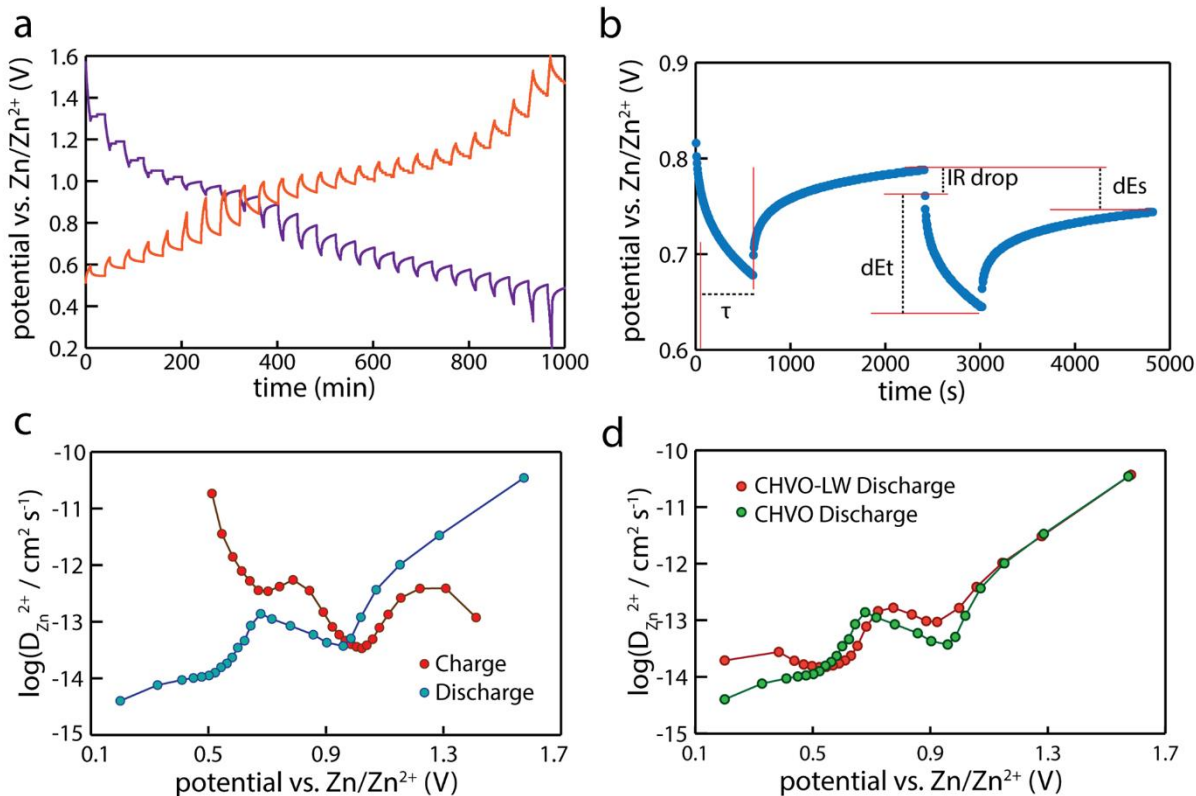
Figure 19: a) GITT profile of CHVO product, b) two selected steps the of GITT profile, c) change in CHVO diffusion coefficient across charge and discharge cycles, d) comparative discharge diffusion coefficients between CHVO and CHVO-LW water samples.

An *ex-situ* XPS analysis was conducted to understand the chemistry behind the charge-storage mechanism of CHVO material. **Figure 20a** shows the high-resolution V 2p spectrum of the pristine electrode (note: this electrode was kept in a coin-cell for 24h before disassembly and analysis). The $V2p_{3/2}$ peak can be deconvoluted into two components at 517.1 and 516.1 eV, which were attributed to +5 and +4 oxidation states. The peak area ratio between these two components was nearly 1:1 denoting an average oxidation state of +4.5 for V. The reduction of the pristine material from +4.7 to +4.5, indicates the partial insertion of Zn^{2+} during the rest period of the cell. After discharging the battery to 0.2 V, two new components appear at 515.6 and 513.8 eV, which can be attributed to +3 and +2 oxidation states of V (**Figure 20b**). Moreover, the intensity of the +5 $V2p_{3/2}$ peak diminished, while +4 peak disappeared. These

observations clearly indicate, the rich redox chemistry of the CHVO material and its reduction upon successful insertion of Zn^{2+} ions as expected. **Figure 20c** displays the high-resolution V 2p spectrum of the CHVO electrode after charging the battery to 1.6 V. Clearly, the intensity of the $V2p_{3/2}$ component at 517.1 eV increased, indicating the re-oxidation of the CHVO material. However, +3 and +2 oxidation states of V were also evident, indicating some irreversibility. This also accounts for the irreversible capacity in the first cycle. **Figure 20d-f** shows high resolution Zn 2p spectra of pristine, discharged (0.2 V) and charged (1.6 V) electrodes. The pristine electrode (soaked in electrolyte) shows the Zn 2p doublet centred at 1021.7 and 1044.8 eV, which is attributed to $2p_{3/2}$ and $2p_{1/2}$ of surface adsorbed Zn^{2+} ions. In fact, adsorption (or partial insertion) of Zn^{2+} ions result in the reduction of CHVO to a certain degree as observed in high resolution V2p spectra of the pristine electrode, even before discharging the cell. Interestingly, after full discharge to 0.2 V, a new Zn2p doublet centred at 1018.1 and 1041.2 eV can be observed, which is attributed $2p_{3/2}$ and $2p_{1/2}$ of Zn^{2+} ions inserted within the VO_5 pyramids and VO_6 octahedral layers of the CHVO material. After charging the electrode to 1.6 V, the intensity of this peak dramatically decreased, indicating the de-insertion of Zn^{2+} ions. However, some Zn^{2+} ions are irreversibly trapped within the CHVO electrode. Although trapped Zn^{2+} ions decrease the initial coulombic efficiency of the battery, these ions are expected to improve the overall conductivity of the material in the long run.
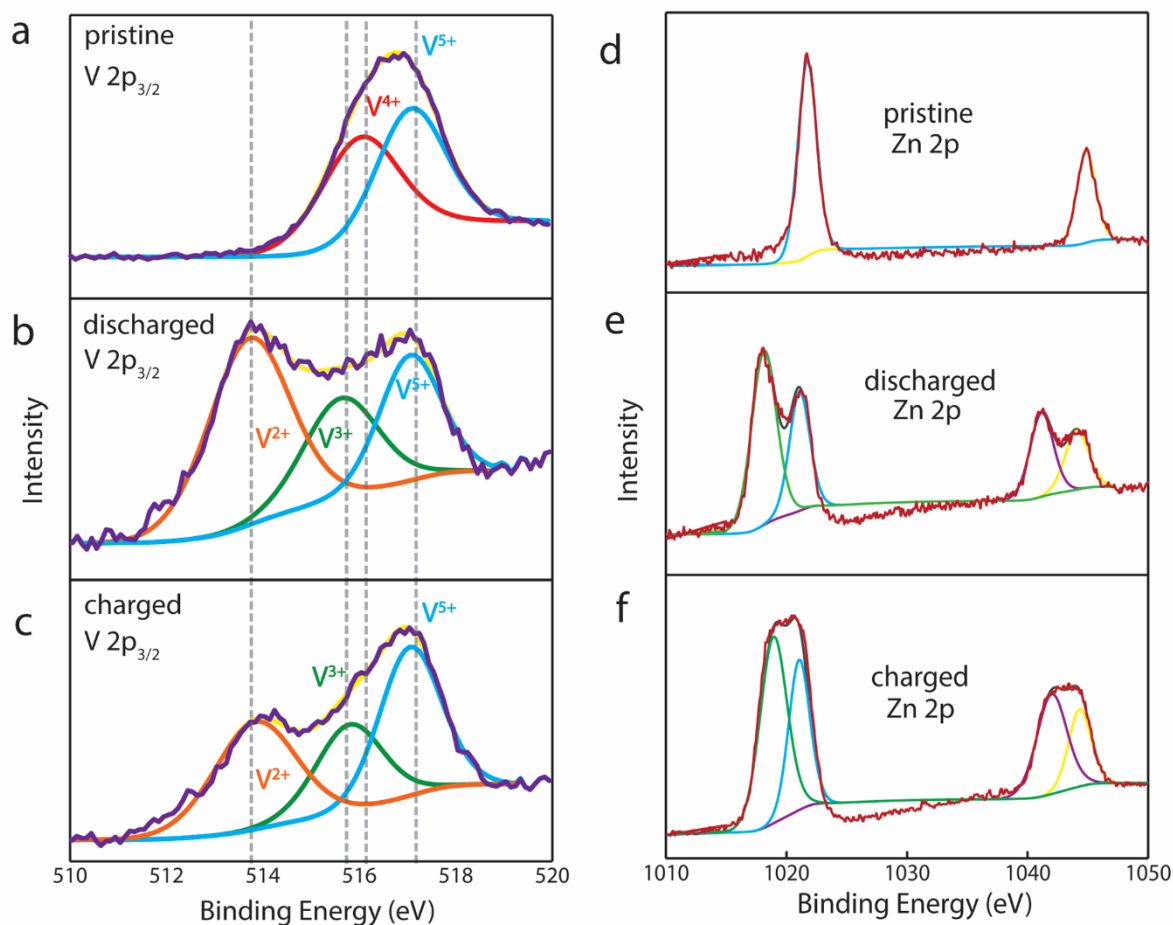
Figure 20: V2p *ex situ* XPS curves of a) pristine, b) discharged, and c) discharged samples, and Zn2p *ex situ* XPS curves of d) pristine, e) discharged, and f) discharged samples.

This material has shown to produce highly electrochemically capable ZIB cells. The data collected, whilst not reaping the highest possible results a zinc battery can provide, do show notable performance and also explore the prospect of simple, hydrated vanadium containing compounds. Other material of this nature does not often fare this well, investigation of literature yields a comparable material only reaching a capacity of 221 mAh g^{-1} at 0.1 A g^{-1} and a cyclability of 1000 cycles at 10 A g^{-1}. This competing material however, despite lacking in capacity and longevity showed exceptional capacity retention and should be duly considered for techniques and design strategies for future electrode materials.[77]

Not only does this material show promising electrochemical performance, but the resulting cell also has a notable shelf life. An experimental cell after fabrication was allowed to remain at rest for approximately three months, however during this time there was a significant amount of self-discharge resulting from deterioration of the AM or unexpected side reactions, however these were not detrimental to the functionality of the cell as demonstrated in **Figure 21**.
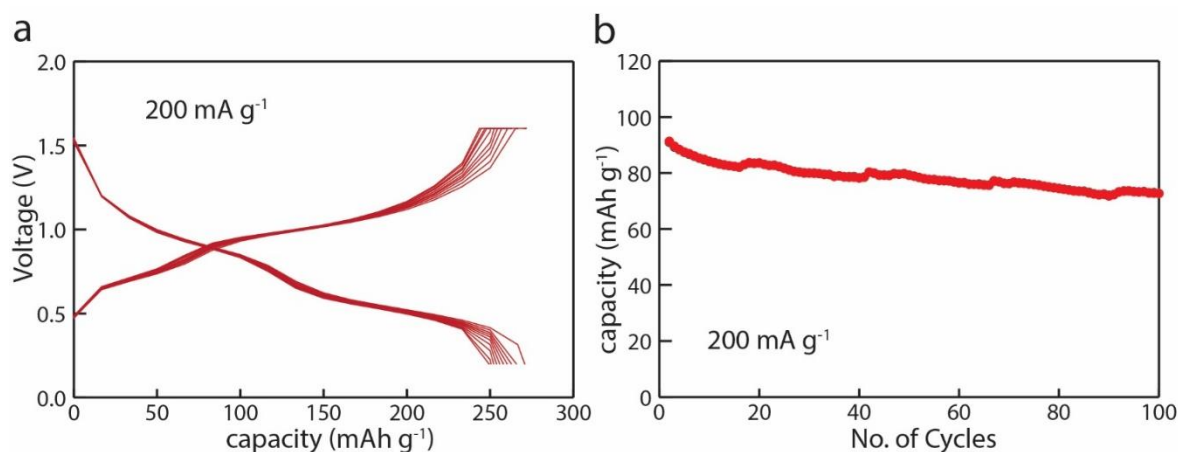
Figure 21: Electrochemical performance of HW CC cell after remaining at rest for 3 months (shelf-life test)

Chapter 6: Discussion and Concluding Statements
6.1. Experimental Project Summary

The above chapters give insight to my experimental project surrounding the use of a hydrated, carbon integrated, layered vanadium oxide nanomaterial as a cathode material for zinc ion battery systems. All stages of a standard, lab-scale cell production procedure are involved, including the solvothermal synthesis, annealing, aging and water addition to create the active material, as well as electrolyte preparation, slurry mixing, and cell fabrication. The cells then underwent various electrochemical tests. In the initial stage of this experimentation many aspects of the process contributed to the premature failure of the cells upon cycling. The first steps taken to troubleshoot this issue was to carefully examine all components involved. The

Zn(SO_4) electrolyte was replaced with the bulky-salt solution Zn(CF_3SO_3)$_2$ to assist the transport of the Zn^{2+} ions as per the information discovered during the writing of the review paper. This showed promising results as the cells were able to achieve 15-20 cycles as opposed 5 cycles in the previous case. After this, the cycled cells were disassembled. It was discovered that the cathode material was not remaining adhered to the foil current collector during cycling, this provided two options for resolution; calendaring, or using a current collector with a rough surface to encourage adhesion. As the laboratory space available did not have the means or equipment for calendaring, the current collector route was further investigated. Initially stainless-steel foil and carbon coated stainless steel foil were being used, this was then changed to Ni foam, carbon cloth, and stainless steel mesh. Ni foam proved to be incompatible with the zinc battery system, however both stainless steel mesh and carbon cloth produced promising results with high specific capacities and cycling lives of over 100 cycles. There was also small concern given to the mildly hydrophobic nature of the carbon cloth, however having the electrodes undergo plasma cleaning to resolve this showed a drop in electrochemical performance presumably due to the interference with the carbon framework within the active material, and as such this method was abandoned and extra attention was taken to ensure that the electrolyte had penetrated the carbon cloth during cell fabrication. Comparative experimentation was then conducted using a material that instead of aging was to be mixed with water to increase the hydration ratio. This material was only found to work to a moderate performance, and thus investigations were initiated into the cause of the downfall. Upon conducting XPS analysis it was determined that the presence of water during the mixing procedure was protecting the material from oxidising, as a result, it still contained large amounts of V(III), and as such the target material had not been obtained. To rectify this, the new method to produce a high water ratio version of the target material was to undergo the usual 20 days of aging before the water mixing stage. This alteration to the synthesis procedure

did correct the material yielded without sacrificing the cells' performance and was used to obtain the reported electrochemical data.

Material characterisation played a large role in this project and was thoroughly undertaken in order confirm the make-up and structure of the material including the presence of the carbon framework, the amount of hydration in each version, and to confirm the enlargement of the interlayer spacing as a result of these assets. As noted in the submitted article, the character analysis of the material showed it to be the target material with a notable carbon framework, water contents of 2.7 and 0.4 per formula unit of $V_5O_{12} \cdot nH_2O$, and interlayer spacings of 13 and 12.8 Å respectively.

The results of the electrochemical experimentation showed that synthesised $V_5O_{12} \cdot 2.7H_2O$ material to be a high-performance material as it showed a relatively high specific capacity 396 mAh g^{-1} at 250 mA g^{-1}) compared to many ZIB systems as demonstrated in *Table 1* of the review paper. It also compared well in terms of cyclability reaching over 3300 cycles at 4 A g^{-1}.

The proposed mechanism for the CHVO material is derived from the data obtained via ex situ XPS analysis. The basic dis/charge mechanism is depicted in figure 22 showing the reversible redox reaction cause by the de/intercalation of Zn^{2+} ions into the material. During discharge the reduction of the $V^{4+/5+}$ into $V^{2+/3+}$ with minimal amount of the original oxidation state remaining. However, the reaction is shown not to be completely reversible as small $V^{2+/3+}$ peaks are still present in the ex situ XPS spectra after the cell has been charged and the oxidation reaction completed. This phenomenon accounts for the notable drop in capacity during the initial cycles of the battery cells' galvanostatic testing.
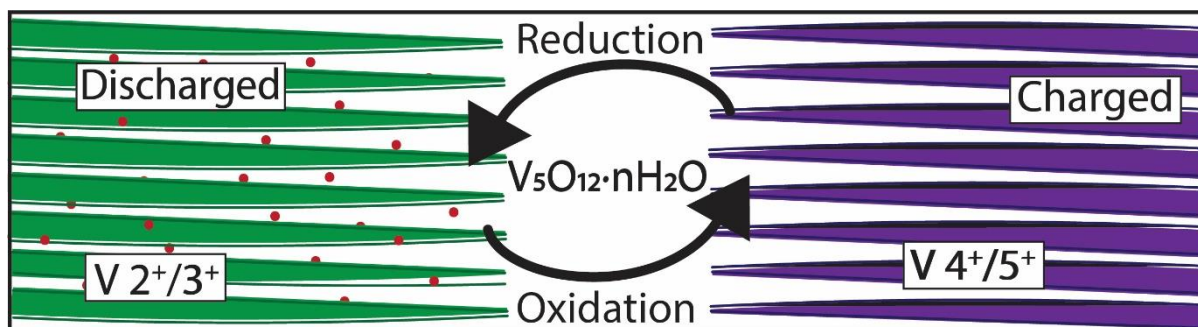
Figure 22: Schematic depicting basic insertion mechanism and resultant oxidation states of CHVO material

6.2. Relevance to Thesis Objective

The introductory chapter of this thesis highlights significant gaps in the knowledge and development of zinc ion batteries, namely that concerning cathodic active materials and their Zn^{2+} intercalation capabilities. Many cathodes struggle with ion diffusion due to limited interlayer spacing and electrostatic interactions between the tunnel walls and the Zn^{2+}, with additional concerns surrounding the conductivity of the materials. The previously disclosed review article discusses a wide variety of in-development techniques that can be incorporated into the synthesis procedure in order to resolve a specific issue impacting the overall and/or an aspect of the cells' electrochemical performance. Notable examples include the integration of structural molecules, carbon/graphite enhancement, and specific engineering of the materials' morphology. These tactics can be utilised in tandem or independently at the discretion of the individual researcher or team.

The project highlighted in this thesis explores the use of all of the aforementioned techniques in a layered vanadium oxide material. This carbon integrated, hydrated, vanadium oxide (CHVO), $V_5O_{12} \cdot 2.7H_2O$, is being used for the first time in a zinc ion battery system.

The objective of the thesis is to document the successful synthesis and implementation of an inorganic ZIB cathodic nanomaterial that performs to a high standard in a full coin-cell format.

The resulting was a high purity cathode nanomaterial with suitable interlayer spacing for optimal zinc ion insertion and reaction sites without sacrificing the longevity or structural stability of the cell in addition to increased conductivity and tunnel lubricating effects.

6.3. Scientific Importance

The ongoing development of energy storage systems is extremely critical for both the scientific and industrial communities. With current universal energy consumption trends and forecasts painting a bleak picture for the future of the currently in place systems, researchers are scrambling to develop a new and innovative alternative.

For the time being, lithium battery systems are admirably fulfilling the role, however between their dwindling material availability, and plethora of safety and environmental concerns, they are not an ideal system for the World to turn to looking to the future. Due to this dilemma, the scientific community is putting much emphasis on rectifying the issue that plague varying alternate metal ion battery systems to investigate and justify their potential as a wide-use ESS in preparation for the on-coming swell in demand. To this end, the insight gained through this project makes notable contribution to the ever-increasing knowledge pool of materials, techniques, variables, and investigations. Not only did we perform a complex analysis of hydration, carbon additives, and morphology manipulation in a new form of a highly renowned cathode material, we also conducted comparative experimentation, studying the effects of varying the water ratio within the material structure, and the current collector substrate onto which the active material was coated. Both of these additional items are not only relevant for our material, but also for any layered cathode structure being developed for implementation into zinc ion battery systems. From this, we can clearly see the high scientific value that projects such as this provide to the community. By increasing the amount of relevant and usable information available to the wider research community, we are ever building-up the

development of technologies that will enable the Worlds' progression into a clean, reliable, and renewable future.

6.4. List of Relevant Publications

Vanadium-Containing Layered Materials as High-Performance Cathodes for Aqueous Zinc-Ion Batteries

Advanced Materials Technologies

DOI: 10.1002/admt.202100505

Carbon-integrated vanadium oxide hydrate as a high-performance cathode material for aqueous zinc-ion batteries

ACS Applied Energy Materials (Accepted for Publication)

DOI: 10.1021/acsaem.1c03517

ORCID ID: https://orcid.org/0000-0001-6604-9075

Bibliography

1.   Li, R.; Zhang, H.; Zheng, Q.; Li, X., Porous V_2O_5 Yolk–Shell Microspheres for Zinc Ion Battery Cathodes: Activation Responsible for Enhanced Capacity and Rate Performance. *J. Mater. Chem. A* **2020,** *8* (10), 5186-5193.

2.   Wang, X.; Li, Y.; Wang, S.; Zhou, F.; Das, P.; Sun, C.; Zheng, S.; Wu, Z.-S., 2d Amorphous V2o5/Graphene Heterostructures for High-Safety Aqueous Zn-Ion Batteries with Unprecedented Capacity and Ultrahigh Rate Capability. *Adv. Energy Mater.* **2020,** *10* (22), 2000081.

3.   Zhang, N.; Dong, Y.; Jia, M.; Bian, X.; Wang, Y.; Qiu, M.; Xu, J.; Liu, Y.; Jiao, L.; Cheng, F., Rechargeable Aqueous Zn–V_2O_5 Battery with High Energy Density and Long Cycle Life. *ACS Energy Lett.* **2018,** *3* (6), 1366-1372.

4.   Chen, S.; Li, K.; Hui, K. S.; Zhang, J., Regulation of Lamellar Structure of Vanadium Oxide Via Polyaniline Intercalation for High-Performance Aqueous Zinc-Ion Battery. *Adv. Funct. Mater.* **2020,** *30* (43), 2003890.

5.   Chen, X.; Wang, L.; Li, H.; Cheng, F.; J., C., Porous V_2O_5 Nanofibers as Cathode Materials for Rechargeable Aqueous Zinc-Ion Batteries. *Journal of Energy Chemistry* **2019,** *38*, 20-25.

6.   Javed, M. S.; Lei, H.; Wang, Z.; Liu, B.-t.; Cai, X.; Mai, W., 2d V_2O_5 Nanosheets as a Binder-Free High-Energy Cathode for Ultrafast Aqueous and Flexible Zn-Ion Batteries. *Nano Energy* **2020,** *70*, 104573.

7.   Luo, H.; Wang, B.; Wang, F.; Yang, J.; Wu, F.; Ning, Y.; Zhou, Y.; Wang, D.; Liu, H.; Dou, S., Anodic Oxidation Strategy toward Structure-Optimized V_2O_3 Cathode Via Electrolyte Regulation for Zn-Ion Storage. *ACS Nano* **2020,** *14* (6), 7328-7337.

8.   Ding, Y.; Peng, Y.; Chen, S.; Zhang, X.; Li, Z.; Zhu, L.; Mo, L.-E.; Hu, L., Hierarchical Porous Metallic V_2O_3@C for Advanced Aqueous Zinc-Ion Batteries. *ACS Appl. Mater. Inter.* **2019,** *11* (47), 44109-44117.

9.   Ding, J.; Du, Z.; Gu, L.; Li, B.; Wang, L.; Wang, S.; Gong, Y.; Yang, S., Ultrafast Zn2+ Intercalation and Deintercalation in Vanadium Dioxide. *Adv. Mater.* **2018,** *30* (26), 1800762.

10.   Chen, L.; Ruan, Y.; Zhang, G.; Wei, Q.; Jiang, Y.; Xiong, T.; He, P.; Yang, W.; Yan, M.; An, Q.; Mai, L., Ultrastable and High-Performance Zn/VO_2 Battery Based on a Reversible Single-Phase Reaction. *Chem. Mater.* **2019,** *31* (3), 699-706.

11.   Li, Z.; Ganapathy, S.; Xu, Y.; Zhou, Z.; Sarilar, M.; Wagemaker, M., Mechanistic Insight into the Electrochemical Performance of Zn/VO$_2$ Batteries with an Aqueous Znso4 Electrolyte. *Adv. Energy Mater.* **2019,** *9* (22), 1900237.

12.   Cao, Z.; Wang, L.; Zhang, H.; Zhang, X.; Liao, J.; Dong, J.; Shi, J.; Zhuang, P.; Cao, Y.; Ye, M.; Shen, J.; Ajayan, P. M., Localized Ostwald Ripening Guided Dissolution/Regrowth to Ancient Chinese Coin-Shaped VO$_2$ Nanoplates with Enhanced Mass Transfer for Zinc Ion Storage. *Adv. Funct. Mater.* **2020,** *30* (25), 2000472.

13.   Lin, Y.; Zhou, F.; Xie, M.; Zhang, S.; Deng, C., V$_6$O$_{13}$−Δ@C Nanoscrolls with Expanded Distances between Adjacent Shells as a High-Performance Cathode for a Knittable Zinc-Ion Battery. *ChemSusChem* **2020,** *13* (14), 3696-3706.

14.   Liao, M.; Wang, J.; Ye, L.; Sun, H.; Wen, Y.; Wang, C.; Sun, X.; Wang, B.; Peng, H., A Deep-Cycle Aqueous Zinc-Ion Battery Containing an Oxygen-Deficient Vanadium Oxide Cathode. *Angew. Chem., Int. Ed.* **2020,** *59* (6), 2273-2278.

15.   Zhang, N.; Jia, M.; Dong, Y.; Wang, Y.; Xu, J.; Liu, Y.; Jiao, L.; Cheng, F., Hydrated Layered Vanadium Oxide as a Highly Reversible Cathode for Rechargeable Aqueous Zinc Batteries. *Adv. Funct. Mater.* **2019,** *29* (10), 1807331.

16.   Feng, J.; Wang, Y.; Liu, S.; Chen, S.; Wen, N.; Zeng, X.; Dong, Y.; Huang, C.; Kuang, Q.; Zhao, Y., Electrochemically Induced Structural and Morphological Evolutions in Nickel Vanadium Oxide Hydrate Nanobelts Enabling Fast Transport Kinetics for High-Performance Zinc Storage. *ACS Appl. Mater. Interfaces* **2020,** *12* (22), 24726-24736.

17.   Li, G.; Yang, Z.; Jiang, Y.; Jin, C.; Huang, W.; Ding, X.; Huang, Y., Towards Polyvalent Ion Batteries: A Zinc-Ion Battery Based on Nasicon Structured Na$_3$V$_2$(PO$_4$)$_3$. *Nano Energy* **2016,** *25*, 211-217.

18.   Zhang, H.; Liu, X.; Li, H.; Qin, B.; Passerini, S., High-Voltage Operation of a V$_2$O$_5$ Cathode in a Concentrated Gel Polymer Electrolyte for High-Energy Aqueous Zinc Batteries. *ACS Appl. Mater. Inter.* **2020,** *12* (13), 15305-15312.

19.   Islam, S.; Alfaruqi, M. H.; Putro, D. Y.; Soundharrajan, V.; Sambandam, B.; Jo, J.; Park, S.; Lee, S.; Mathew, V.; Kim, J., K$^+$ Intercalated V$_2$O$_5$ Nanorods with Exposed Facets as Advanced Cathodes for High Energy and High Rate Zinc-Ion Batteries. *J. Mater. Chem. A* **2019,** *7* (35), 20335-20347.

20.   Islam, S.; Alfaruqi, M. H.; Sambandam, B.; Putro, D. Y.; Kim, S.; Jo, J.; Kim, S.; Mathew, V.; Kim, J., A New Rechargeable Battery Based on a Zinc Anode and a NaV$_6$O$_{15}$ Nanorod Cathode. *Chem. Commun.* **2019,** *55* (26), 3793-3796.

21.   Mathew, V.; Sambandam, B.; Kim, S.; Kim, S.; Park, S.; Lee, S.; Alfaruqi, M. H.; Soundharrajan, V.; Islam, S.; Putro, D. Y.; Hwang, J.-Y.; Sun, Y.-K.; Kim, J., Manganese and Vanadium Oxide Cathodes for Aqueous Rechargeable Zinc-Ion Batteries: A Focused

View on Performance, Mechanism, and Developments. *Acs. Energy. Lett.* **2020,** *5* (7), 2376-2400.

22.   Yang, Z.; Zhang, J.; Kintner-Meyer, M. C. W.; Lu, X.; Choi, D.; Lemmon, J. P.; Liu, J., Electrochemical Energy Storage for Green Grid. *Chemical Reviews* **2011,** *111* (5), 3577-3613.

23.   Song, M.; Tan, H.; Chao, D.; Fan, H. J., Recent Advances in Zn-Ion Batteries. *Adv. Funct. Mater.* **2018,** *28* (41), 1802564.

24.   Geng, H.; Cheng, M.; Wang, B.; Yang, Y.; Zhang, Y.; Li, C. C., Zinc-Ion Batteries: Electronic Structure Regulation of Layered Vanadium Oxide Via Interlayer Doping Strategy toward Superior High-Rate and Low-Temperature Zinc-Ion Batteries. *Adv. Funct. Mater.* **2020,** *30* (6), 2070034.

25.   Carbone, R., *Energy Storage in the Emerging Era of Smart Grids*. BoD–Books on Demand: 2011.

26.   Vikstrom, H.; Davidsson, S.; Hook, M., Lithium Availability and Future Production Outlooks. *Appl. Energ.* **2013,** *110*, 252-266.

27.   Wei, T. Y.; Li, Q.; Yang, G. Z.; Wang, C. X., Pseudo-Zn-Air and Zn-Ion Intercalation Dual Mechanisms to Realize High-Areal Capacitance and Long-Life Energy Storage in Aqueous Zn Battery. *Adv. Energy. Mater.* **2019,** *9* (34).

28.   Zhang, N.; Jia, M.; Dong, Y.; Wang, Y. Y.; Xu, J. Z.; Liu, Y. C.; Jiao, L. F.; Cheng, F. Y., Hydrated Layered Vanadium Oxide as a Highly Reversible Cathode for Rechargeable Aqueous Zinc Batteries. *Adv. Funct. Mater.* **2019,** *29* (10).

29.   Wang, Q.; Sun, J.; Chu, G., Lithium Ion Battery Fire and Explosion. *Fire Safety Science* **2005,** *8*, 375-382.

30.   MacNeil, D. D.; Dahn, J. R., The Reaction of Charged Cathodes with Nonaqueous Solvents and Electrolytes - Ii. $LiMn_2O_4$ Charged to 4.2 V. *J. Electrochem. Soc.* **2001,** *148* (11), A1211-A1215.

31.   MacNeil, D. D.; Dahn, J. R., The Reactions of $Li_{0.5}COO_2$ with Nonaqueous Solvents at Elevated Temperatures. *J. Electrochem. Soc.* **2002,** *149* (7), A912-A919.

32.   Jiang, H.; Zhang, Y.; Pan, Z.; Xu, L.; Zheng, J.; Gao, Z.; Hu, T.; Meng, C.; Wang, J., $Nh_4V_3O_8 \cdot 0.5H_2O$ Nanobelts with Intercalated Water Molecules as a High Performance Zinc Ion Battery Cathode. *Mater. Chem. Front.* **2020,** *4* (5), 1434-1443.

33.   Liu, Z.; Huang, Y.; Huang, Y.; Yang, Q.; Li, X.; Huang, Z.; Zhi, C., Voltage Issue of Aqueous Rechargeable Metal-Ion Batteries. *Chem. Soc. Rev.* **2020**.

34.   Xu, C.; Li, B.; Du, H.; Kang, F., Energetic Zinc Ion Chemistry: The Rechargeable Zinc Ion Battery. *Angew. Chem* **2012,** *51* (4), 933-5.

35.   Hu, E.; Yang, X. Q., Rejuvenating Zinc Batteries. *Nat. Mater.* **2018,** *17* (6), 480-481.

36.   Zhu, C. Y.; Fang, G. Z.; Zhou, J.; Guo, J. H.; Wang, Z. Q.; Wang, C.; Li, J. Y.; Tang, Y.; Liang, S. Q., Binder-Free Stainless Steel@Mn3o4 Nanoflower Composite: A High-Activity Aqueous Zinc-Ion Battery Cathode with High-Capacity and Long-Cycle-Life. *J. Mater. Chem. A* **2018,** *6* (20), 9677-9683.

37.   Qiu, N.; Yang, Z.; Wang, Y.; Zhu, Y.; Liu, W., A High-Power and Long-Life Aqueous Rechargeable Zn-Ion Battery Based on Hierarchically Porous Sodium Vanadate. *Chem. Commun.* **2020,** *56* (64), 9174-9177.

38.   Zhang, N.; Cheng, F.; Liu, Y.; Zhao, Q.; Lei, K.; Chen, C.; Liu, X.; Chen, J., Cation-Deficient Spinel Znmn2o4 Cathode in $Zn(CF_3SO_3)_2$ Electrolyte for Rechargeable Aqueous Zn-Ion Battery. *J Am Chem Soc* **2016,** *138* (39), 12894-12901.

39.   Wang, Y.; Takahashi, K.; Lee, K.; Cao, G. Z., Nanostructured Vanadium Oxide Electrodes for Enhanced Lithium-Ion Intercalation. *Adv. Funct. Mater.* **2006,** *16* (9), 1133-1144.

40.   Ming, J.; Guo, J.; Xia, C.; Wang, W. X.; Alshareef, H. N., Zinc-Ion Batteries: Materials, Mechanisms, and Applications. *Mat. Sci. Eng. R* **2019,** *135*, 58-84.

41.   Xu, X.; Xiong, F.; Meng, J.; Wang, X.; Niu, C.; An, Q.; Mai, L., Vanadium-Based Nanomaterials: A Promising Family for Emerging Metal-Ion Batteries. *Adv. Funct. Mater.* **2020,** *30* (10), 1904398.

42.   Zhang, M.; Liang, R.; Or, T.; Deng, Y.-P.; Yu, A.; Chen, Z., Recent Progress on High-Performance Cathode Materials for Zinc-Ion Batteries. *Small Structures* **2021,** *2* (2), 2000064.

43.   Fernando, J. F. S.; Siriwardena, D. P.; Firestein, K. L.; Zhang, C.; von Treifeldt, J. E.; Lewis, C.-E. M.; Wang, T.; Dubal, D. P.; Golberg, D. V., Enriched Pseudocapacitive Lithium Storage in Electrochemically Activated Carbonaceous Vanadium(Iv, V) Oxide Hydrate. *J. Mater. Chem. A* **2020,** *8* (26), 13183-13196.

44.   Augustyn, V.; Simon, P.; Dunn, B., Pseudocapacitive Oxide Materials for High-Rate Electrochemical Energy Storage. *Energ. Environ. Sci.* **2014,** *7* (5), 1597-1614.

45.   Beaudrouet, E.; La Salle, A. L. G.; Guyomard, D., Nanostructured Manganese Dioxides: Synthesis and Properties as Supercapacitor Electrode Materials. *Electrochim. Acta* **2009,** *54* (4), 1240-1248.

46.   Wan, F.; Niu, Z., Design Strategies for Vanadium-Based Aqueous Zinc-Ion Batteries. *Angew. Chem* **2019,** *58* (46), 16358-16367.

47.   Xu, G.; Liu, X.; Huang, S.; Li, L.; Wei, X.; Cao, J.; Yang, L.; Chu, P. K., Freestanding, Hierarchical, and Porous Bilayered $Na_xV_2O_5 \cdot NH_2O$/RGO/CNT Composites as High-Performance Cathode Materials for Nonaqueous K-Ion Batteries and Aqueous Zinc-Ion Batteries. *ACS Appl. Mater. Inter.* **2020,** *12* (1), 706-716.

48.   Li, Z.; Ren, Y.; Mo, L.; Liu, C.; Hsu, K.; Ding, Y.; Zhang, X.; Li, X.; Hu, L.; Ji, D.; Cao, G., Impacts of Oxygen Vacancies on Zinc Ion Intercalation in Vo2. *ACS Nano* **2020,** *14* (5), 5581-5589.

49.   Yan, M.; He, P.; Chen, Y.; Wang, S.; Wei, Q.; Zhao, K.; Xu, X.; An, Q.; Shuang, Y.; Shao, Y.; Mueller, K. T.; Mai, L.; Liu, J.; Yang, J., Water-Lubricated Intercalation in V2o5·Nh2o for High-Capacity and High-Rate Aqueous Rechargeable Zinc Batteries. *Adv. Mater.* **2018,** *30* (1), 1703725.

50.   Chen, T.; Zhu, X.; Chen, X.; Zhang, Q.; Li, Y.; Peng, W.; Zhang, F.; Fan, X., VS_2 Nanosheets Vertically Grown on Graphene as High-Performance Cathodes for Aqueous Zinc-Ion Batteries. *J. Power Sources* **2020,** *477*, 228652.

51.   Pan, Z.; Yang, J.; Yang, J.; Zhang, Q.; Zhang, H.; Li, X.; Kou, Z.; Zhang, Y.; Chen, H.; Yan, C.; Wang, J., Stitching of $Zn_3(OH)_2V_2O_7 \cdot 2H_2O$ 2d Nanosheets by 1d Carbon Nanotubes Boosts Ultrahigh Rate for Wearable Quasi-Solid-State Zinc-Ion Batteries. *ACS Nano* **2020,** *14* (1), 842-853.

52.   Fernando, J. F. S.; Zhang, C.; Firestein, Konstantin L.; Nerkar, J. Y.; Golberg, D. V., Zno Quantum Dots Anchored in Multilayered and Flexible Amorphous Carbon Sheets for High Performance and Stable Lithium Ion Batteries. *J. Mater. Chem. A* **2019,** *7* (14), 8460-8471.

53.   Wei, T.; Li, Q.; Yang, G.; Wang, C., Pseudo-Zn–Air and Zn-Ion Intercalation Dual Mechanisms to Realize High-Areal Capacitance and Long-Life Energy Storage in Aqueous Zn Battery. *Adv. Energy Mater.* **2019,** *9* (34), 1901480.

54.   Fang, G. Z.; Zhou, J.; Pan, A. Q.; Liang, S. Q., Recent Advances in Aqueous Zinc-Ion Batteries. *Acs. Energy. Lett.* **2018,** *3* (10), 2480-2501.

55.   Zhang, N.; Cheng, F.; Liu, Y.; Zhao, Q.; Lei, K.; Chen, C.; Liu, X.; Chen, J., Cation-Deficient Spinel $ZnMn_2O_4$ Cathode in $Zn(CF_3SO_3)_2$ Electrolyte for Rechargeable Aqueous Zn-Ion Battery. *J. Am. Chem. Soc.* **2016,** *138* (39), 12894-12901.

56.   Liu, Z.; Huang, Y.; Huang, Y.; Yang, Q.; Li, X.; Huang, Z.; Zhi, C., Voltage Issue of Aqueous Rechargeable Metal-Ion Batteries. *Chem. Soc. Rev.* **2020,** *49* (1), 180-232.

57.   Narayanasamy, M.; Kirubasankar, B.; Shi, M.; Velayutham, S.; Wang, B.; Angaiah, S.; Yan, C., Morphology Restrained Growth of V_2O_5 by the Oxidation of V-Mxenes as a Fast Diffusion Controlled Cathode Material for Aqueous Zinc Ion Batteries. *Chem. Commun.* **2020,** *56* (47), 6412-6415.

58.   Ponrouch, A.; Bitenc, J.; Dominko, R.; Lindahl, N.; Johansson, P.; Palacin, M. R., Multivalent Rechargeable Batteries. *Energy Storage Mater* **2019,** *20*, 253-262.

59.   Zhou, W.; Chen, J.; Chen, M.; Wang, A.; Huang, A.; Xu, X.; Xu, J.; Wong, C.-P., An Environmentally Adaptive Quasi-Solid-State Zinc-Ion Battery Based on Magnesium Vanadate Hydrate with Commercial-Level Mass Loading and Anti-Freezing Gel Electrolyte. *J. Mater. Chem. A* **2020,** *8* (17), 8397-8409.

60.   Xu, C.; Chen, Y.; Shi, S.; Li, J.; Kang, F.; Su, D., Secondary Batteries with Multivalent Ions for Energy Storage. *Sci Rep* **2015,** *5*, 14120.

61.   Chang, Z.; Yang, Y.; Wang, X.; Li, M.; Fu, Z.; Wu, Y.; Holze, R., Hybrid System for Rechargeable Magnesium Battery with High Energy Density. *Scientific Reports* **2015,** *5* (1), 11931.

62.   Ru, Y.; Zheng, S.; Xue, H.; Pang, H., Different Positive Electrode Materials in Organic and Aqueous Systems for Aluminium Ion Batteries. *J. Mater. Chem. A* **2019,** *7* (24), 14391-14418.

63.   Wippermann, K.; Schultze, J. W.; Kessel, R.; Penninger, J., The Inhibition of Zinc Corrosion by Bisaminotriazole and Other Triazole Derivatives. *Corrosion Science* **1991,** *32* (2), 205-230.

64.   Shin, J.; Lee, J.; Park, Y.; Choi, J. W., Aqueous Zinc Ion Batteries: Focus on Zinc Metal Anodes. *Chemical Science* **2020,** *11* (8), 2028-2044.

65.   Tang, B. Y.; Shan, L. T.; Liang, S. Q.; Zhou, J., Issues and Opportunities Facing Aqueous Zinc-Ion Batteries. *Energ. Environ. Sci.* **2019,** *12* (11), 3288-3304.

66.   Xia, C.; Guo, J.; Lei, Y.; Liang, H.; Zhao, C.; Alshareef, H. N., Rechargeable Aqueous Zinc-Ion Battery Based on Porous Framework Zinc Pyrovanadate Intercalation Cathode. *Adv. Mater.* **2018,** *30* (5), 1705580.

67.   Jiang, H.; Zhang, Y.; Pan, Z.; Xu, L.; Zheng, J.; Gao, Z.; Hu, T.; Meng, C., Facile Hydrothermal Synthesis and Electrochemical Properties of $(NH_4)_2V_{10}O_{25} \cdot 8H_2O$ Nanobelts for High-Performance Aqueous Zinc Ion Batteries. *Electrochim. Acta* **2020,** *332*, 135506.

68.   Wang, X.; Li, Y.; Wang, S.; Zhou, F.; Das, P.; Sun, C.; Zheng, S.; Wu, Z.-S., Zinc-Ion Batteries: 2d Amorphous V_2O_5/Graphene Heterostructures for High-Safety Aqueous Zn-Ion Batteries with Unprecedented Capacity and Ultrahigh Rate Capability. *Adv. Energy. Mater.* **2020,** *10* (22), 2070100.

69.   Hou, Z.; Tan, H.; Gao, Y.; Li, M.; Lu, Z.; Zhang, B., Tailoring Desolvation Kinetics Enables Stable Zinc Metal Anodes. *J. Mater. Chem. A* **2020,** *8* (37), 19367-19374.

70.   Xue, T.; Fan, H. J., From Aqueous Zn-Ion Battery to Zn-Mno2 Flow Battery: A Brief Story. *Journal of Energy Chemistry* **2021,** *54*, 194-201.

71.   Selvakumaran, D.; Pan, A. Q.; Liang, S. Q.; Cao, G. Z., A Review on Recent Developments and Challenges of Cathode Materials for Rechargeable Aqueous Zn-Ion Batteries. *J. Mater. Chem. A* **2019,** *7* (31), 18209-18236.

72.   Cao, J.; Zhang, D.; Zhang, X.; Sawangphruk, M.; Qin, J.; Liu, R., A Universal and Facile Approach to Suppress Dendrite Formation for a Zn and Li Metal Anode. *J. Mater. Chem. A* **2020,** *8* (18), 9331-9344.

73.   Wang, L.; Wu, Z.; Jiang, M.; Lu, J.; Huang, Q.; Zhang, Y.; Fu, L.; Wu, M.; Wu, Y., Layered Vse2: A Promising Host for Fast Zinc Storage and Its Working Mechanism. *J. Mater. Chem. A* **2020,** *8* (18), 9313-9321.

74.   Yang, G.; Li, Q.; Ma, K.; Hong, C.; Wang, C., The Degradation Mechanism of Vanadium Oxide-Based Aqueous Zinc-Ion Batteries. *J. Mater. Chem. A* **2020,** *8* (16), 8084-8095.

75.   Zhang, N.; Cheng, F.; Liu, J.; Wang, L.; Long, X.; Liu, X.; Li, F.; Chen, J., Rechargeable Aqueous Zinc-Manganese Dioxide Batteries with High Energy and Power Densities. *Nat. Commun.* **2017,** *8* (1), 405.

76.   Chen, D.; Lu, M.; Wang, B.; Cheng, H.; Yang, H.; Cai, D.; Han, W.; Fan, H. J., High-Mass Loading V3o7·H2o Nanoarray for Zn-Ion Battery: New Synthesis and Two-Stage Ion Intercalation Chemistry. *Nano Energy* **2021,** *83*, 105835.

77.   Zhang, Q.; Zhang, Y.; Fu, L.; Liu, S.; Yang, H., A Novel and Improved Hydrophilic Vanadium Oxide-Based Cathode for Aqueous Zn-Ion Batteries. *Electrochim. Acta* **2020,** *354*, 136721.

78.   Zhang, Y.; Ang, E. H.; Dinh, K. N.; Rui, K.; Lin, H.; Zhu, J.; Yan, Q., Recent Advances in Vanadium-Based Cathode Materials for Rechargeable Zinc Ion Batteries. *Mater. Chem. Front.* **2021,** *5* (2), 744-762.

79.   Liu, X.; Xu, G.; Zhang, Q.; Huang, S.; Li, L.; Wei, X.; Cao, J.; Yang, L.; Chu, P. K., Ultrathin Hybrid Nanobelts of Single-Crystalline VO2 and Poly(3,4-Ethylenedioxythiophene) as Cathode Materials for Aqueous Zinc Ion Batteries with Large Capacity and High-Rate Capability. *J. Power Sources* **2020,** *463*, 228223.

80.   Liu, Y.; Li, C.; Xu, J.; Ou, M.; Fang, C.; Sun, S.; Qiu, Y.; Peng, J.; Lu, G.; Li, Q.; Han, J.; Huang, Y., Electroactivation-Induced Spinel ZnV2O4 as a High-Performance Cathode Material for Aqueous Zinc-Ion Battery. *Nano Energy* **2020,** *67*, 104211.

81.   Zhang, N.; Chen, X.; Yu, M.; Niu, Z.; Cheng, F.; Chen, J., Materials Chemistry for Rechargeable Zinc-Ion Batteries. *Chem. Soc. Rev.* **2020,** *49* (13), 4203-4219.

82.   Yang, J.; Lana, T.; Liub, J.; Songa, Y.; Wei, M., Supercapacitor Electrode of Hollow Spherical V_2O_5 with a High Pseudocapacitance in Aqueous Solution. *Electrochim. Acta* **2013,** *105*, 489-495.

83.   Zhu, Q.; Xiao, Q.; Zhang, B.; Yan, Z.; Liu, X.; Chen, S.; Ren, Z.; Yu, Y., Vs4 with a Chain Crystal Structure Used as an Intercalation Cathode for Aqueous Zn-Ion Batteries. *J. Mater. Chem. A* **2020,** *8* (21), 10761-10766.

84.   Chen, L.; Yang, Z.; Wu, J.; Chen, H.; Meng, J., Energy Storage Performance and Mechanism of the Novel Copper Pyrovanadate $Cu_3V_2O_7(OH)_2 \cdot 2H_2O$ Cathode for Aqueous Zinc Ion Batteries. *Electrochim. Acta* **2020,** *330*, 135347.

85.   Liu, F.; Chen, Z.; Fang, G.; Wang, Z.; Cai, Y.; Tang, B.; Zhou, J.; Liang, S., V2o5 Nanospheres with Mixed Vanadium Valences as High Electrochemically Active Aqueous Zinc-Ion Battery Cathode. *Nano-Micro Letters* **2019,** *11* (1), 25.

86.   Zhou, J.; Shan, L. T.; Wu, Z. X.; Guo, X.; Fang, G. Z.; Liang, S. Q., Investigation of V2o5 as a Low-Cost Rechargeable Aqueous Zinc Ion Battery Cathode. *Chem. Commun.* **2018,** *54* (35), 4457-4460.

87.   Hu, P.; Yan, M.; Zhu, T.; Wang, X.; Wei, X.; Li, J.; Zhou, L.; Li, Z.; Chen, L.; Mai, L., Zn/V2o5 Aqueous Hybrid-Ion Battery with High Voltage Platform and Long Cycle Life. *ACS Appl. Mater. Inter.* **2017,** *9* (49), 42717-42722.

88.   Dai, X.; Wan, F.; Zhang, L.; Cao, H.; Niu, Z., Freestanding Graphene/Vo2 Composite Films for Highly Stable Aqueous Zn-Ion Batteries with Superior Rate Performance. *Energy Stor. Mater.* **2019,** *17*, 143-150.

89.   Liu, Y.; Hu, P.; Liu, H.; Wu, X.; Zhi, C., Tetragonal Vo2 Hollow Nanospheres as Robust Cathode Material for Aqueous Zinc Ion Batteries. *Materials Today Energy* **2020,** *17*, 100431.

90.   Tamilselvan, M.; Sreekanth, T. V. M.; Yoo, K.; Kim, J., Binder-Free Coaxially Grown V6o13 Nanobelts on Carbon Cloth as Cathodes for Highly Reversible Aqueous Zinc Ion Batteries. *Applied Surface Science* **2020,** *529*, 147077.

91.   Shi, W.; Yin, B.; Yang, Y.; Sullivan, M. B.; Wang, J.; Zhang, Y.-W.; Yu, Z. G.; Lee, W. S. V.; Xue, J., Unravelling V_6O_{13} Diffusion Pathways Via CO_2 Modification for High-Performance Zinc Ion Battery Cathode. *ACS Nano* **2021,** *15* (1), 1273-1281.

92.   Wang, X.; Ye, L.; Zou, Y.; Zhao, L.; Jiang, Q., Constructing Ultra-Long Life and Super-Rate Rechargeable Aqueous Zinc-Ion Batteries by Integrating Mn Doped V_6O_{13} Nanoribbons with Sulfur-Nitrogen Modified Porous Carbon. *Materials Today Energy* **2021,** *19*, 100593.

93.   Hu, J.; Chen, H.; Xiang, K.; Xiao, L.; Chen, W.; Liao, H.; Chen, H., Preparation for V6o13@Hollow Carbon Microspheres and Their Remarkable Electrochemical Performance for Aqueous Zinc-Ion Batteries. *Journal of Alloys and Compounds* **2021,** *856*, 157085.

94.   Tian, M.; Liu, C.; Zheng, J.; Jia, X.; Jahrman, E. P.; Seidler, G. T.; Long, D.; Atif, M.; Alsalhi, M.; Cao, G., Structural Engineering of Hydrated Vanadium Oxide Cathode by K+ Incorporation for High-Capacity and Long-Cycling Aqueous Zinc Ion Batteries. *Energy Storage Mater* **2020,** *29*, 9-16.

95.   Zhao, H.; Fu, Q.; Yang, D.; Sarapulova, A.; Pang, Q.; Meng, Y.; Wei, L.; Ehrenberg, H.; Wei, Y.; Wang, C.; Chen, G., In Operando Synchrotron Studies of Nh4+ Preintercalated $V_2O_5 \cdot nH_2O$ Nanobelts as the Cathode Material for Aqueous Rechargeable Zinc Batteries. *ACS Nano* **2020,** *14* (9), 11809-11820.

96.   Kundu, D.; Adams, B. D.; Duffort, V.; Vajargah, S. H.; Nazar, L. F., A High-Capacity and Long-Life Aqueous Rechargeable Zinc Battery Using a Metal Oxide Intercalation Cathode. *Nature Energy* **2016,** *1* (10), 16119.

97.   Geng, H.; Cheng, M.; Wang, B.; Yang, Y.; Zhang, Y.; Li, C. C., Electronic Structure Regulation of Layered Vanadium Oxide Via Interlayer Doping Strategy toward Superior High-Rate and Low-Temperature Zinc-Ion Batteries. *Adv. Funct. Mater.* **2020,** *30* (6), 1907684.

98.   Li, J.; McColl, K.; Lu, X.; Sathasivam, S.; Dong, H.; Kang, L.; Li, Z.; Zhao, S.; Kafizas, A. G.; Wang, R.; Brett, D. J. L.; Shearing, P. R.; Corà, F.; He, G.; Carmalt, C. J.; Parkin, I. P., Multi-Scale Investigations of Δ-$Ni_{0.25}V_2O_5 \cdot NH_2O$ Cathode Materials in Aqueous Zinc-Ion Batteries. *Adv. Energy Mater.* **2020,** *10* (15), 2000058.

99.   Liu, Y.; Li, Q.; Ma, K.; Yang, G.; Wang, C., Graphene Oxide Wrapped CuV_2O_6 Nanobelts as High-Capacity and Long-Life Cathode Materials of Aqueous Zinc-Ion Batteries. *ACS Nano* **2019,** *13* (10), 12081-12089.

100.   Liu, C.; Tian, M.; Wang, M.; Zheng, J.; Wang, S.; Yan, M.; Wang, Z.; Yin, Z.; Yang, J.; Cao, G., Catalyzing Zinc-Ion Intercalation in Hydrated Vanadates for Aqueous Zinc-Ion Batteries. *J. Mater. Chem. A* **2020,** *8* (16), 7713-7723.

101.   Chen, S.; Zhang, Y.; Geng, H.; Yang, Y.; Rui, X.; Li, C. C., Zinc Ions Pillared Vanadate Cathodes by Chemical Pre-Intercalation Towards Long Cycling Life and Low-Temperature Zinc Ion Batteries. *J. Power Sources* **2019,** *441*, 227192.

102.   Liu, C.; Massé, R.; Nan, X.; Cao, G., A Promising Cathode for Li-Ion Batteries: Li3v2(Po4)3. *Energy Stor. Mater.* **2016,** *4*, 15-58.

103. He, P.; Yan, M.; Zhang, G.; Sun, R.; Chen, L.; An, Q.; Mai, L., Layered Vs2 Nanosheet-Based Aqueous Zn Ion Battery Cathode. *Adv. Energy. Mater.* **2017,** *7* (11), 1601920.

104. Liu, S.; Chen, X.; Zhang, Q.; Zhou, J.; Cai, Z.; Pan, A., Fabrication of an Inexpensive Hydrophilic Bridge on a Carbon Substrate and Loading Vanadium Sulfides for Flexible Aqueous Zinc-Ion Batteries. *ACS Appl. Mater. Inter.* **2019,** *11* (40), 36676-36684.

105. Cao, H.; Zheng, Z.; Meng, J.; Xiao, X.; Norby, P.; Mossin, S., Examining the Effects of Nitrogen-Doped Carbon Coating on Zinc Vanadate Nanoflowers Towards High Performance Lithium Anode. *Electrochim. Acta* **2020,** *356*, 136791.

106. Deng, S.; Yuan, Z.; Tie, Z.; Wang, C.; Song, L.; Niu, Z., Electrochemically Induced Metal–Organic-Framework-Derived Amorphous V_2O_5 for Superior Rate Aqueous Zinc-Ion Batteries. *Angewandte Chemie International Edition* **2020,** *59* (49), 22002-22006.

107. Chen, H.; Chen, L.; Meng, J.; Yang, Z.; Wu, J.; Rong, Y.; Deng, L.; Shi, Y., Synergistic Effects in V3o7/V2o5 Composite Material for High Capacity and Long Cycling Life Aqueous Rechargeable Zinc Ion Batteries. *J. Power Sources* **2020,** *474*, 228569.

108. Bin, D.; Liu, Y.; Yang, B.; Huang, J.; Dong, X.; Zhang, X.; Wang, Y.; Xia, Y., Engineering a High-Energy-Density and Long Lifespan Aqueous Zinc Battery Via Ammonium Vanadium Bronze. *ACS Appl. Mater. Inter.* **2019,** *11* (23), 20796-20803.

109. Wan, F.; Huang, S.; Cao, H.; Niu, Z., Freestanding Potassium Vanadate/Carbon Nanotube Films for Ultralong-Life Aqueous Zinc-Ion Batteries. *ACS Nano* **2020,** *14* (6), 6752-6760.

110. Ma, L.; Li, N.; Long, C.; Dong, B.; Fang, D.; Liu, Z.; Zhao, Y.; Li, X.; Fan, J.; Chen, S.; Zhang, S.; Zhi, C., Achieving Both High Voltage and High Capacity in Aqueous Zinc-Ion Battery for Record High Energy Density. *Adv. Funct. Mater.* **2019,** *29* (46), 1906142.

111. Liang, X.; Hao, J.; Tan, B.; Lu, X.; Li, W., Binder-Free CaV_3O_7 Nanobelts with Rich Oxygen Defects as High Energy Cathode for Aqueous Zn-Ion Battery. *J. Power Sources* **2020,** *472*, 228507.

112. Jo, J. H.; Aniskevich, Y.; Kim, J.; Choi, J. U.; Kim, H. J.; Jung, Y. H.; Ahn, D.; Jeon, T.-Y.; Lee, K.-S.; Song, S. H.; Kim, H.; Ragoisha, G.; Mazanik, A.; Streltsov, E.; Myung, S.-T., New Insight on Open-Structured Sodium Vanadium Oxide as High-Capacity and Long Life Cathode for Zn–Ion Storage: Structure, Electrochemistry, and First-Principles Calculation. *Adv. Energy Mater.* **2020,** *10* (40), 2001595.

113. Xu, L.; Zhang, Y.; Zheng, J.; Jiang, H.; Hu, T.; Meng, C., Ammonium Ion Intercalated Hydrated Vanadium Pentoxide for Advanced Aqueous Rechargeable Zn-Ion Batteries. *Materials Today Energy* **2020,** *18*, 100509.

114.   Deng, W.; Zhou, Z.; Li, Y.; Zhang, M.; Yuan, X.; Hu, J.; Li, Z.; Li, C.; Li, R., High-Capacity Layered Magnesium Vanadate with Concentrated Gel Electrolyte toward High-Performance and Wide-Temperature Zinc-Ion Battery. *ACS Nano* **2020,** *14* (11), 15776-15785.

115.   Wang, X.; Zhang, Z.; Xiong, S.; Tian, F.; Feng, Z.; Jia, Y.; Feng, J.; Xi, B., A High-Rate and Ultrastable Aqueous Zinc-Ion Battery with a Novel $MgV_2O_6 \cdot 1.7H_2O$ Nanobelt Cathode. *Small* **2021,** *17* (20), 2100318.

116.   Wu, H.; Ming, F.; Lei, Y.; Zhang, W.; Alshareef, H. N., Anisotropic Growth of Al-Intercalated Vanadate by Tuning Surface Hydrophilicity for High-Rate Zn-Ion Storage. *Small Structures* **2020,** *1* (1), 2000040.

117.   Qian, l.; Wei, T.; Ma, K.; Yang, G.; Wang, C., Boosting the Cyclic Stability of Aqueous Zinc-Ion Battery Based on Al-Doped $V_{10}O_{24} \cdot 12H_2O$ Cathode Materials. *ACS Appl. Mater. Inter.* **2019,** *11* (23), 20888-20894.

118.   Wan, F.; Zhang, L.; Dai, X.; Wang, X.; Niu, Z.; Chen, J., Aqueous Rechargeable Zinc/Sodium Vanadate Batteries with Enhanced Performance from Simultaneous Insertion of Dual Carriers. *Nat Commun* **2018,** *9* (1), 1656.

119.   Wang, M.; Zhang, J.; Zhang, L.; Li, J.; Wang, W.; Yang, Z.; Zhang, L.; Wang, Y.; Chen, J.; Huang, Y.; Mitlin, D.; Li, X., Graphene-Like Vanadium Oxygen Hydrate (Voh) Nanosheets Intercalated and Exfoliated by Polyaniline (Pani) for Aqueous Zinc-Ion Batteries (Zibs). *ACS Appl. Mater. Inter.* **2020,** *12* (28), 31564-31574.

120.   Yaghoobnejad Asl, H.; Sharma, S.; Manthiram, A., The Critical Effect of Water Content in the Electrolyte on the Reversible Electrochemical Performance of Zn–Vpo4f Cells. *J. Mater. Chem. A* **2020,** *8* (17), 8262-8267.

121.   Chang, N.; Li, T.; Li, R.; Wang, S.; Yin, Y.; Zhang, H.; Li, X., An Aqueous Hybrid Electrolyte for Low-Temperature Zinc-Based Energy Storage Devices. *Energy Environ. Sci.* **2020,** *13* (10), 3527-3535.

122.   Mackanic, D. G.; Chang, T.-H.; Huang, Z.; Cui, Y.; Bao, Z., Stretchable Electrochemical Energy Storage Devices. *Chem. Soc. Rev.* **2020,** *49* (13), 4466-4495.

123.   Pang, Y.; Cao, Y.; Chu, Y.; Liu, M.; Snyder, K.; MacKenzie, D.; Cao, C., Additive Manufacturing of Batteries. *Adv. Funct. Mater.* **2020,** *30* (1), 1906244.

124.   Zhang, M.; Mei, H.; Chang, P.; Cheng, L., 3d Printing of Structured Electrodes for Rechargeable Batteries. *J. Mater. Chem. A* **2020,** *8* (21), 10670-10694.

125.   Hu, Y. S.; Demir-Cakan, R.; Titirici, M. M.; Müller, J. O.; Schlögl, R.; Antonietti, M.; Maier, J., Superior Storage Performance of a Si@Siox/C Nanocomposite as Anode Material for Lithium-Ion Batteries. *Angew. Chem* **2008,** *47* (9), 1645-9.